A NEUTRON-GAMMA COINCIDENCE COUNTING SYSTEM FOR THE INVESTIGATION OF BROMINE DELAYED-NEUTRON PRECURSORS

by

Mahmoud M. Farghaly

B.S., University of Alexandria, 1967
M.S., University of Sao Paulo, 1971

a Masters Thesis

submitted in partial fulfillment of the
requirements for the degree

Master of Science

Department of Nuclear Engineering

KANSAS STATE UNIVERSITY

Manhattan, Kansas

1975

Approved: M S Kirk
Major Professor

TABLE OF CONTENTS

LIST OF FIGURES

List of Figures (Continued)

LIST OF TABLES

NOMENCLATURE

A	Atomic weight of U-235
A_n	Delayed-neutron precursor activity resulting in neutron emission
A_γ	Gamma rays emitted per second
$A_{n\gamma}$	Delayed-neutron precursor activity resulting in coincident n-γ emission
A_{sat}	Saturated activity
$A_n^{(Br)}$	Bromine saturated delayed-neutron activity
$A_\gamma^{(Br)}$	Number of delayed gamma rays produced per second by saturated bromine isotopes
$A_{n\gamma}^{(Br)}$	Coincident n-γ rate from saturated bromine fission products
B_n	Neutron binding energy of the emitter
C_T	True coincidence count rate
C_R	Random coincidence count rate
E_{cc}	Effective cutoff energy for cadmium
E_{res}	Resonance energy
E_{Tc}	Thermal cutoff energy
F_{CD}	Cadmium cover flux depression factor
FR	Fission rate
$\|M\|^2$	Square of the matrix element for β-decay
m	Mass of ^{235}U in the sample
m_c	Mass of the covered foil
m_b	Mass of the bare foil
N_n	Neutron count rate
N_γ	Gamma count rate
N_i	Average number of gamma rays per decay of isotope i
N^{235}	number of nuclei of ^{235}U in the sample

N_{avog}	Avogadro's number
N_D	Number of nuclei in the foil
n	Detector efficiency (used in Appendix B)
P_n	Delayed-neutron emission probability
P_{n_i}	Delayed neutron emission probability of the precursor i
p_i	Fraction of the i-th precursor nuclei which decay by both neutron and gamma emission
Q_β	Beta decay Q-value of the precursor
$\hat{R}_b$	Bare foil activity per unit mass
$\hat{R}_c$	Covered foil activity per unit mass
R	True-to-random coincidence ratio
t_1	Irradiation time
t_2	Cooling time
t_3	Counting time
$T_{1/2}$	Half-live
Y_c	Cummulative yield
Y_i^j	Fractional fission yield of the isotope i in the element j
Γ_n/Γ_t	Ratio of the neutron width to the total width
Γ_n	Partial width for neutron decay
Γ_γ	Partial width for gamma decay
γ	Percentage of nuclei that decay by observed decay mode
λ	Decay constant
ε_n	Absolute neutron detector efficiency
ε_γ	Absolute gamma detector efficiency
τ	Resolving time
ω	Energy level density function in emitter

Chapter I.

INTRODUCTION

Delayed-particle emission is known both from neutron-deficient nuclei (alphas and protons) and from neutron-rich nuclei (neutrons) [1]. Delayed-proton emission was first observed in 1962, whereas the emission of delayed neutrons had been discovered in 1939 [1]. After the discovery of nuclear fission it was considered that newborn fragments having a large excess of neutrons over stable nuclei would emit prompt neutrons either at the instant of fission or very soon thereafter. However, some serious discussion centered on the idea that a fission fragment may undergo several steps of β-decay and still reach a state where de-excitation by neutron emission is possible. In fact the emission of delayed neutrons was observed by Roberts, Mayer, and Wang [2] early in 1939 before the existence of the prompt neutrons had been proven [1].

The delayed neutrons are those neutrons emitted when a particular radioactive nuclide, called the precursor, decays by β^- emission to a level in the daughter nucleus which lies at a higher excitation energy than the neutron separation energy for the daughter. This highly excited state in the daughter nucleus generally decays by neutron emission; the daughter nucleus is called the delayed-neutron emitter. A diagram illustrating the process is shown in Figure 1.

Although the discovery and the qualitative interpretation of delayed neutrons dates from 1939, and although delayed neutrons have both practical and fundamental importance, theoretical investigations of delayed-neutron phenomena are hindered by the lack of direct experimental data on delayed

THIS BOOK CONTAINS NUMEROUS PAGES WITH DIAGRAMS THAT ARE CROOKED COMPARED TO THE REST OF THE INFORMATION ON THE PAGE.

THIS IS AS RECEIVED FROM CUSTOMER.

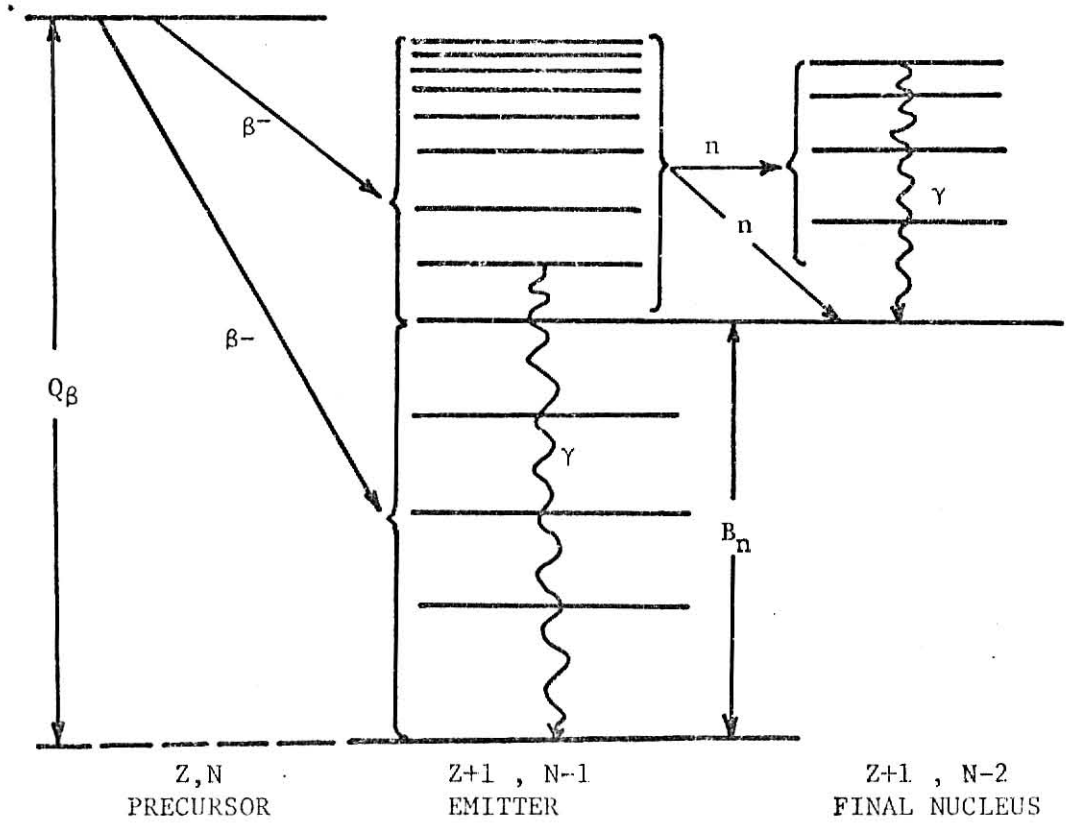

Figure 1. Schematic representation of delayed-neutron emission; Q_β is the beta decay energy of the precursor and B_n is the neutron binding energy of the emitter.

neutrons and delayed-neutron precursors and by the large charge separation of delayed-neutron precursors from the line of beta stability, where most nuclear data exists. Experimental investigations are also hindered by the separation of precursors from the beta-stability line. Accelerator-produced charged-particle reactions leading directly to precursors, emitters or final nuclei are generally not practical. Also, because of the distance from the stability line, the precursor half-lives are short, and fast radiochemical separations of precursors produced as fission products are difficult. The current status of delayed-neutron measurements is reviewed briefly in section (II.1).

Delayed-neutron measurements are of current importance for fast reactor design, nondestructive assay of fissionable materials by fast-neutron interrogation, and nuclear structure studies. Recent work has included measurements on absolute delayed-neutron yields, dependence of the yields on the energy of the neutron inducing fission, delayed-neutron group yields and abundances and delayed-neutron energy spectra. Further, progress in delayed-neutron physics depends strongly upon extensive measurements of delayed-neutron energy spectra and delayed-neutron decay modes.

The need for further delayed-neutron measurements is discussed in section (II.3). Two of the experiments requiring immediate attention are 1) the measurement of delayed-neutron energy spectra with good resolution and 2) the measurement of the decay modes of delayed-neutron emitters. As long ago as 1967 the importance of these measurements was emphasized by Jahnsen, Pappas, and Tunnal [1]. Their paper discusses the experimental and theoretical work required to develop the field of delayed-neutron physics. Their conclusions were that, first of all, knowledge is required on the detailed shapes of the delayed neutron spectra, and a decision as to whether these are line spectra (as they most likely will be) or continuous spectra.

Secondly, the importance of the measurement of neutron branchings, n-γ coincidences and, if possible, β-n-γ coincidences was emphasized.

Further studies should result in information not only of major interest for the delayed-neutron problem itself, but might also throw some light on parameters of importance for the understanding of the nuclear structural properties involved in the decay process (e.g., the square of the matrix element $|M|^2$, the level density function ω, the ratio of the neutron width to total width Γ_n/Γ_t, Q_β and B_n), and should of course be of importance in the practical aspects of delayed-neutron emission.

The measurement of delayed-neutron spectra has recently been receiving attention by several experimental groups world-wide [13,14,24,25]; the investigation of delayed-neutron decay modes of bromine precursors produced as fission products of an irradiated sample of uranium is the subject of this work and is discussed in Chapter III.

Chapter II.

REVIEW OF DELAYED NEUTRON MEASUREMENTS AND CALCULATIONS

II.1 Significance

The basic interest in delayed-neutron emission for nuclear physics stems from its importance in the study of nuclear structure and transitions and for mass and binding energy formulae in the neutron rich region far off the beta-stability line [3]. For nuclear engineering, delayed-neutron data has been of great importance for thermal and fast reactor design and for the development of nondestructive assay techniques for fissionable materials [4,5]. The basic input data required for all reactor physics and design calculations include: (a) fundamental nuclear cross sections, (b) physical properties of materials, and (c) fission parameters including yields and energy distributions of the delayed and prompt fission neutrons. The accuracy of all reactor physics and design calculations is ultimately limited by three main sources of errors: 1) uncertainties in calculational methods, 2) uncertainties in physical compositions, masses, dimensions, etc. of the system, and 3) uncertainties in the general input data including basic cross-sections, fission parameters, physical characteristics, etc. Of major importance among the fission parameters are the number and energy distributions of the delayed-neutrons. This is especially true in the case of the large fast power breeder reactors. The importance of the accuracy of these data for reactor design has been emphasized by Keepin [6] and Yiftah [7]. The excellent references by Keepin [8], Jahnsen, Pappas, and Tunnal [1] and Tomlinson and Hermann [9] review delayed-neutron knowledge up to 1965, 1968, and 1972, respectively. Many investigations have been attempted with the purpose of identifying the delayed-neutron precursors and of measuring the absolute delayed-neutron yields for important isotopes.

II.2 Delayed-neutron Yields, Precursor Identification, and P_n Values

The number of delayed neutrons emitted per low-energy fission is in the range of 0.006 to 0.016 depending on the fission source [3]. Regularities are observed, such as that the delayed-neutron yield increases with the mass number of the fissioning nuclide within an isotopic series and decreases with increasing atomic number of the nuclide within an isobaric series. Also the delayed-neutron yield depends on the energy of the fission-inducing neutron. These regularities are consistant with the systematics of fission, and are linked with the increasing abundance of delayed-neutron precursors as the production and relative distribution of neutron rich nuclides increases beyond the closed neutron shells.

Analysis of the composite decay of the delayed neutrons observed with different fission sources (ranging from Th-232 to Cf-252, fission either spontaneous or induced by thermal to 15 MeV neutrons) showed that the precursor decay can be characterized by six groups with approximate half-lives of 55 sec, 22 sec, 6 sec, 2 sec, 0.5 sec, and 0.2 sec [3,5,9]. The isotopes primarily responsible for the activity of groups 1, 2, and 3 (longest lived ones) have been identified and their half-lives determined [3,9]; also the probability P_n that a delayed-neutron precursor will decay by neutron emission has been determined with varying degrees of accuracy for many precursors [3,9]. A summary of some of these results is shown in Tables 1 and 2. In recent work Kratz and Hermann [10] have identified two new delayed-neutron bromine precursors with half-lives of 0.63 sec and 0.25 sec which were assigned to Br-91 and Br-92, respectively. The other known bromine precursors are Br-87, Br-88, Br-89, and Br-90.

Reactor physics and design problems are concerned primarily with absolute yields (i.e., the number of delayed neutrons produced per fission) and energy

Table 1. Comparison between group (i = 1,2,3) yields and detailed precursor contributions from different fission reactions. (From Ref.3)

Group No. (i)	d.n. precursor	$T_{1/2}$ (s)	P_n (%)	^{233}U thermal fission Y_c (%)	^{233}U thermal fission $n/10^4$ fission	^{235}U thermal fission Y_c (%)	^{235}U thermal fission $n/10^4$ fission	^{239}Pu thermal fission Y_c (%)	^{239}Pu thermal fission $n/10^4$ fission	^{252}Cf spontaneous fission Y_c (%)	^{252}Cf spontaneous fission $n/10^4$ fission
1	^{87}Br	55	2.5	3.58	8.96	2.28	5.7	0.79	1.97	0.21	0.52
	^{133}Sn	7	(0.2)	0.09	(0.02)	0.42	(0.1)	0.13	0.03	0.02	0.004
					8.98		5.8		2.0		0.52
	Group yield:			(5.7 ± 0.3)		(5.2 ± 0.5)		(2.1 ± 0.6)		(0)	
2	^{88}Br	16	4	3.03	12.14	2.78	11.1	0.85	3.41	0.174	0.70
	^{137}I	24	4.8	2.75	13.20	4.11	19.7	3.0	14.42	1.69	8.11
	^{141}Cs	25	0.073	3.66	0.27	4.60	0.3	3.16	0.23	3.2	0.23
	^{134}Sb	11	0.08	0.714	0.06	2.19	0.2	0.93	0.07	0.25	0.02
	^{134}Sn	7	(6.1)	0.095	0.58	0.09	(0.5)	0.015	0.09	0.003	0.02
					26.25		31.8		18.22		9.08
	Group yield:			(19.7 ± 0.9)		(34.6 ± 1.8)		(18.2 ± 2.3) [1]		(26.7 ± 3.5)	
3	^{87}Se	6	0.4	1.04	0.42	1.09	0.4	0.244	0.10	0.05	0.02
	^{89}Br	4.5	7	1.63	11.42	2.42	16.9	0.502	3.52	0.10	0.70
	^{92}Rb	4.5	0.012	4.52	0.05	5.18	0.06	2.25	0.03	0.498	0.01
	^{93}Rb	6	1.8	2.58	4.64	4.0	7.2	1.61	2.90	0.285	0.51
	^{139}I	6	2.5	1.31	3.27	2.68	6.7	1.34	3.36	0.788	1.97
					19.80		31.3		9.91		3.21
	Group yield:			(16.6 ± 2.7)		(31.0 ± 3.6)		(12.9 ± 3)		(18.9 ± 3.0)	

Table 2. Summary of known and expected contributions to delayed neutron groups 4, 5, and 6 in ^{235}U thermal fission. (From Ref. 3)

Group No.	d.n. precursor	$T_{1/2}$ (s)	P_n %	Thermal fission of U^{235} Y_c %	Thermal fission of U^{235} n/10^4 fission
4	Ge-84	?	(8.9)	0.093	(0.83)
	As-84	?	(1.3)	0.646	(0.84)
	As-85	2	10.5	0.485	8.0
	As-86	?	(16.6)	0.31	(5.15
	Se-88	2	6.4	0.65	4.18
	Br-90	1.6	12	1.75	21.0
	Br-92	?	(20.2)	0.07	(1.4)
	Kr-92	1.9	0.04	1.68	0.07
	Kr-93	1.3	3.3	0.53	1.75
	Rb-94	2.7	7.5	1.9	14.2
	Y -98	2	0.8	2.9	2.3
	Sb-135	1.7	8.0	0.485	3.9
	Te-137	?	(1.0)	0.63	(0.63)
	I -139	2	6.0	1.1	6.6
	I -140	0.8	12	0.236	2.8
	Xe-141	1.7	0.054	1.14	0.06
	Xe-142	1.2	0.45	0.31	0.14
	Cs-142	2	1.5	3.1	4.6
	Cs-143	1.7	3.0	1.43	4.3
	Cs-144	1.0	3.6	0.41	1.5
	Cs-145	?	(4.7)	0.054	(0.25)
					84.48
		Group yield (3)			(62.4 ± 2.6)
5,6	Br-91	0.5	(13.8)	0.40	(5.52)
	Kr-94	0.2	(4.7)	0.08	(0.38)
	Kr-95	?	(8.3)	0.01	(0.08)
	Rb-95	0.4	7.1	0.66	4.7
	Rb-96	0.2	17.7	0.17	2.15
	Rb-97	0.14	20	0.02	0.4
	Sb-136		(13)	0.094	(1.22)
	I -141	0.3	(11.1)	0.032	(0.35)
	Xe-143		1.5	0.05	0.08
	Xe-144		1	5×10^{-5}	0
					14.88
		Group yield (3)			(24.8 ± 1.7)

spectra of delayed neutrons. There is a clear need for more accurate and complete delayed-neutron energy-spectrum measurements, as well as further high-energy delayed-neutron yield data, for all of the main fission species [6].

Several studies have been conducted with the purpose of determining the absolute delayed-neutron yields; a good reference for such studies is that of Keepin, Wimmet, and Zeigler [11]. Recent values have been reviewed by Evans, Thorpe, and Krick [12] and by Tuttle [45].

II.3 Calculation of P_n Values and Delayed-neutron Energy Spectra

Delayed neutron emission is made possible by the fact that the greater the distance from stability, the less the neutron binding energy B_n and the greater the mass difference between adjacent isobars, and hence the total β-decay energy Q_β. Thus at a certain or greater distance from stability $Q_\beta - B_n > 0$, and β-decay from a nuclide (Z,N) can populate states above the neutron binding energy in the daughter nuclide (Z+1,N-1). This may then promptly emit a neutron giving the nuclide (Z+1,N-2) or de-excite through gamma emissions to its ground state (Figure 1).

Any comprehensive theory of delayed-neutron emission should account for the existence of the known delayed-neutron precursors, the observed energy spectra, and the observed delayed-neutron emission probabilities (P_n). The probability for delayed neutron emission P_n is defined [8,26,27] as the fraction of β-decays from the precursor leading to neutron-emitting states in the emitter. Using the decay scheme shown in Figure 1, it should be possible, in principle, to calculate P_n values. To do so, it is necessary to know the level density in the emitter, the number of beta decays going to each level, the mode of decay (γ or n) of each level and whether or not any neutron decay goes to excited rather than ground states in the final nucleus. Several attempts have been made at the

calculation of the P_n values by Pappas [24], Pappas and Rudstam [15] and Keepin [28]. Tomlinson [46] has used the following expression for a P_n-value calculation

$$P_n = \frac{\int_{B_n}^{Q_\beta} \frac{\Gamma_n}{\Gamma_n \quad \Gamma_\gamma} \cdot (Q_\beta - E)^5 \, \omega dE}{\int_0^{Q_\beta} (Q_\beta - E)^5 \, \omega dE}$$

where

ω = level density at energy E in the emitter.

Γ_n and Γ_γ are the partial widths for neutron and gamma decay, respectively. This expression was simplified by assuming that when Q_β was more than 50 keV greater than B_n, Γ_γ was zero; Q_β and B_n were estimated using mass formulas [23]. Figure (2) shows emperical plots of P_n values made by Tomlinson using a number of experimental values of P_n and the general shapes of the theoretical curves as a guide. These plots can be used to estimate P_n values for unknown precursors. A summary of Q_β, B_n, and P_n data taken from reference (3) is shown in Table (3).

Delayed-neutron energy spectra were measured in 1956 by Bachelor and Hyder [13]; their work provided some important data using low resolution measurements. Recently, Shalev and Cuttler [14], Shalev and Rudstam [47], and Sloan and Woodruff [48] have improved the situation somewhat by providing a few higher resolution spectra. Figure 3 shows such spectra. Theoretical calculations have been carried out by Gauvin and de Tourreil [49] in attempts to include the correct expressions for beta-decay probability, the level densities and the gamma-neutron completion in the de-excitation of the emitter for the precursors ^{87}Br, ^{88}Br, ^{137}I, ^{85}As, and $^{93-97}$Rb. The results of their trials are shown in Figure (4) for group 1 (^{87}Br) and in Figure (5) for group 2. In Figure (5), the values were obtained by combining spectra for ^{88}Br and ^{137}I. In both groups 1 and 2 the theoretical spectra reproduce the main features of the Batchelor and Hyder

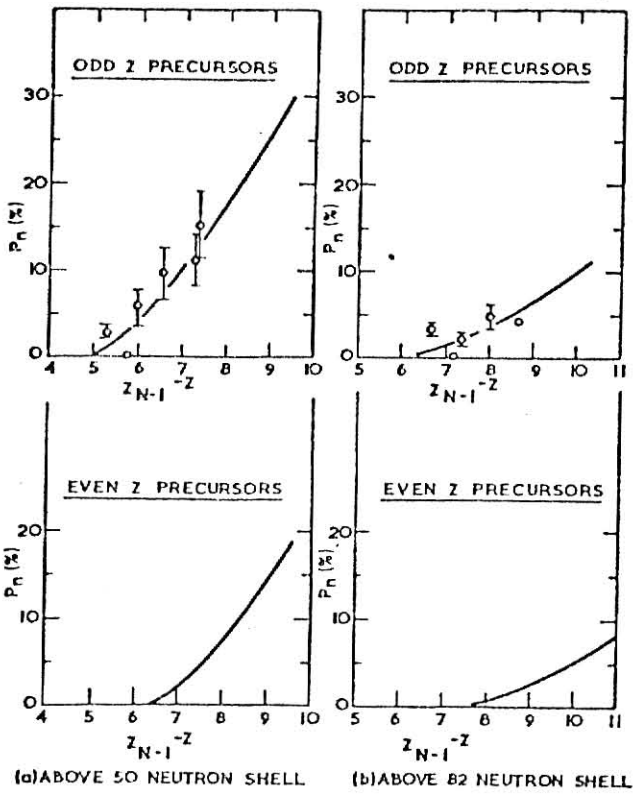

Figure 2. Semiempirical plots of delayed-neutron emission probabilities. $Z_N - Z$ is a parameter denoting the distance of the precursor from the line of stability. (From Ref. 46)

Table 3. Estimated and Experimental Delayed-Neutron Emission Probabilities (From Ref. 3)

d.n. precursor	Q_β^*	B_n^*	$Q_\beta - B_n$	P_n (calc.)**	P_n (exp.)***	Ratio (calc./exp.)	Cumulative fission yield in ^{235}U; (%)	d.n. yield (n/10^4 fissions of ^{235}U)	
								calculated	experimental
^{84}Ge	7.54	4.15	3.39	8.9 ± 1.1	-	-	0.093	0.83	-
^{84}As	9.09	9.06	0.03	~1.3	-	-	0.646	0.84	-
^{85}As	9.05	4.10	4.95	15.8 ± 1.8	16.5 ± 6	0.96	0.485	7.66	8.00
^{86}As	11.35	6.22	5.13	16.6 ± 1.9	-	-	0.31	5.15	-
^{87}Se	7.27	6.40	0.87	~1.1	0.4 ± 0.1	2.75	1.09	1.2	0.44
^{88}Se	6.33	4.85	1.48	2.5 ± 1.9	6.4 ± 2.5	0.39	0.65	1.62	4.16
^{87}Br	6.68	5.46	1.22	1.9 ± 1.4	2.5 ± 0.5	0.76	2.28	4.33	5.7
^{88}Br	8.98	7.15	1.83	3.5 ± 2.7	4 ± 1	0.88	2.78	9.73	11.12
^{89}Br	8.04	5.22	2.82	6.8 ± 0.8	7 ± 2	0.97	2.42	16.46	16.94
^{90}Br	10.33	6.21	4.12	12 ± 1.4	12 ± 3	1.00	1.75	21.0	21.0
^{91}Br	9.18	4.57	4.61	13.8 ± 1.6	-	-	0.40	5.52	-
^{92}Br	12.01	6.21	5.80	20.2 ± 2.3	-	-	0.07	1.4	-
^{92}Kr	5.31	5.06	0.25	< 0.5	0.04 ± 0.007	-	1.68	< 0.84	0.07
^{93}Kr	8.15	6.30	1.85	3.5 ± 2.7	3.3 ± 0.5	1.06	0.53	1.85	1.75
^{94}Kr	6.56	4.33	2.23	4.7 ± 0.5	-	-	0.08	0.38	-
^{95}Kr	9.45	6.22	3.23	8.3 ± 1.0	-	-	0.01	0.08	-
^{93}Rb	7.80	7.35	0.45	< 0.5	0.012 ± 0.004	-	5.18	< 2.09	0.06
^{94}Rb	6.62	5.14	1.48	2.5 ± 1.9	1.8 ± 0.5	1.39	4.0	10.0	7.2
^{95}Rb	9.45	7.17	2.28	4.8 ± 0.5	7.5 ± 1.9	0.64	1.9	9.1	14.2
^{96}Rb	7.87	4.64	3.23	8.3 ± 1.0	7.1 ± 0.9	1.2	0.66	5.5	4.7
^{97}Rb	10.76	6.62	4.14	12.1 ± 1.4	12.7 ± 1.5	0.96	0.17	2.05	2.15
^{97}Y	9.03	3.92	5.11	16.6 ± 1.9	>20	0.83	0.02	0.3	> 0.4
^{98}Y	5.35	5.22	0.13	< 0.5	-	-	4.75	< 2.3	-
^{98}Y	8.24	7.55	0.69	~0.8	0.8 ± 0.4	1.00	2.9	2.3	2.3
^{99}Y	6.51	4.44	2.07	4.2 ± 0.5	-	-	0.54	2.27	-

Table 3. (cont.)

d.n. precursor	Q_β^*	B_n^*	$Q_\beta - B_n$	P_n (calc.)**	P_n (exp.)***	Ratio (calc./exp.)	Cumulative fission yield in ^{235}U; (%)	d.n. yield ($n/10^4$ fissions of ^{235}U)	
								calculated	experimental
^{133}Sn	7.24	7.11	0.13	< 0.5	-	-	0.42	< 0.21	-
^{134}Sn	6.07	3.43	2.64	6.1 ± 0.7	-	-	0.086	0.52	-
^{134}Sb	8.70	7.35	1.35	2.2 ± 1.7	0.08 ± 0.02	-	2.19	4.82	0.18
^{135}Sb	7.52	3.86	3.66	10 ± 1.1	8 ± 2	1.25	0.485	4.85	3.88
^{135}Sb	9.54	5.20	4.34	13 ± 1.5	-	-	0.094	1.22	-
^{136}Te	4.47	4.02	0.45	< 0.5	-	-	2.02	< 1.01	-
^{137}Te	6.48	5.63	0.85	~1	-	-	0.63	0.63	-
^{137}I	5.79	4.45	1.34	2.2 ± 1.7	4.8 ± 1.3	0.46	4.11	9.1	19.7
^{138}I	7.80	5.86	1.94	3.8 ± 2.9	2.5 ± 0.6	1.52	2.68	10.2	6.73
^{139}I	6.67	3.89	2.88	6.7 ± 0.8	6 ± 2	1.12	1.10	7.98	6.60
^{140}I	8.93	5.35	3.58	9.8 ± 1.1	12 ± 8	0.82	0.236	2.28	2.83
^{141}I	7.42	3.52	3.90	11.1 ± 1.3	-	-	0.032	0.35	-
^{141}Xe	5.85	5.79	0.06	< 0.5	0.054 ± 0.009	-	1.14	<0.57	0.06
^{142}Xe	4.34	3.93	0.41	< 0.5	0.45 ± 0.08	-	0.31	< 0.15	0.14
^{143}Xe	6.65	5.59	1.06	1.5 ± 1.1	-	-	0.05	0.08	-
^{144}Xe	4.67	3.85	0.82	~1	-	-	0.00005	~0	-
^{145}Xe	7.14	5.81	1.33	2.2 ± 1.7	-	-	~0	~0	-
^{141}Cs	4.97	4.65	0.32	< 0.5	0.073 ± 0.011	-	4.60	< 2.30	0.33
^{142}Cs	7.24	6.20	1.04	1.5 ± 1.1	0.27 ± 0.1	5.56	3.1	4.64	0.84
^{143}Cs	5.73	4.09	1.64	3.0 ± 2.3	1.13 ± 0.25	2.66	1.43	4.29	1.61
^{144}Cs	8.05	6.16	1.89	3.8 ± 2.7	1.10 ± 0.3	3.27	0.41	1.48	0.45
^{145}Cs	6.07	3.83	2.24	4.7 ± 0.5	-	-	0.054	0.25	-

THIS BOOK CONTAINS NUMEROUS PAGES WITH ILLEGIBLE PAGE NUMBERS THAT ARE CUT OFF, MISSING OR OF POOR QUALITY TEXT.

THIS IS AS RECEIVED FROM THE CUSTOMER.

ILLEGIBLE DOCUMENT

THE FOLLOWING DOCUMENT(S) IS OF POOR LEGIBILITY IN THE ORIGINAL

THIS IS THE BEST COPY AVAILABLE

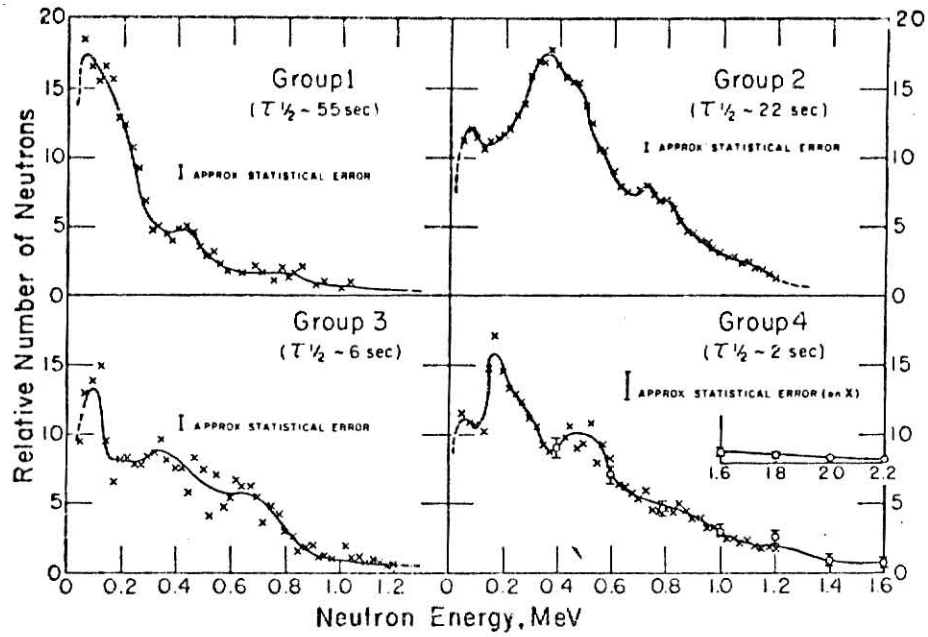

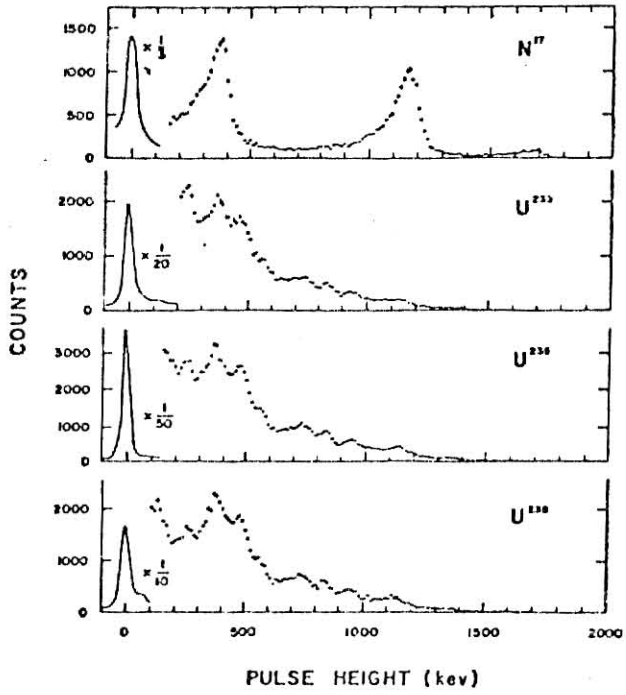

Figure 3. Experimental delayed neutron spectra. The upper group spectra are from Bachelor and Hyder (Ref. 13). The lower gross spectra for ^{17}N, ^{233}U, ^{235}U and ^{236}U are from Shalev and Cuttler (Ref. 14).

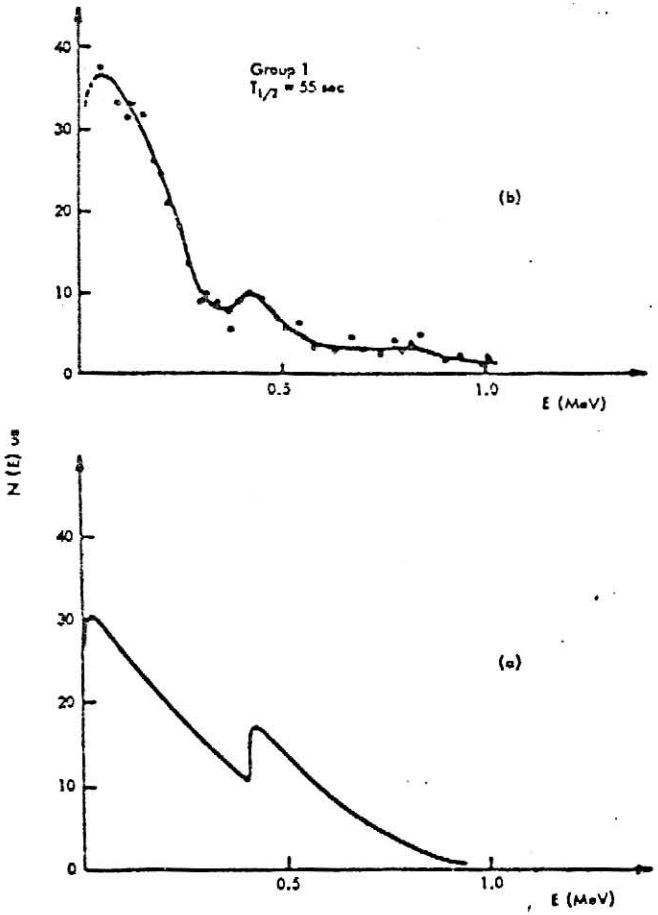

Figure 4. (a) Calculated Energy Spectrum for ^{87}Br

(b) Experimental Spectrum for group 1.

(From Ref. 46)

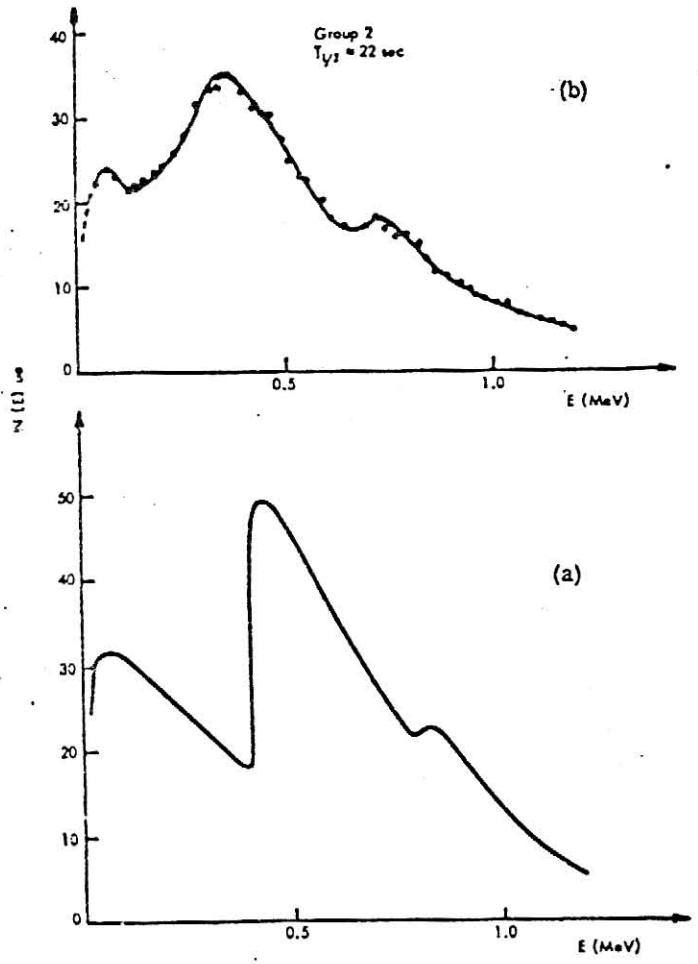

Figure 5. (a) Calculated Energy Spectrum for group 2(^{88}Br+^{137}I)

(b) Experimental Spectrum for group 2.

(From Ref. 46)

experimental spectra. The actual delayed-neutron spectra, however, are much more complex than the old Batchelor and Hyder measurements indicate.

A comparison by Takahashi [16] of the theoretical and experimental delayed-neutron energy spectrum for the precursor ^{137}I is shown in Figure 6 as an illustration of relatively recent delayed-neutron calculations. The experimental spectrum is the recent, fairly high-resolution one of Shalev and Rudstam [47]. In this calculation as in all other delayed-neutron spectra calculations, the lack of experimental nuclear structure data is the primary limitation.

II.4 Delayed-neutron/Gamma-ray Coincidence Measurements

Gamma rays in coincidence with delayed-neutrons following the decay of ^{95}Rb, ^{90}Br, and ^{85}As have been detected according to the recent work done by Crawford et al [24]. This work has been performed using an on-line separator to select the fission products of mass 85, 90, and 95. The fission products were collected on a continuous-loop moving tape system and passed with a minimum of distance to a roller system which concentrated 1.5 m of tape in a zig-zag pattern between two detectors and then to a reservoir which held some 800 m of tape. The tape speed was chosen to optimize the yield of the isotope of interest on the basis of its known half-life. The two detectors used were a 3 x 3 in. NaI(Tl) for gammas and a 12.7 cm x 5 cm NE213 liquid scintillator for neutrons. The pulse height spectrum was recorded for all events in the NaI(Tl) detector which were detected in coincidence with those in the neutron detector. Table 4 shows some of the results obtained from this work.

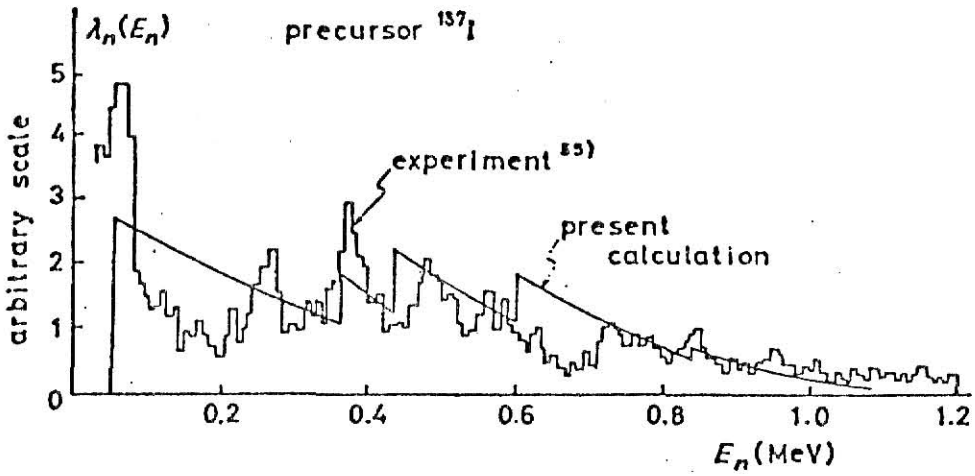

Figure 6. Comparison of calculated and experimental delayed-neutron spectra for ^{137}I. The calculation was performed by Takahashi (Ref.16); experimental data is from Shalev and Rudstam (Ref. 47).

Table 4. Rb, Br, and As Delayed-Neutron Precursor Gamma Energies [24]

Precursor	True single neutron detection rate sec^{-1}	Total coincidence rate sec^{-1}	E_γ keV	Photopeak count rate min^{-1}
^{95}Rb	1.5	0.22	845	1.3
^{90}Br	2.6	0.25	417	1.9
^{85}As	2.6	0.17	304	
			687	uncertain
			1440	uncertain

Gunther, Siegert, Wuensch, and Wollnik [25] have investigated the gamma rays emitted by short-lived Rb, Sr, and Y isotopes. Delayed neutron emission to excited states was indicated. The thermally ionizable Rb and Cs fission products were formed by irradiating 500 mg of ^{235}U in a flux of 10^7 neutrons/cm^2-sec in a neutron beam tube. The uranium was loaded into the pores of five 20 x 20 x 0.7 mm thick carbon pieces. They were heated to 1600°C assuring a quick diffusion of the thermalized Rb fission products to the surface and an ionization efficiency of about 100%. The ions then were accelerated to an energy of 15 keV and separated in an on-line separator according to mass by a sector magnet of 21 cm radius. By chopping the neutron beam, they were able to observe an overall delay time of about 60 msec for the Rb fission products from their production to their detection behind the separator and the gamma spectra were recorded for ^{95}Rb, ^{96}Rb, and ^{97}Rb with half-lives of 383 msec, 199 msec, and 172 msec, respectively. Gamma energies in the level schemes of Sr, Y, and Zr isotopes were distinguished by the known half-lives of the decaying Rb, Sr, and Y isotopes (see Table 5) using a moving tape of variable speed.

Table 5. Gamma-ray energies (keV) in the decay schemes of $^{95,96,97}Sr$, $^{95,96,97}Y$, and $^{95,97}Zr$

	Level scheme	Half-life of mother	Pn value (%)	γ-lines (MeV) and intensities											
daughters of ^{95}Rb	^{95}Sr	^{95}Rb: 0.38 sec	8	26%	24%	100%	4%	6%	11%	33%	7%	10%	7%		
				204	329	352	564	578	660	681	769	1001	1258		
				(190)		(360)	(560)			(680)			(1270)		
	^{95}Y	^{95}Sr: 26 sec		100%	4%	11%	10%	4%	6%						
				686	777	827	945	982	1278						
				(686)	(777)	(827)	(945)	(983)	(1278)						
	^{95}Zr	^{95}Y: 11 min		12%	28%	100%	27%								
				433	919	953	1325								
daughters of ^{96}Rb	^{96}Sr	^{96}Rb: 0.2 sec	13	4%	8%	6%	10%	100%	8%	9%	4%	4%			
				412	593	606	691	813	978	1036	1179?	1335?			
								(813)							
	^{96}Y	^{96}Sr: 1.2 sec		94%	13%	12%	100%	21%	6%						
				122	279	530	809	931	1306?						
				(121)	(279)	(530)	(809)	(931)							
	^{96}Zr	^{96}Y: 10 sec		-											
daughters of ^{97}Rb	^{97}Sr	^{97}Rb: 0.17 sec	27	9%	100%	10%	14%	18%	38%	79%	56%	29%	21%	34%	52%
				141?	167	355?	367?	418	519	585	599	652?	697?	1097?	1258?
	^{97}Y	^{97}Sr: 0.4 sec		100%	25%	22%	71%								
				123	308	434	953								
	^{97}Zr	^{97}Y: 1.1 sec		22%	25%	40%	60%	100%	38%						
				280	530	893	1091	1104	1125						

The maximum error is ±1 keV. For each γ-line the relative intensity with an abosolute error of 5%. Values shown in brackets are known from previous measurements[6,10,11]. In the mass chains of the decaying ^{96}Rb several lines are marked with a question mark (see also Figure 1). In these cases the intensity was insufficient to determine the half-lives exactly and thus it was not possible to determine without doubt whether these γ-line belonged to the level schemes of Sr, Y, or Zr. (Reference 25)

The gamma spectra were measured with a Ge(Li) detector with a volume of 80 cm^3. In order to reduce the background only those γ-rays were accepted which were coincident with the preceding β^- particle registered in a Si surface-barrier detector. The recorded gamma spectra of the decaying fission products ^{95}Rb, ^{96}Rb, and ^{97}Rb and of their daughters obtained from this work are shown in Figure 4. From the results shown in Figure 7, they were able to assign the different gamma lines to level schemes of Sr, Y, or Zr isotopes. The isotopes identified by label (n) in the spectrum obtained from this work (see Fig. 7) indicates that the γ-lines observed belong to the final nucleus of a delayed neutron emitter. P_n values obtained for ^{96}Sr (12%) and ^{97}Sr (31%) by comparing gamma-ray intensities from ^{95}Y, ^{96}Y, and ^{97}Y agree well with previously measured values (13% and 27%, respectively).

II.5 Need for Further Measurements

On reviewing the information and the data on delayed-neutron physics since its discovery up until the present time, it is apparent that nearly every aspect of delayed-neutron physics requires further investigation. The most accurate and satisfactory data exists for

1) absolute delayed-neutron yields for thermal and fission-spectrum-induced fission of the most practically important nuclides,
2) group periods and abundances for the above,
3) the identification of precursors for groups 1-4, and
4) half-lives and P_n values for the above groups and precursors.

Of the many deficiencies in present delayed-neutron data several of the most important are:

1) According to Saphier and Yiftah [17], the absolute delayed-neutron yields should be measured with a standard deviation of ± 2%. There is a discrepancy of 17% for U-238 between the two carefully performed

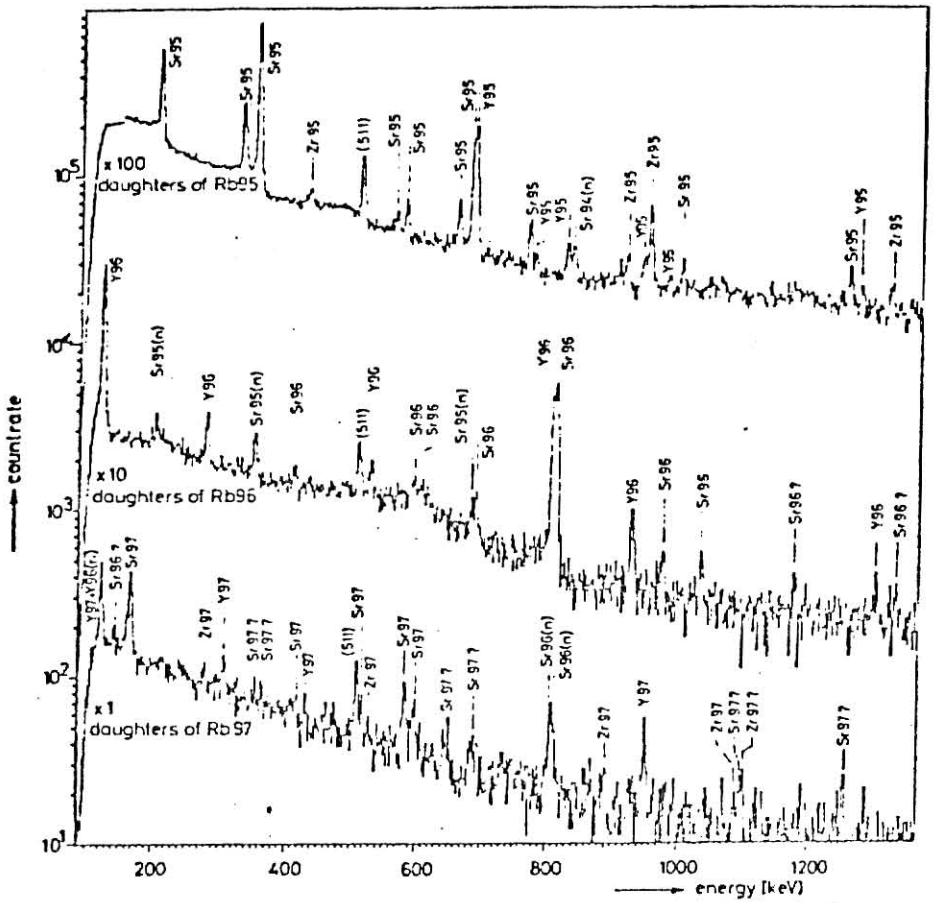

Figure 7. The β-coincident γ-spectra of Rb-95, Rb-96 and Rb-97 and their daughters. For each γ-line an indication as to whether it belongs to the level scheme of a Sr, Y, or Zr isotope is given. The distinction between diffirent elements was made by the diffirent half-lives of the preceding nuclei. In some cases the lable (n) is added indicating that this γ-line belongs to the final nucleus of a delayed neutron emitter. In a few cases question marks are added to the symbol of Sr, Y, or Zr. They characterize weak γ-lines for which a precise determination of their half-lives was not possible; there existed some doubts as to the identification of these elements. (From Ref. 25)

masurements of Keepin, Wimmett, and Zeigler [11] and Masters, Thorpe, and Smith [18]. Presently there are no ± 2% standard deviation measurements.

2) Only recently, the dependence of delayed-neutron yields on the energy of the neutrons inducing fission has been found to be consistent with the qualitative theoretical predictions. Earlier measurements by Shpakov [19] and McGarry [20] indicated large increases in yield with increasing neutron energy. This was inconsistent with arguments forwarded by Keepin [21]. Recent measurements by Masters, Thorpe, and Smith [18] and by Krick and Evans [22,12] have shown decreasing yields with increasing neutron energy, a result consistent with qualitative predictions. However, many measurements are still needed, particularly from 5 to 14 MeV neutron energy. This range is of a particular importance for nondestructive assay of fissionable materials with 14 MeV neutrons and is also extremely interesting with regard to fission physics.

3) Even for fissions induced by low energy neutrons, the energy dependence of the yield is not well determined. In particular the apparent lower yields observed for thermal fission relative to 1-4 MeV fission are unexpected, are of importance for reactor design, and require further investigations.

4) Delayed-neutron yield measurements need to be made on elements such as U-234, U-236, Pu-240, Pu-241, and Pu-242 for which little-to-no data are known.

5) Energy-dependent period and abundance data are very scarce, except for thermal, fission spectrum, 3-MeV, and 14-MeV neutrons.

6) Extensive measurements remain to be done on delayed-neutron energy spectra and delayed-neutron decay modes. Gross spectra are needed

for the major fissionable isotopes as a function of the energy of the neutron inducing fission for reactor and safeguards research. These results as well as separated precursor neutron spectra are needed to further the understanding of delayed-neutron physics. The investigation of the delayed-neutron emission process requires measurements of P_n values and precursor decay modes and energies.

II.6 The Present Investigation

For future progress in delayed-neutron physics, measurements of individual precursor delayed-neutron spectra and decay modes are required. Since several groups are presently involved in delayed-neutron spectra measurements, this work is concerned with the measurement of the decay modes of delayed-neutron precursors, about which very little is known. From the mass formulas of Garvey et al [23] it is estimated that it is energetically possible for most delayed-neutron precursors to decay via excited states in the final nucleus. Table 6 tabulates principal precursors, decay energies ($Q_\beta - B_n$) and excited states energies, where known [23]. The investigation of delayed-neutron precursor decay modes ideally would involve a β-n-γ triple coincidence experiment on individual precursors, with the simultaneous measurements of the energies of the three particles. This is not practical. However, a practical experiment may be the measurement of n-γ coincidences on either separated or unseparated precursors. The present experiment is designed to study the feasibility of n-γ coincidence measurements using radiochemically separated bromine delayed-neutron precursors.

Table 6. 1) Values of $(Q_\beta - B_n)$ calculated from tables of Garvey et al. (reference 23)
2) Percent contribution to groups taken from reference 3.

Group	Precursor	percent contribution to group	Emitter	Product	Known product energy levels (MeV)	$(Q_\beta - B_n)$ (MeV)
1	Br-87	100	Kr-87	Kr-86	1.56	1.22
2	I -137	62	Xe-137	Xe-136	1.32 2.64	1.34
	Br-88	35	Kr-88	Kr-87	0.55 1.52 2.17	1.83
3	I -138	21	Xe-138	Xe-137		1.94
	Br-89	54	Kr-89	Kr-88		2.82
	Rb-93	23	Sr-93	Sr-92		1.48
4	Br-90	25	Kr-90	Kr-89		4.12
	Rb-94	17	Sr-94	Sr-93		2.28
	As-85	9	Se-85	Se-74		4.95
	I -139	8	Xe-139	Xe-138		2.78
	As-86	6 (calc)	Se-86	Se-85		5.13
	Cs-142	5	Ba-142	Ba-141		0.32
	Cs-143	5	Ba-143	Ba-142		1.64
	Se-88	5	Br-88	Br-87		1.48

Chapter III.

EXPERIMENTAL SYSTEM AND DESIGN

III.1 Introduction

As discussed in section II.6, the purpose of this present experiment is to develop a neutron-gamma coincidence counting system for the investigation of bromine delayed-neutron precursor decay modes. Since the half-lives of the delayed-neutron precursors are of the order of 0.2-55 seconds, individual precursor decays can be separated in time from other nuclear events if count rates are kept low. If a delayed-neutron emitter decays by neutron emission to an excited state in the final nucleus and if the excited state is not long lived, neutron--gamma coincidences can be observed.

The experiment requires a source of delayed neutron precursors, neutron and gamma-ray detectors and suitable electronics. These items are discussed separately in the following sections.

III.2 Production and Transport System of the Fission Products

The only realistic source of delayed-neutron precursors is fission products. Because of the short delayed-neutron precursor half-lives, the precursor supply has to be constantly activated in order to provide relatively high neutron source activity.

Since the main purpose of this present work is to investigate the bromine delayed-neutron precursors, the sample used as a precursor supply was obtained by dissolving 2 g of natural uranium in 15 ml of a solution composed of 1M HNO_3 and 0.5M $KBrO_3$. A gas flow system was first attempted using a gas pump as shown in Figure 8. The system was tested in the chemistry lab by making a saturated vapor of bromine flow in a closed loop through the

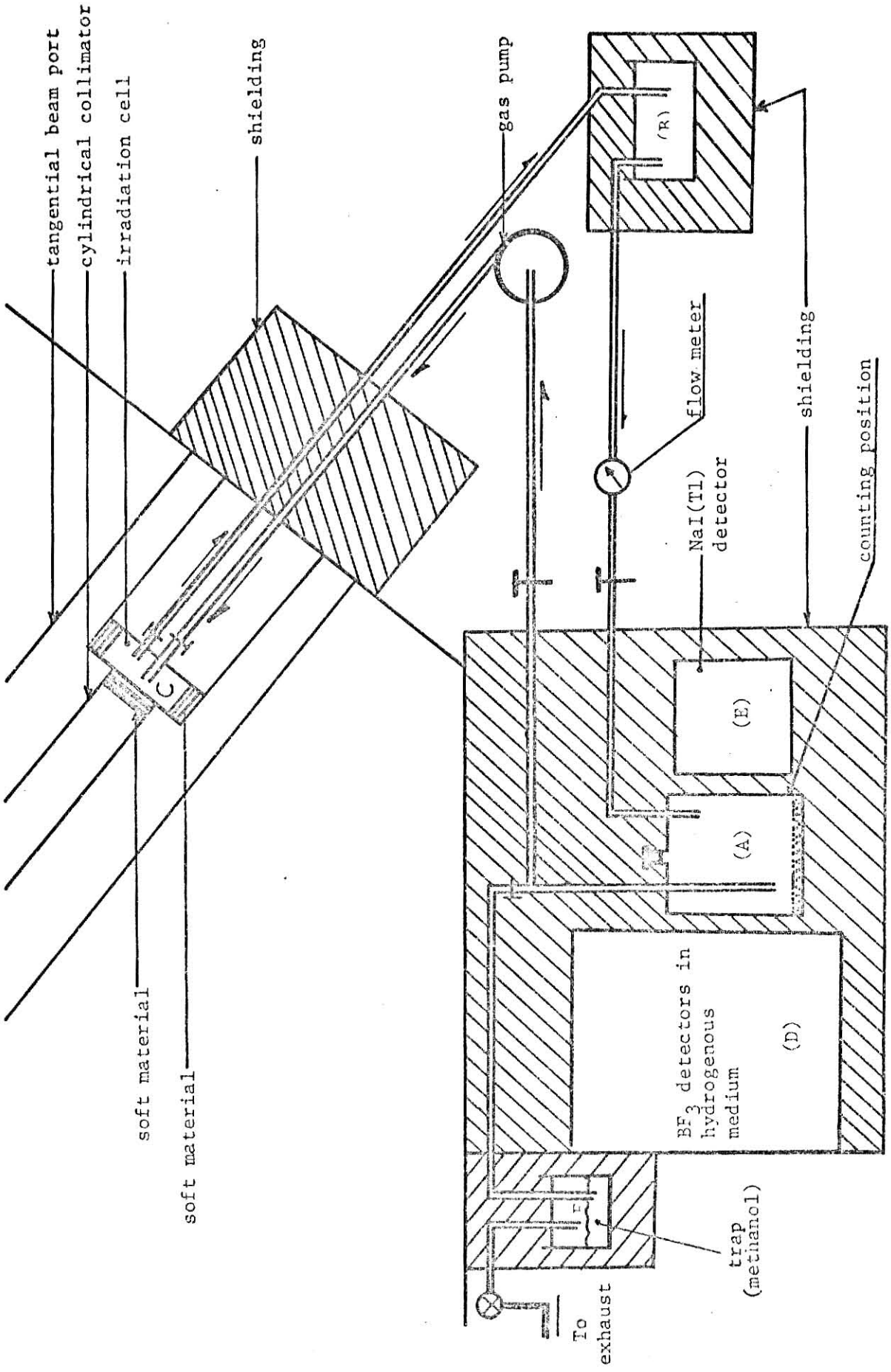

Figure 8. Closed Loop Experimental Setup

tygon tubes, then pumped into the irradiation cell and back to the bromine reservoir where the flow was mixed with more saturated bromine vapor and the cycle continued. It was found that the tygon tubes act as a good absorber for bromine and therefore reduce the efficiency of the transport system to an unacceptable extent, even if glass tubing is used everywhere but in the peristaltic pump. Another gas flow system was then developed based on the system used by Perlow and Stehney [33] in which fission-product bromine was swept out of the sample solution undergoing constant irradiation by slow neutrons and was subsequently absorbed in a small volume of CCl_4 to provide a counting source of continuously-maintained activity. Figure 9 schematically represents the main elements of the gas flow system. This form of the sample possesses good emmanation properties for gaseous fission products when used at low flux levels. The solution was contained in the irradiation cell "C" and was first irradiated by a collimated beam of neutrons through a cylindrical collimator inside the tangental beam port of the TRIGA Mark II nuclear reactor at Kansas State University according to Reactor Experiment #37 (see Appendix A). The flux required for the experiment was determined as discussed in Section (III.4.3). Flux measurements inside the tangential beam port were performed in a separate experiment by the foil activation technique (see Appendix B). The sample location was then determined.

A small empty glass vessel was located downstream from the irradiation cell to catch any active solution that might be carried out of it by foaming. A stream of nitrogen flowing at a rate of about 1000 cc/min was passed through a cell containing saturated bromine vapor and the mixture was bubbled through the sample solution in the irradiation cell. The BrO_3^- ion serves a dual purpose. By virtue of its reaction with Br^- to form Br_2, bromides could

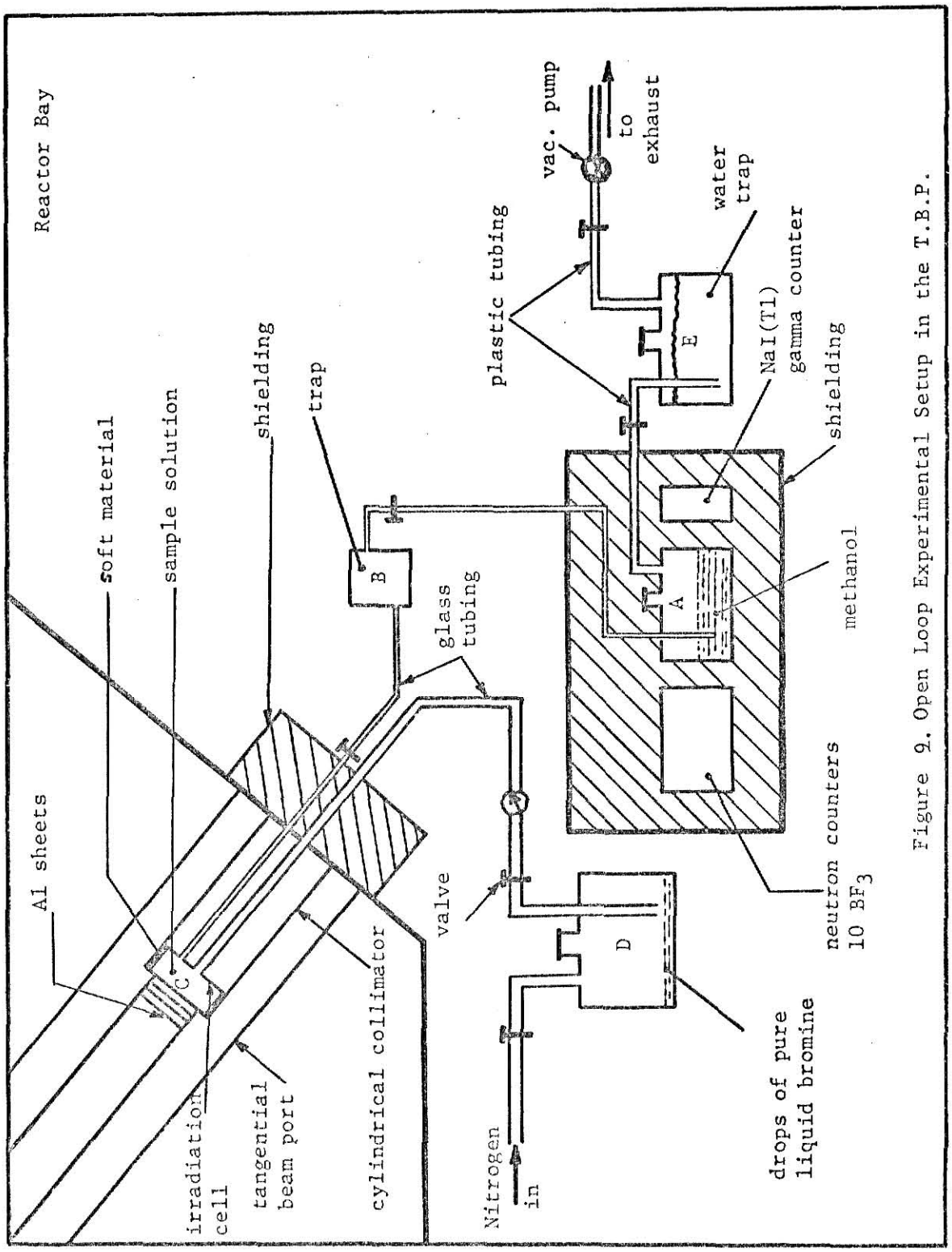

Figure 9. Open Loop Experimental Setup in the T.B.P.

not accumulate in the cell. The second purpose of BrO_3^- was to oxidize iodine formed in its lower valence states to the nonvolatile IO_3^- form, and thereby prevent its escape into the nitrogen stream [33]. The stream after leaving the irradiation cell passed through the trap unit "B" to trap any uranium solution carried out from the cell. The gas flow passed through a methanol trap in the container "A" where bromine remained and from there to trap "E" to the exhaust vent of the reactor bay. Methanol was used in this experiment rather than CCl_4 to trap the bromine. The container "A" represents also the counting position which was located between two detectors, one for gamma counting and the other for neutron counting. This counting system is discussed in more detail in section III.3. The neutron flux at the tangential beam port at low reactor power levels with the one inch collimator in place was found to be inadequate to produce the required fission product activity. Therefore it was decided to use the thermal column as an irradiation facility. Again, the flux was measured at some points in the thermal column and the irradiation position was established to be 3 ft inside the graphite thermal column. Figure 12 shows the final arrangement of the experimental setup using the thermal column of the KSU TRIGA Mark II nuclear reactor.

III.3 Detection System

III.3.1 Neutron-gamma coincidence detector

As shown in Chapter IV, the fission product activity must be kept extremely low to produce a useful true-to-random coincidence ratio. This in turn requires extremely high detection efficiency for the neutron and gamma detectors to maintain a reasonable count rate. The neutron-gamma coincidence consists mainly of the neutron detector, the gamma detector, and associated electronics.

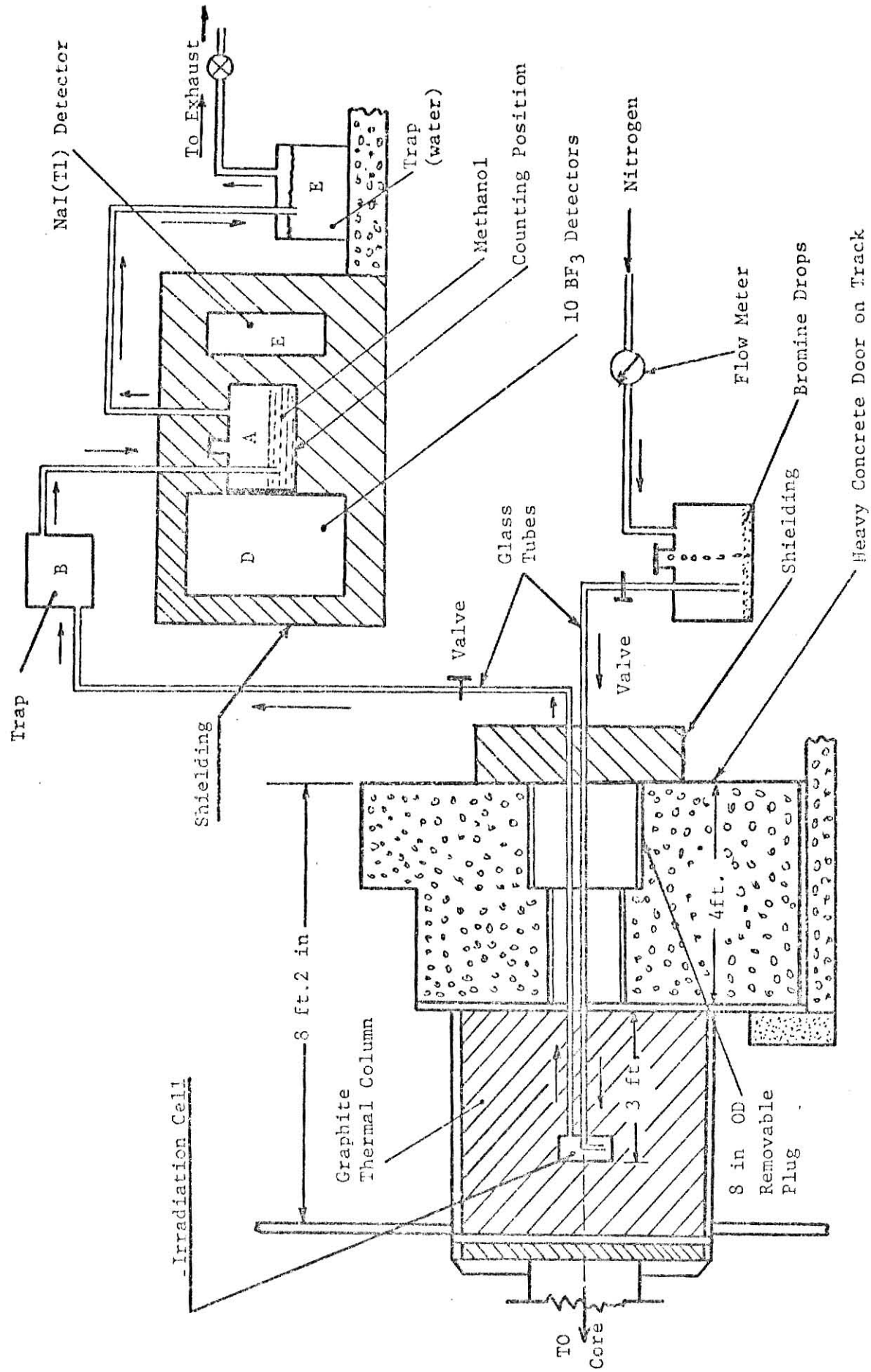

Figure 10. Experimental setup using the thermal column

III.3.1.1 Delayed-neutron detection system

The neutron detection system was built with 10 BF_3 proportional counters [34] connected in parallel and arranged in an array inside a large paraffin block (Figure 11) serving as a thermalizing medium for the neutrons. As was mentioned before, high detection efficiencies are required for this kind of experiment; therefore ^{3}He-filled proportional counters would serve the purpose better due to their high detection efficiency, low background and excellent gamma insensitivity. However, due to the lack of availability of this type of counters, BF_3 counters were used. Since it is not desirable for this experiment to restrict the energy range of the detected neutrons, the neutron detector must have a reasonably small efficiency variation from ∿ 0 to 2 MeV neutron energy. This requirement is met satisfactorily with a modified long counter [28].

A brief review of BF_3-filled detector operation is presented below. These proportional counters employ the $^{10}B(n,\alpha)$ reaction as follows:

$$^1_0n + {}^{10}_5B \rightarrow {}^7_3Li + {}^4_2He + 2.78 \text{ MeV} \qquad \text{(a)}$$

$$\rightarrow {}^7_3Li^* + {}^4_2He + 2.31 \text{ MeV} \qquad \text{(b)}$$

$$^7_3Li^* \rightarrow {}^7_3Li + \gamma + 0.48 \text{ MeV} \qquad \text{(c)}$$

The probability of reaching the ground state (reaction (a) above) is about 6% for thermal neutrons. The most commonly used detectors (and the ones used for this system) are BF_3 tubes enriched to 96% in ^{10}B. The reaction cross section for thermal neutrons is 3840 barns and has a 1/v dependence in the thermal energy range. BF_3 counters are most sensitive to thermal neutrons; the gas in the counters serves both as the neutron sensitive

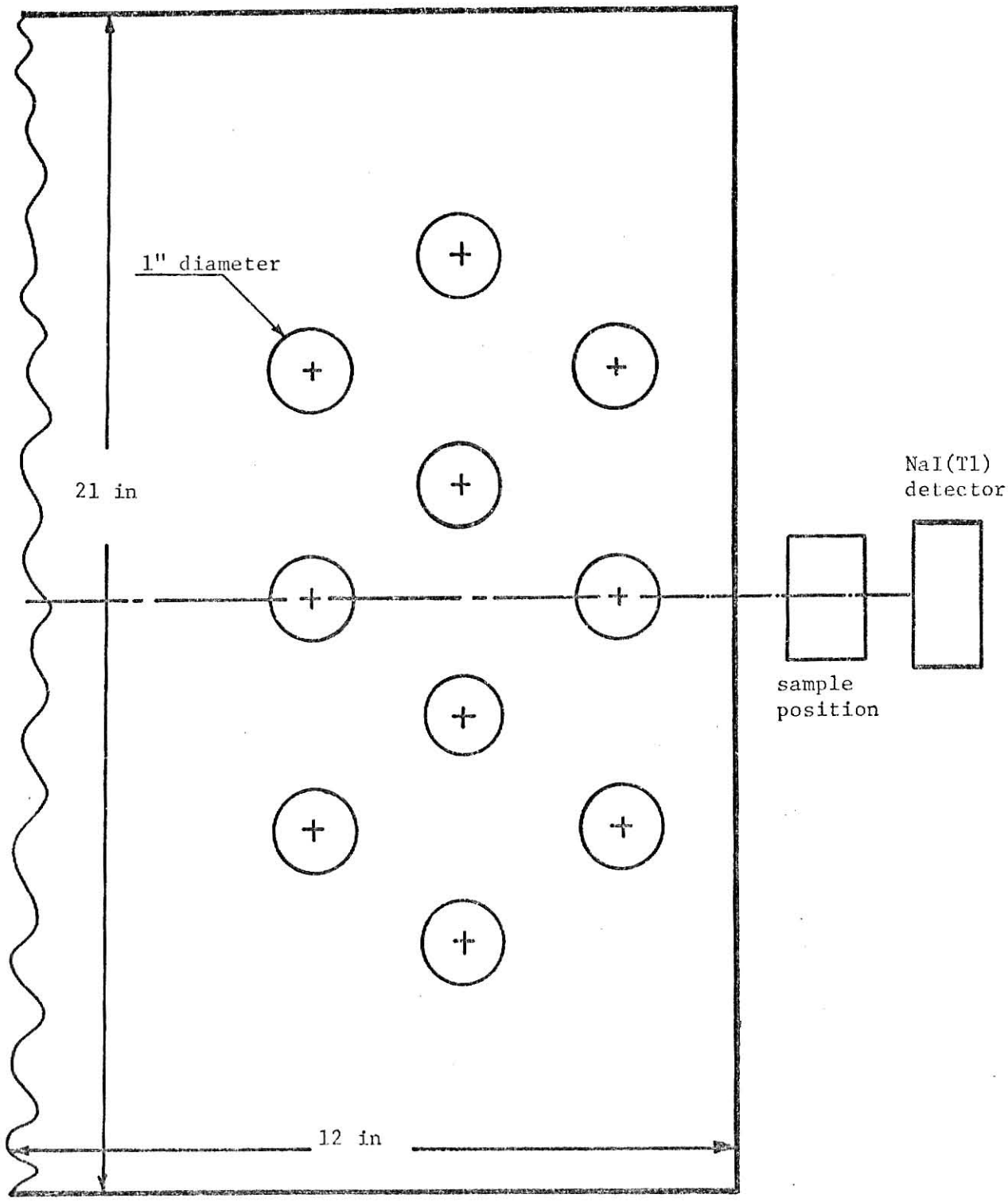

Figure 11. Arrangement of the BF_3 Tubes in the Paraffin Box

material and as the ionizing gas. An increase in sensitivity of BF_3 tubes is achieved by increasing the pressure and/or the counter size. This, however, can result in higher operating voltages together with poorer pulse-height resolution. Reaction (c) above is a potential problem in this experiment. This reaction occurs with 94% probability and can generate a true, but undesired, neutron-gamma coincidence. ^3He detectors are better in this sense since they do not produce secondary gammas. The absolute efficiency of a neutron detector is defined as the fraction of neutrons produced which result in counts. The efficiency of a moderated BF_3 detector depends on the size and shape of the detector, the location of the neutron source and the pressure of the filling gas in the counting tubes.

Two types of Reuter-Stokes [34] BF_3 counters were used in this experiment, one of which has a sensitive length of 8.125 inches, 1 inch diameter and a filling gas pressure of 76 cm Hg while the other has a 12.5 inch sensitive length, is 1 inch in diameter and has a pressure of 40 cm Hg. Six tubes of the first type and four of the second type were used. The ten tubes were tested individually. The plateau curves of each type were obtained using a californium-252 source (source strength: 1.6×10^6 neutrons/sec) and the operating voltages were established in the plateau regions as shown in Figures 12 and 13. The pulse height distributions for both types of BF_3 tubes were also obtained, again using the moderated neutrons from the Cf-252 source. Figures 14-a and 14-b represent typical pulse height distributions from the 76 cm Hg and the 40 cm Hg tubes, respectively, using a Technical Measurements Corporation Model 402 pulse height analyzer. The absolute efficiency for the whole setup of BF_3 tubes arranged as shown in Figure 11 was determined using the ^{252}Cf source located at a distance of 3 inches outward from the center of the paraffin-box surface nearest the BF_3 counters. The absolute efficiency was found to be $4.0 \pm 0.13\%$ for ^{252}Cf-spectrum neutrons.

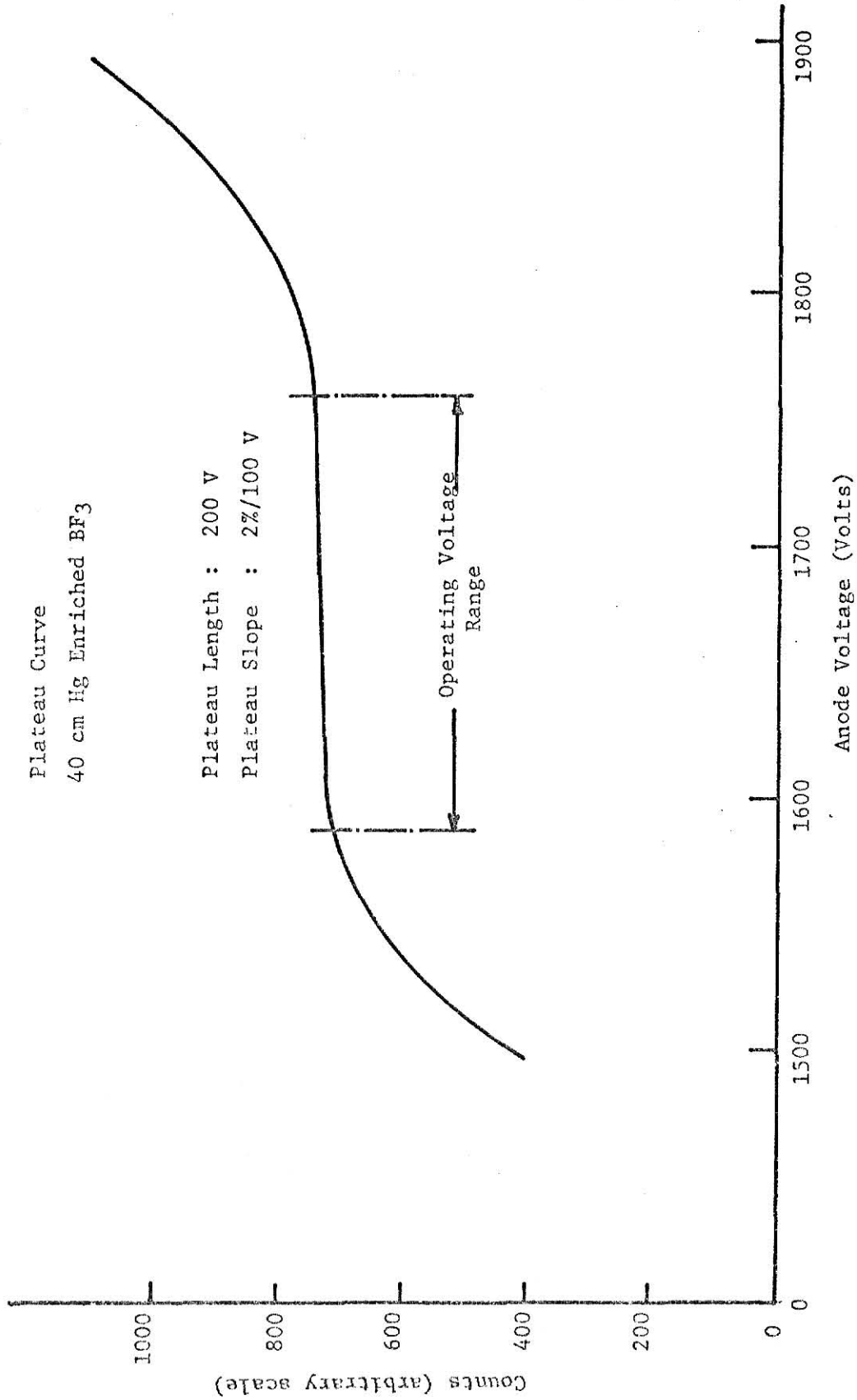

Figure 12

Plateau Curve

40 cm Hg Enriched BF_3

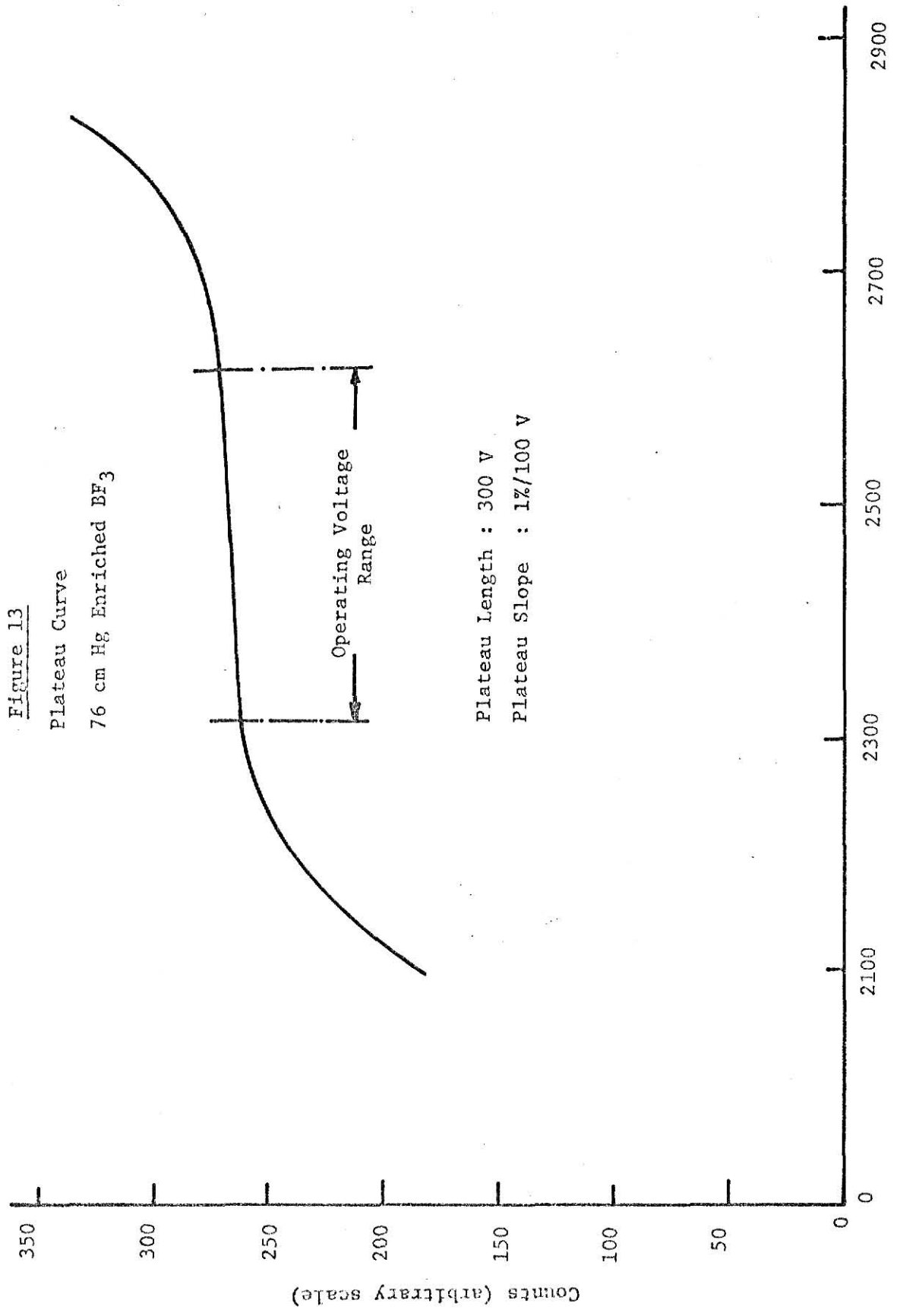

Figure 13

Plateau Curve

76 cm Hg Enriched BF_3

Figure 14

Pulse Height Distributions

(a)

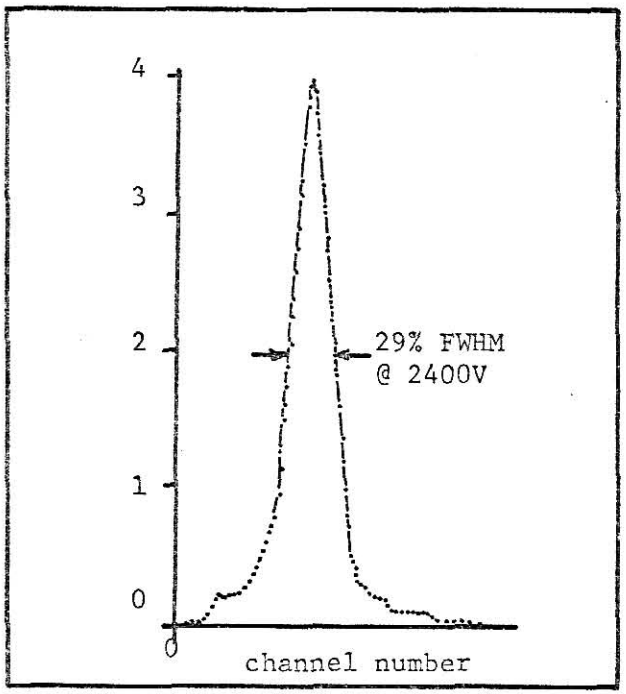

Pulse Height Distribution from the
76 cm Hg Enriched BF_3 Tube

(b)

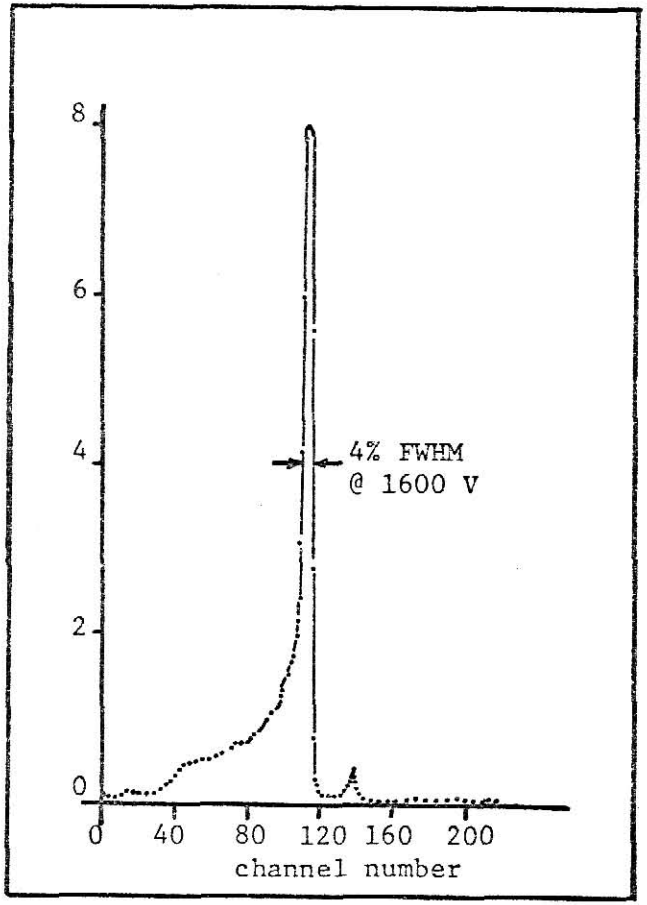

Pulse Height Distribution from the
40 cm Hg Enriched BF_3 Tube

III.3.1.2 Gamma detection system

For the gamma detection system, a large NaI(Tl) detector was used for the purpose of this experiment. A 3 x 3 inch NaI(Tl) crystal with a 3 inch photomultiplier tube was chosen because it provides good resolution for a scintillation detector and has high efficiency. It was also the largest NaI(Tl) detector available.

The detector was tested using a standard ^{137}Cs source. Figure 15 shows the gamma-ray spectrum obtained using a Technical Measurements Corporation Model 402 pulse height analyzer. The intrinsic efficiency as a function of the gamma energy for various distances between source and detector is shown in Figure 16 [40]. The absolute efficiency of the 3 x 3 inch NaI(Tl) detector was measured using a ^{137}Cs gamma-ray source located at the same position as the activated sample. The measured absolute efficiency was 1.0 ± 0.2%. This value was consistent with the intrinsic efficiency value shown in Figure 16 within the limitations set up by the geometry configuration used for this measurement.

Since the NaI(Tl) crystal may have to be removed approximately 3 to 6 cm from the precursor source to reduce inelastic scattering contributions to the coincidences count (see section III.5.1), the absolute gamma detection efficiency may be as low as 1% for the gamma energies of interest [35]. A diagram of the coincidence counter is shown in Figure 17. The amount of separation of NaI(Tl) crystal from the precursor source, the choice of intervening material and the type and amount of shieldings for the NaI(Tl) detector must be determined experimentally for each attempted measurement. Figure 18 shows the details of the shielding unit built for the coincidence counter.

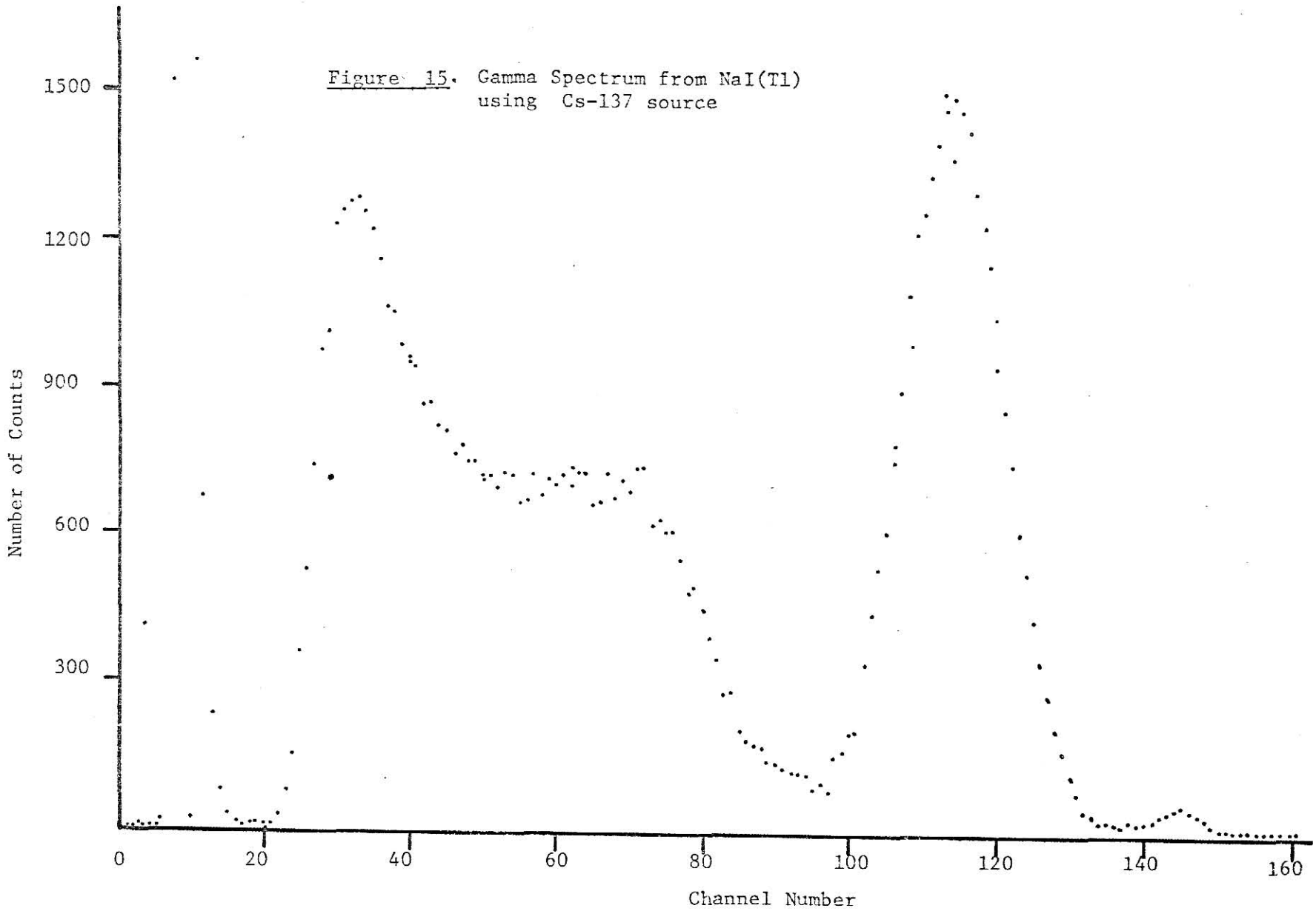

Figure 15. Gamma Spectrum from NaI(Tl) using Cs-137 source

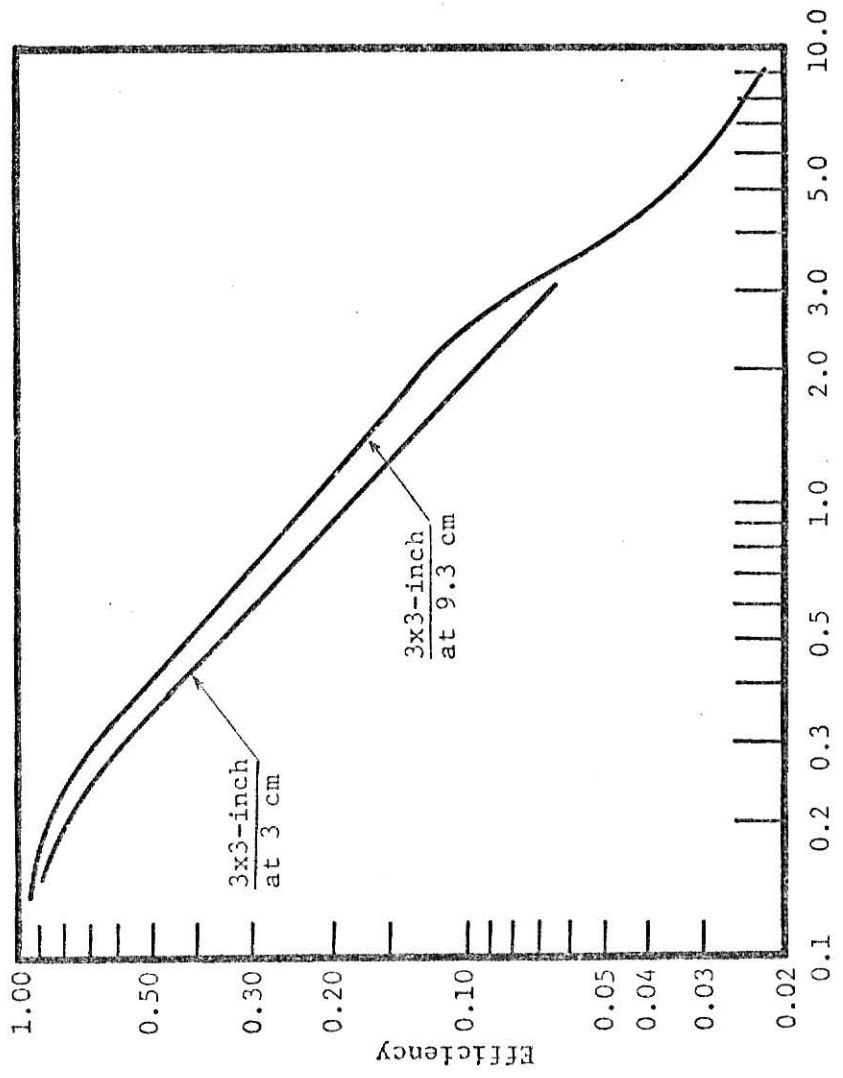

Figure 16. Intrinsic peak efficiency versus gamma energy for NaI(Tl) : 3x3-inch crystal. (From Ref.40)

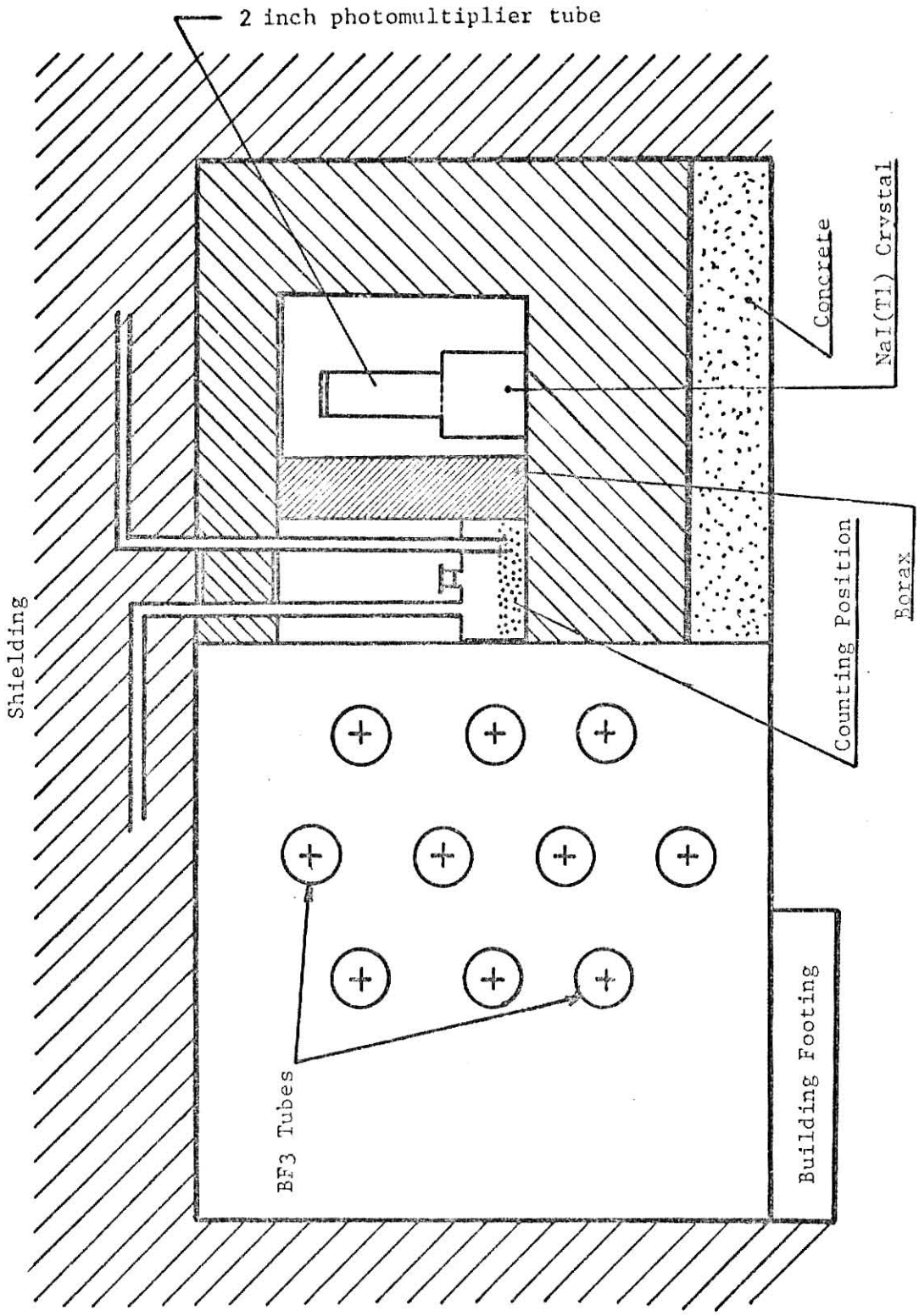

Figure 17. Neutron-Gamma Coincidence Counter

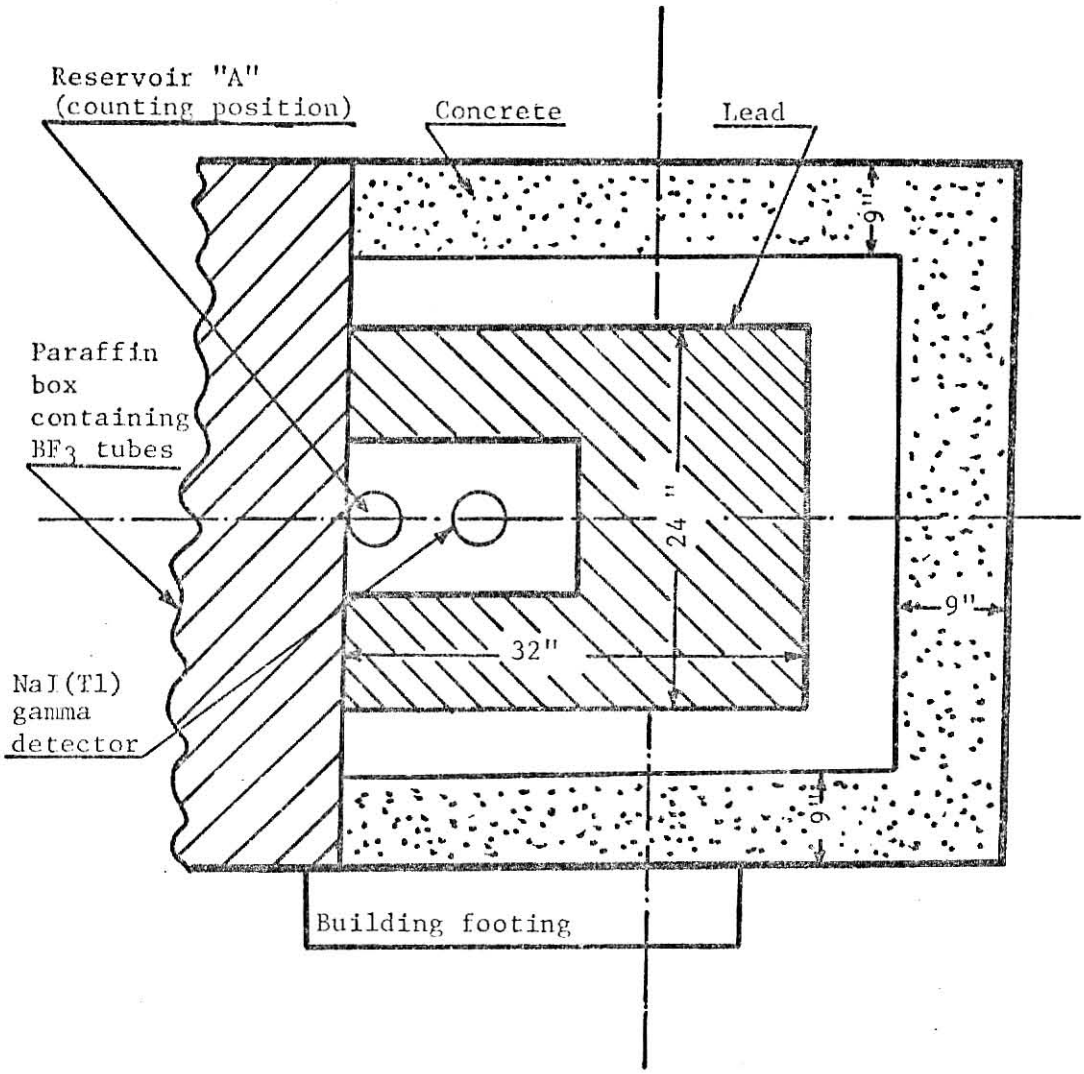

Figure 18

Experimental Shielding unit built for NaI(Tl) Detector, BF_3 Detectors and the Reservoir "A"

III.3.2 Electronics

A block diagram of the electronics used for the coincidence experiment is shown in Figure 19. The 10 BF_3 counters were connected in parallel and were divided into three groups (3 rows), one of which is the closest to the precursor source, another is the furthest, and a third one in between, as shown in Figure 11. The distribution box shown in Figure 20 was constructed so that the response of different counter groups could be easily studied. The electronic circuit of that box was built as recommended by the manufacturer of the BF_3 counters [34].

The block diagram shown in Figure 19 can be divided into two subcircuits- the neutron and the gamma circuits. An input signal in the former one, coming from the neutron detection system, goes through a preamplifier, an amplifier and a single channel analyzer (SCA), the output of which is the gate signal for a linear gate. In the other circuit (gamma circuit), signals coming from the NaI(Tl) detector go through a preamplifier built in the NaI(Tl) unit, an amplifier of the same type as that of the neutron circuit and then through a delay network of approximately 20 μsec delay time, and then into two linear gates. The two linear gates work as coincidence circuits for different purposes, as will be discussed in the following sections. They receive signals from both neutron and gamma circuits.

The function of the linear gate when operated in coincidence mode is to generate an internal gate period when triggered by an appropriate gate signal and to regenerate a linear rectangular pulse if a linear pulse comes in during the gate period. The output pulse amplitude is equal to that of the input linear pulse only when the pulse peak is covered by the internal gate. Signals from the linear gates are reshaped and attenuated to meet the requirements of the input of the pulse height analyzer (PHA). The PHA is of the 400 channel type; in Figure 19, PHA#1 corresponds to the first 200 channels and PHA#2 corresponds to the second 200 channels. Appendix C shows the specifications

Figure 19. Electronic Block Diagram for the Neutron-Gamma Coincidence Counting System

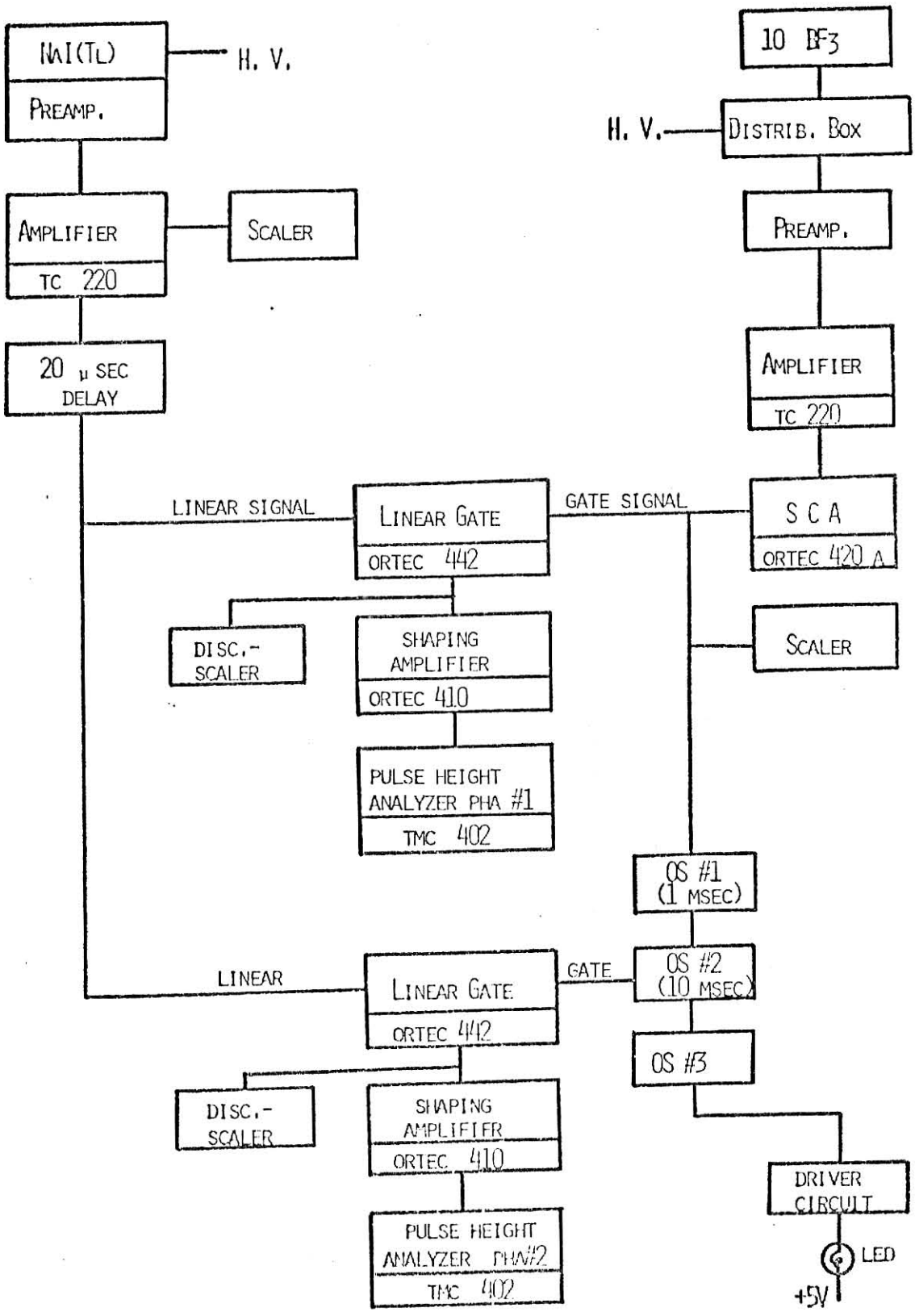

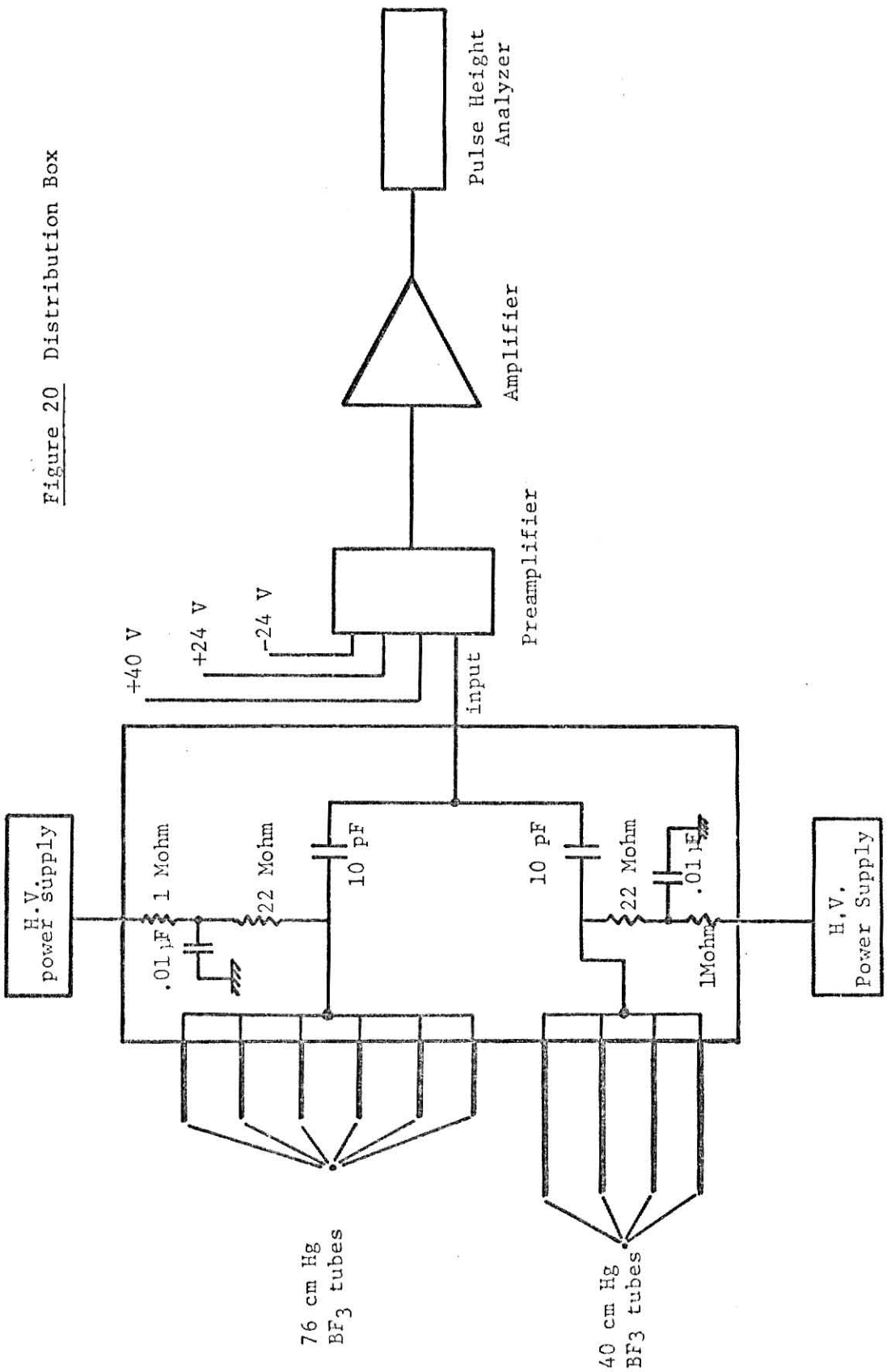

Figure 20 Distribution Box

and general features of the components and equipment shown in the block diagram, Figure 19. A timing diagram is shown in Figure 22.

As discussed below, one can consider the electronic system to be composed of two subsystems - the true and the random coincidence systems.

III.3.2.1 True concidence system

A delayed-neutron decay may be followed by an emission of a gamma photon. The delayed neutrons with which we are dealing are thermalized before reaching the BF_3 tubes. The time that the neutrons might take to reach the BF_3 tubes after being thermalized was estimated to be of the order of 20 μsec (36) whereas the response of a scintillation detector is in the range of 250 nsec. Hence, a gamma signal has to be delayed by ∿ 20 μsec in order to overlap its corresponding neutron gate signal in the linear gate. The resulting coincidences are true coincidences and are detected by the electronics in the upper portion of the block diagram in Figure 19. The energy spectrum of the gamma rays coincident with neutrons as described is collected in PHA#1.

III.3.2.2 Random coincidence system

Actually, in the circuit discussed in the above section, a number of random coincidences are also counted. These are due to neutrons and gamma rays produced within ∿ 20 μsec of one another, but which are not both related to a single decay process. To measure these random coincidences, the neutron gate signals are simply delayed by an arbitrarily long time compared to 20 μsec to make the chance of a true coincidence negligible, whereas the random gammas still meet neutron gate signals with the same probability as before. The delay of the neutron signals is obtained through a time-delay gate unit indicated in the block diagram of Figure 19 by OS#1 and OS#2.

III.3.2.3 Time-delay gate unit

A time-delay gate unit was built to delay the neutron signal by 1.0 msec and then to generate a 10 μsec pulse to trigger the linear gate used for analyzing random coincidences. A block diagram of the circuit is shown in Figure 21. The neutron signal triggers a one-shot multivibrator (OS#1) which generates a 1.0 msec output pulse. When OS#1 resets, another one-shot multivibrator (OS#2) is triggered and generates a 10 μsec pulse for triggering the linear gate. The one-shot multivibrators were designed from standard transistor-transistor logic multivibrator circuits (SN 74121)[37,38] and were constructed in a standard double-width nuclear instrument module (NIM)[37]. Two signals were made available for external use via the front panel of the NIM module. The first was the output of the 1.0 msec one-shot, so the delay time could be readily set and checked with the aid of an oscilliscope; the second was a light pulse generated by a light emitting diode (LED). The output of OS#2 was used to trigger a third one-shot multivibrator (OS#3) which, via a driver circuit, turned on the LED for 0.25 sec. This LED was included to provide a continuous and convenient indication of the neutron count rate. Figure 21 also shows the timing diagram of the waveforms produced from each one-shot. Figure 22 shows the timing diagram of the waveforms at each step of the electronic block diagram (Figure 19).

III.4 Count Rates

III.4.1 General

The following definitions are made for fission products formed in the irradiation position and transported to the counting position in the neutron-gamma coincidence counter.

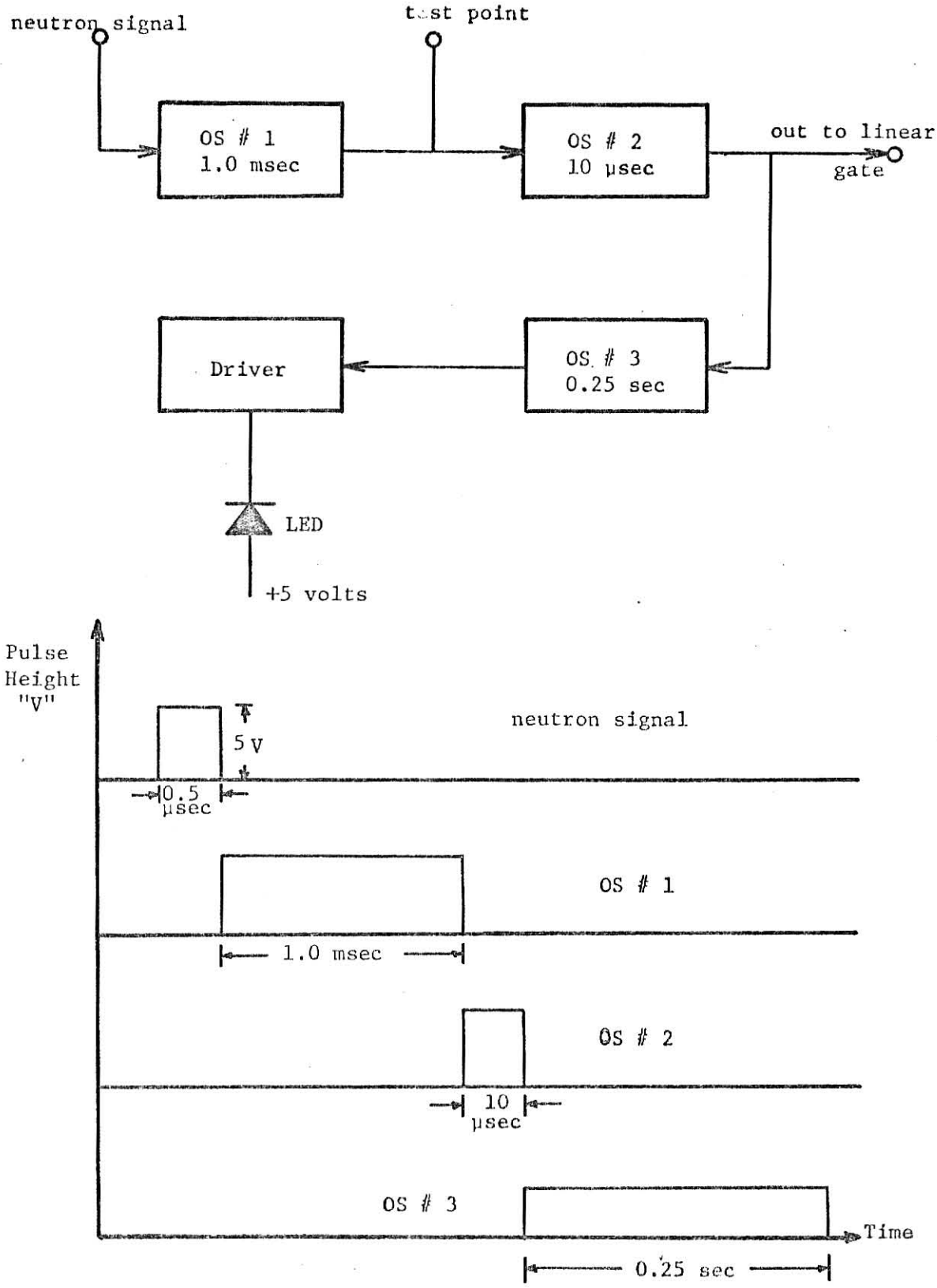

Figure 21. Block and Timing Diagram of the Delay-Time Gate Unit

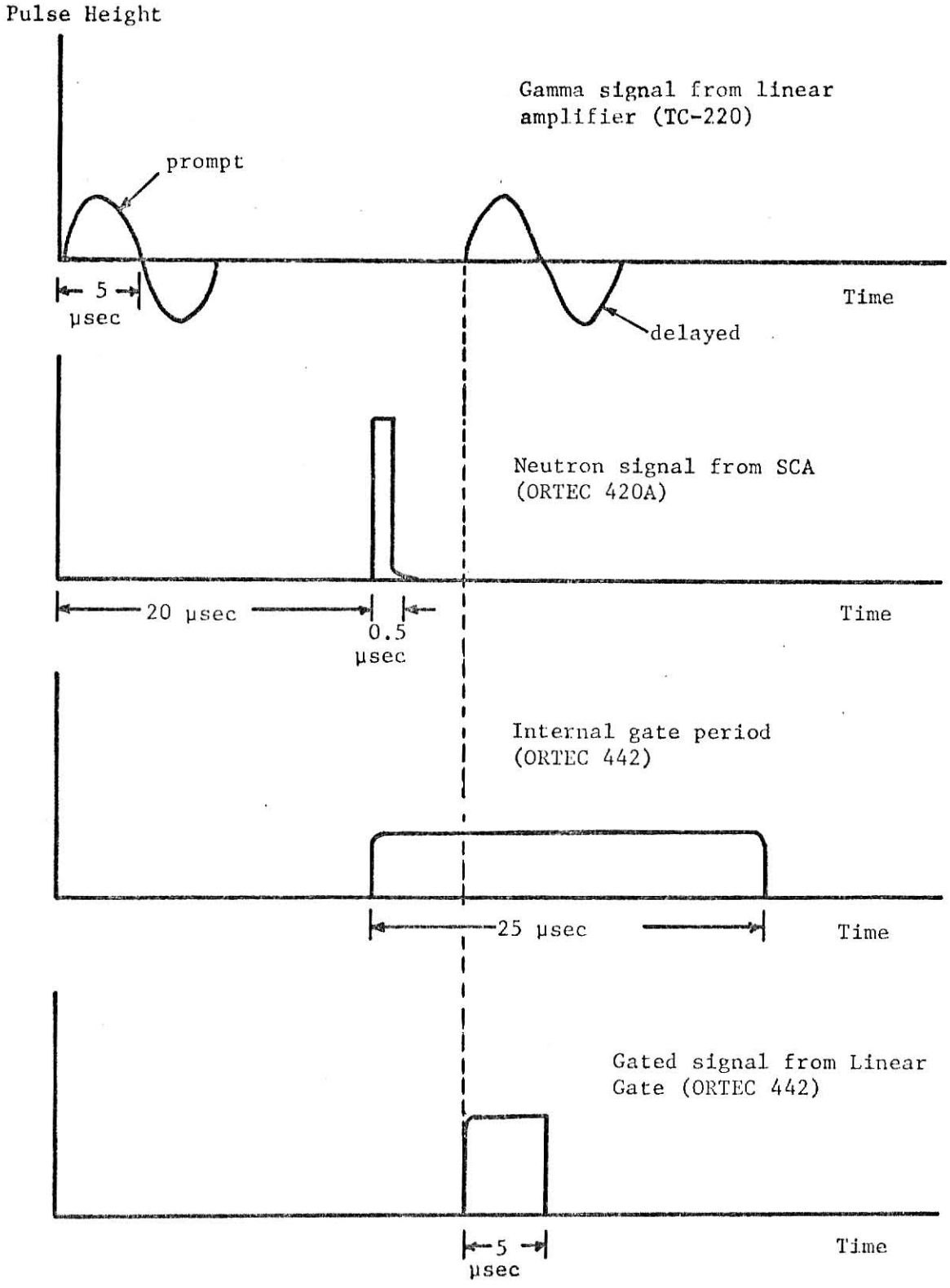

Figure 22, Waveforms and Timing Diagram of the Signals at each step in the Electronic Block Diagram

A_γ = gamma rays emitted per second

A_n = delayed-neutron precursor activity resulting in neutron emission

$A_{n\gamma}$ = delayed neutron precursor activity resulting in coincident n-γ emission.

If the absolute neutron and gamma detector efficiency are denoted by ε_n and ε_γ respectively and if background counts are neglected, the neutron and gamma singles count rates (denoted by N_n and N_γ, respectively) will be

$$N_n = \varepsilon_n A_n \qquad \text{and} \qquad N_\gamma = \varepsilon_\gamma A_\gamma \quad .$$

The true and random coincident count rates (C_T and C_R, respectively) will approximately be

$$C_T = \varepsilon_n \varepsilon_\gamma A_{n\gamma}$$

$$C_R = \tau N_n N_\gamma = \tau \varepsilon_n \varepsilon_\gamma A_n A_\gamma \quad .$$

where τ is the coincidence resolving time, which is determined primarily by the neutron channel. The important true-to-random coincidence ratio R is then

$$R = \frac{C_T}{C_R} = \frac{A_{n\gamma}}{\tau A_n A_\gamma} \quad . \qquad \text{(III.1)}$$

If it is assumed for the purpose of estimating count rates that R = 1 is an acceptable true-to-random ratio, that approximately 10% of the decays to the final nucleus occur via excited states (i.e., $A_n \simeq 10\ A_{n\gamma}$), and that $\tau = 25\ \mu\text{sec}$, then the gamma rays emitted per second at the detector is estimated to be

$$A_\gamma = \frac{A_{n\gamma}}{R\ \tau\ A_n} \qquad \text{(from Eqn. III.I)}$$

$$= \frac{A_{n\gamma}}{(1)(25\times10^{-6}\text{sec})(10A_{n\gamma})} = 4000\ \text{sec}^{-1}.$$

III.4.2 Fission Rate Calculations

The saturated bromine activity A_{sat} can be related to the fission rate FR by the following equation

$$A_{sat} = (FR)\sum_i Y_i \qquad \text{(III.2)}$$

where Y_i is the cummulative fission yield of the bromine isotope i.
The number of delayed gammas produced per second by the bromine isotope i $A_\gamma^{(Br)}$ is then

$$A_\gamma^{(Br)} = (FR)\sum_i Y_i N_i \,, \qquad \text{(III.3)}$$

where N_i = average number of gammas per decay of isotope i.
The saturated delayed-neutron activity (neutrons/sec) is

$$A_n^{(Br)} = (FR)\sum_i Y_i P_{n_i} \,, \qquad \text{(III.4)}$$

where P_{n_i} is the probability that a delayed-neutron precursor will decay by neutron emission [3]. If p_i is the fraction of the i-th precursor nuclei which decay by both neutron and gamma emission, then the coincident n-γ rate from bromine fission products $A_{n\gamma}^{(Br)}$ is

$$A_{n\gamma}^{(Br)} = (FR)\sum_i Y_i P_{n_i} p_i \qquad \text{(III.5)}$$

It is conservatively assumed for the purpose of calculation that $p_i = 0.1$ for all i. It is also assumed that three gamma rays are emitted per decay, i.e., that $N_i = 3$ for all i. The values for P_{n_i} and Y_i used in the above relations are

tabulated in Table 7 [39,3]. The bromine isotopes with A>90 are not included, since their short half-lives allow decay in transit to the detectors.

Table 7. Cummulative yields and P_n values for the bromine isotopes [39,3]

Bromine isotope i	Cummulative Yield Y_i(%)	P_{n_i} (%)
83	0.54	0
84	1.00	0
85	1.33	0
86	1.94	0
87	2.28	2.5
88	2.78	4.0
89	2.42	7.0
90	1.75	12.0

From the data of Table 10 and from the above analysis, the coincidence count rates were estimated on the assumption that the activity at the detector is due to bromine isotopes only. The number of gamma rays per second emitted by the sample was therefore estimated to be

$$A_{\gamma}^{(Br)} = (FR) \sum_i Y_i N_i \cong 0.37(FR), \qquad \text{(III.6)}$$

the neutron-gamma coincident decay rate was estimated to be

$$A_{n\gamma}^{(Br)} = (FR) \sum_i Y_i P_{n_i} p_i = 0.00034(FR),$$

and finally the neutron emission rate was estimated to be

$$A_{n}^{(Br)} = (FR) \sum_i Y_i P_{n_i} = 0.0034(FR).$$

If (as discussed in the previous section) it is assumed that

$$A_{\gamma}^{(Br)} = 4000 \text{ sec}^{-1} ,$$

then from equation III.6

$$(FR) = \frac{4000}{0.37} = 10800 \text{ sec}^{-1}$$

and so

$$A_{n\gamma}^{(Br)} = 3.7 \text{ sec}^{-1}$$

and

$$A_n = 37 \text{ sec}^{-1} .$$

If the neutron and gamma-ray absolute detection efficiencies are $\varepsilon_n = 0.2$ and $\varepsilon_\gamma = 0.1$, respectively, then the true coincidence count rate is

$$C_T = \varepsilon_\gamma \varepsilon_n A_{n\gamma}$$

$$= (0.1)(0.2)(3.7) = 0.074 \text{ sec}^{-1}$$

or about 6000 counts per day. The actual true coincidence count rate for a true-to-random ratio of one will be considerably lower than this, however, since

(1) the decay products of the bromine fission products are also radioactive,

(2) the bromine in the gas-flow system will be activated while passing through the irradiation cell, and

(3) some noble-gas fission products will also be transported to the counting system.

III.4.3 Flux Measurements

The thermal neutron flux required to achieve the desired fission rate in the irradiation position was determined in a separate experiment. The

activation method (see Appendix B) was used to determine the thermal flux in the tangential beam port and later in the thermal column in KSU TRIGA Mk II reactor (see Section IV.2). The flux was determined as a function of distance along the thermal column and the tangential beam port at a power level of 10kW. The irradiation position was then determined accordingly, considering that it was desired to have a total fission rate up to about 10^5 fissions/sec produced in the irradiation cell which contains 2 g of natural uranium dissolved in a 15 ml sample of a solution consisting of 1 M of HNO_3 and 0.5 M of $KBrO_3$. The fission rate FR is related to the thermal flux producing fission by the equation

$$FR \simeq N^{235} \sigma_f \phi_{th} = \frac{N_{avog.}\, m}{A} \cdot \sigma_f \cdot \phi_{th}. \qquad \text{(III.7)}$$

where N^{235} = number of nuclei of U^{235} in the sample

$N_{avog.}$ = Avogardro's number

m = mass of U^{235} in the sample

A = atomic weight of U^{235}

σ_f = fission microscopic cross section.

Considering

σ_f = 580 barns

m = 0.0144 grams

A = 235 g/gmw

$FR \simeq 4 \times 10^5$ fission/sec,

and considering Equation III.6, the thermal flux desired for the experiment was found to be of the order of 10^7 neutrons/cm^2-sec. In order to achieve this flux, the irradiation cell containing the sample solution was located 3 feet inside the graphite of the thermal column as shown in Figure 12, with the reactor operating at a power level of 5 kW.

III.5 Potential Problems

III.5.1 Inelastic Scattering

A true but undesirable coincidence can be produced when a delayed neutron scatters inelastically. If the scattered neutron and deexcitation gamma ray are both detected, an unwanted coincidence occurs. In principle, the background produced by this process is subtractable if the detector materials are well known; in practice, however, this could be difficult when NaI(Tl) is used for gamma-ray detection. It is preferable when using NaI(Tl) detector to sacrifice some gamma detection efficiency for a sharp reduction in gammas from inelastic scattering on ^{127}I and ^{23}Na by removing the NaI(Tl) about 5 cm from the sample location, with polyethylene and borax filling the gap. Since most delayed neutrons have energies below 1.5 MeV, materials with high first and second excited state energy levels are desirable. Isotopes most likely to be exposed to fast neutrons together with their lowest two excited-state energies are listed below [44].

Element	Energies (MeV)	
^{1}H	-	-
^{2}H	-	-
^{3}He	-	-
^{10}B	0.717	1.74
^{11}B	2.14	4.46
^{12}C	4.43	7.66
^{13}C	3.09	3.68
^{27}Al	0.842	1.013
^{54}Fe	1.41	2.53
^{56}Fe	0.847	2.09

III.5.2 Neutron Detector Gamma Rays

It is undesirable if the detection of a delayed neutron produces a gamma ray, since this will generate further true but unwanted coincidences. The capture of a neutron by ^{10}B produces a gamma ray via the 0.48 MeV level in ^{7}Li (see Section IV.3.1.1):

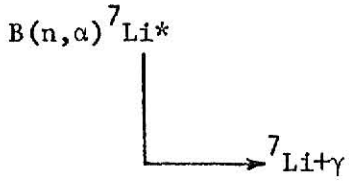

Since the first excited state in ^{7}Li is produced with a 94% probability [40], the use of BF_3 detectors was not a good choice but were used due to the reasons mentioned in Section III.3.1.1. ^{3}He detectors have higher efficiency and do not produce secondary gammas.

III.5.3 Compton Scattering

Because of the large volume of the neutron detector and because of the other shielding material around the NaI(Tl) crystal, a substantial Compton scattering contribution was expected to interfere with the gamma-ray spectral measurements. To investigate how significant this scattering could be, ^{137}Cs and ^{60}Co sources were placed about 6 cm from the 3 x 3" NaI(Tl) detector in air and the gamma spectrum was recorded. The measurement was repeated with the two sources at the same distance from the NaI(Tl) crystal, but with the entire system buried in hydrogeneous materials. The results are shown in Figure 23, which indicates that for gamma energies above 100 keV, the Compton scattering problem is not important.

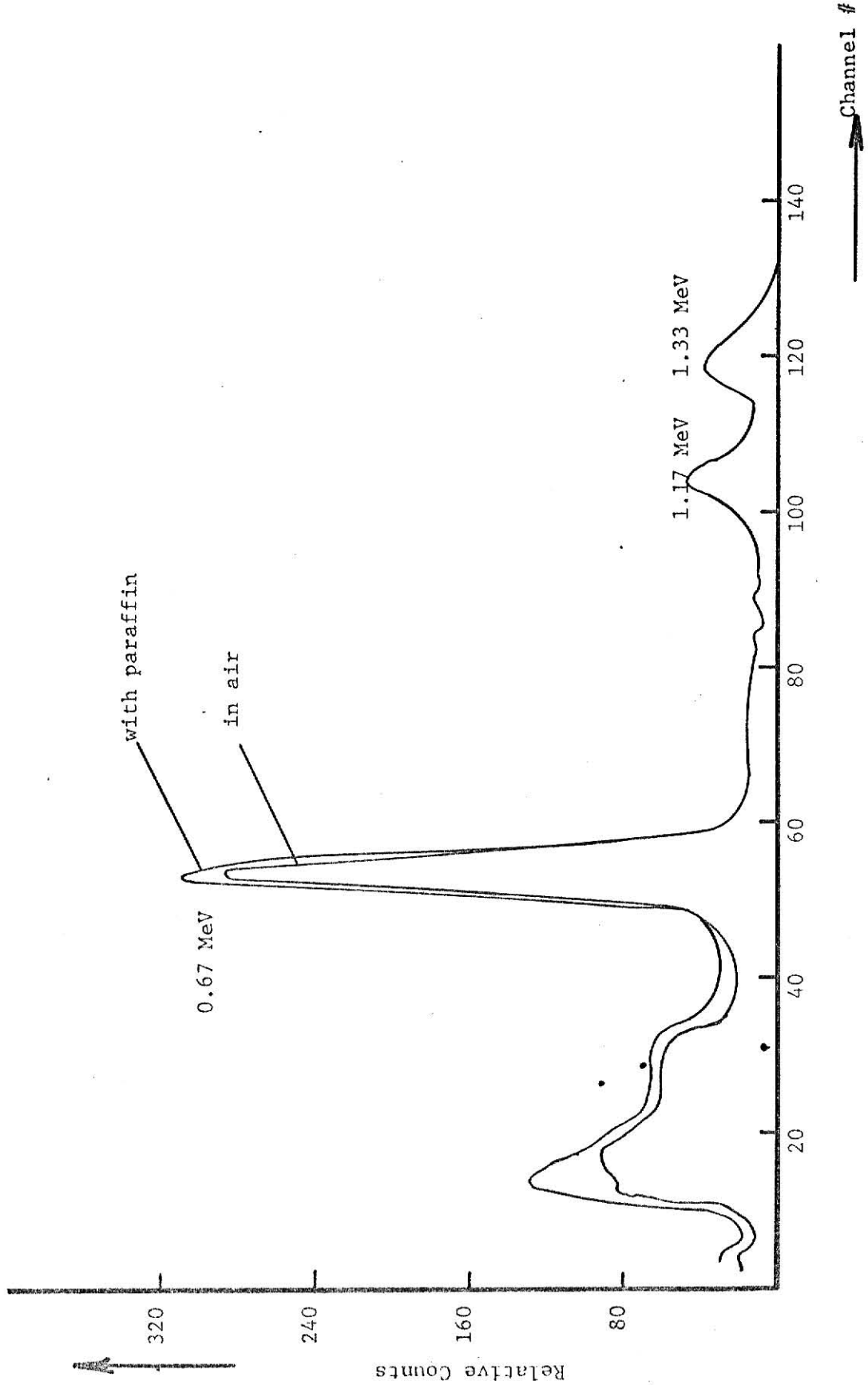

Figure 23. Pulse height distributions obtained with combined Cs-137 and Co-60 sources approximately 3 cm from a 3x3" NaI(Tl) detector. Lower curve is for a medium of air ; upper curve for a medium of paraffin

Chapter IV.

MEASUREMENTS AND RESULTS

The fission-product spectra were first obtained by the use of a 25 cm^3 Ge(Li) spectrometer. The Ge(Li) detector was chosen for this purpose because of its higher resolution compared with that of the NaI(Tl) detector. An electronic block diagram for the Ge(Li) spectrometer is shown in Figure 24. The high resolution of the Ge(Li) detector is necessary for isotope identification. The Ge(Li) detector was first calibrated using ^{60}Co, ^{139}Ce, and ^{137}Cs source sources. Figure 25 shows the calibration curve obtained. The bromine gamma-ray spectrum was then obtained for three different cases, as follows:

A. Continuous sample irradiation and counting for 30 minutes with the reactor at 5 kW and the gas-flow system on,

B. Gas-flow system off and counting the activated sample for 10 minutes with no cooling period,

C. Gas-flow system off and counting the activated samples for 10 minutes after a 45 minute cooling period.

Figures 26, 27, and 28 show, respectively, the spectra obtained from the above three cases. Using the calibration curve (Figure 24), the associated energies of the peaks observed in each one of the three spectra were determined using the program written by Tracor Northern for the NOVA 1220 computer [42]. Table 8 shows the computed energies for the observed peaks and the possible contributors to the peaks together with their half-lives and intensities [41]. Column 5 in Table 8 shows the calculated relative intensities of the possible contributors taking into account the relative efficiency of the Ge(Li) detector (Figure 29) for each energy at the counting position. The peak energies were next assigned to a unique possible contributor taking into consideration half-

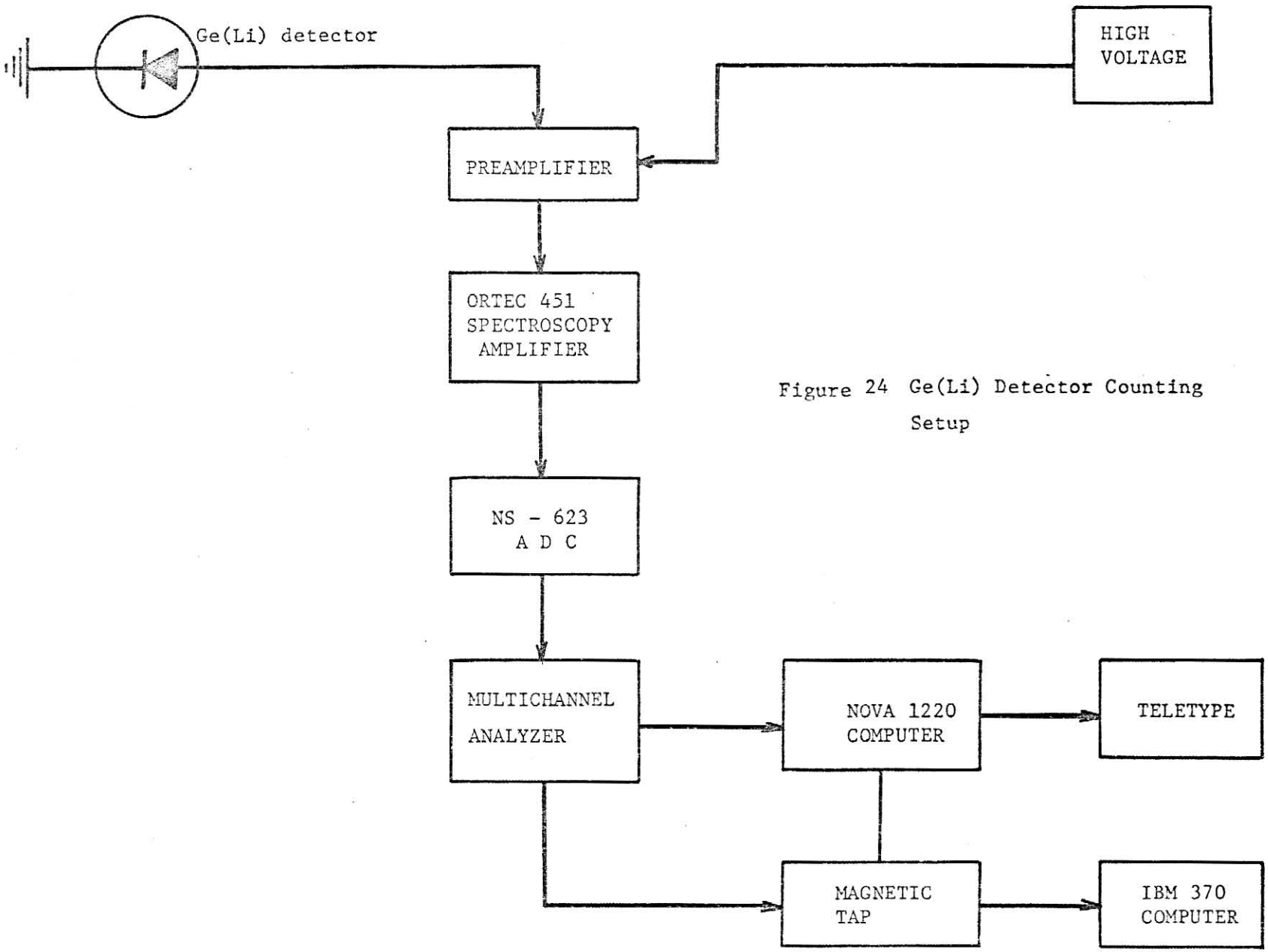

Figure 24 Ge(Li) Detector Counting Setup

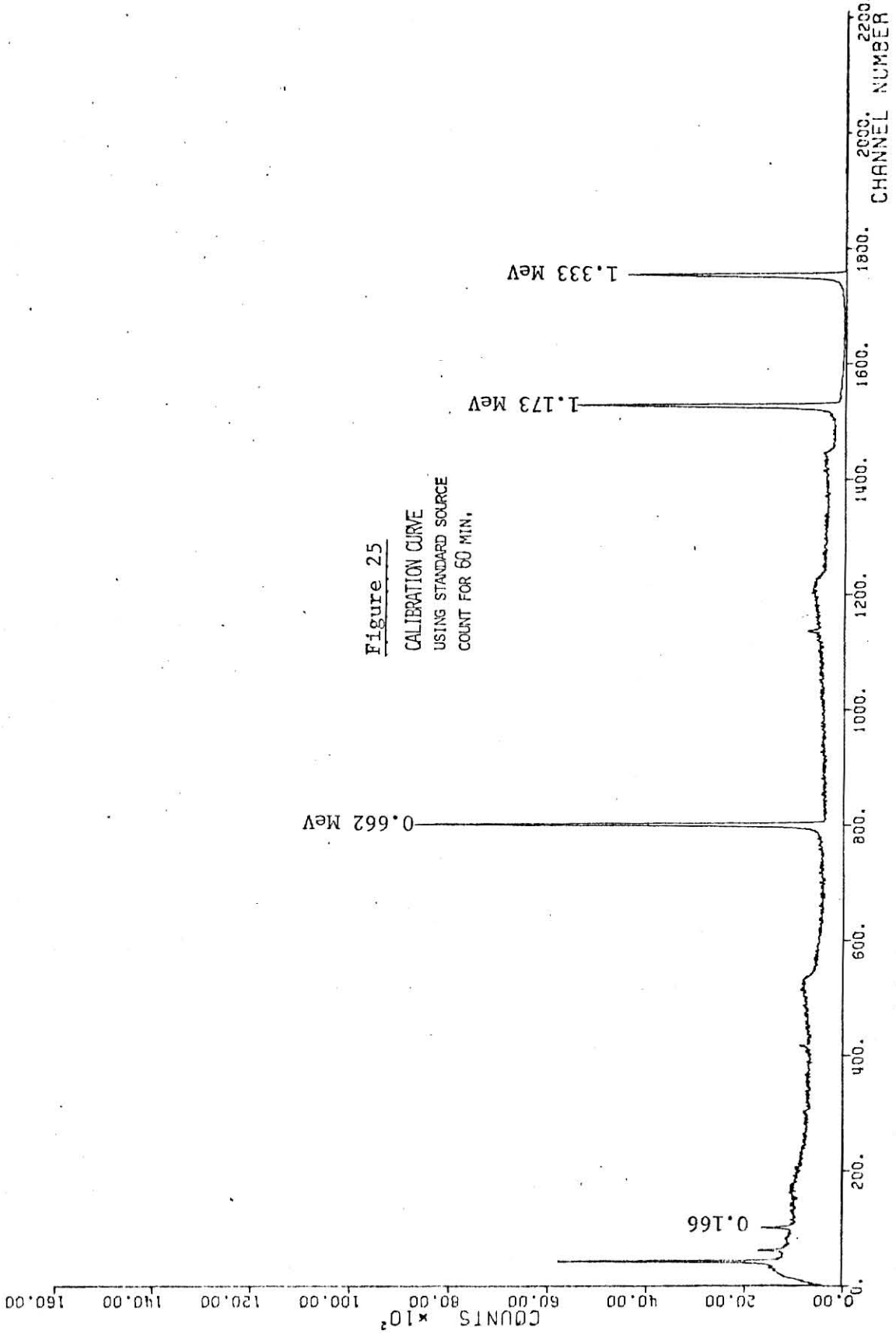

Figure 25

CALIBRATION CURVE

USING STANDARD SOURCE

COUNT FOR 60 MIN.

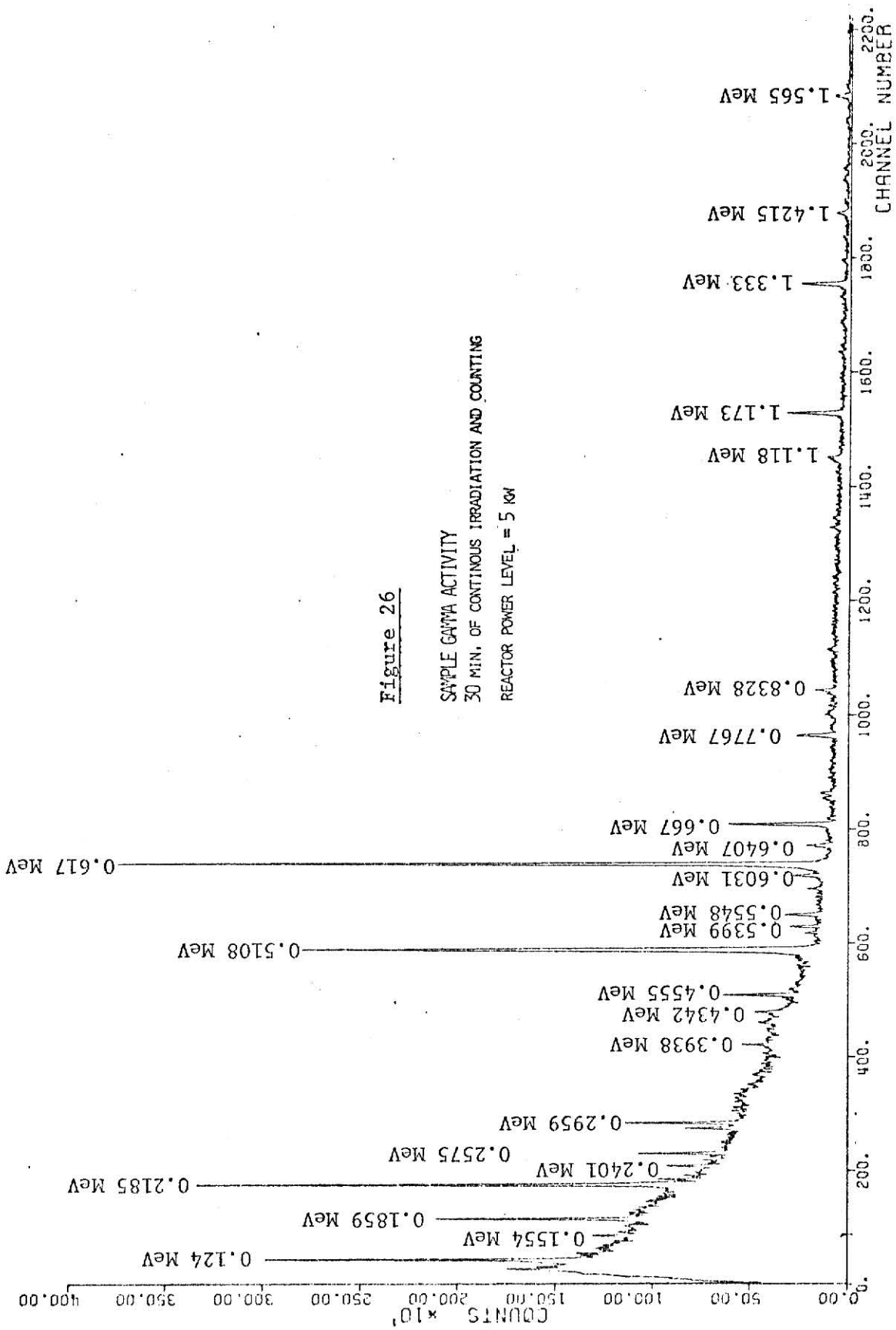

Figure 26

SAMPLE GAMMA ACTIVITY
30 MIN. OF CONTINOUS IRRADIATION AND COUNTING
REACTOR POWER LEVEL = 5 KW

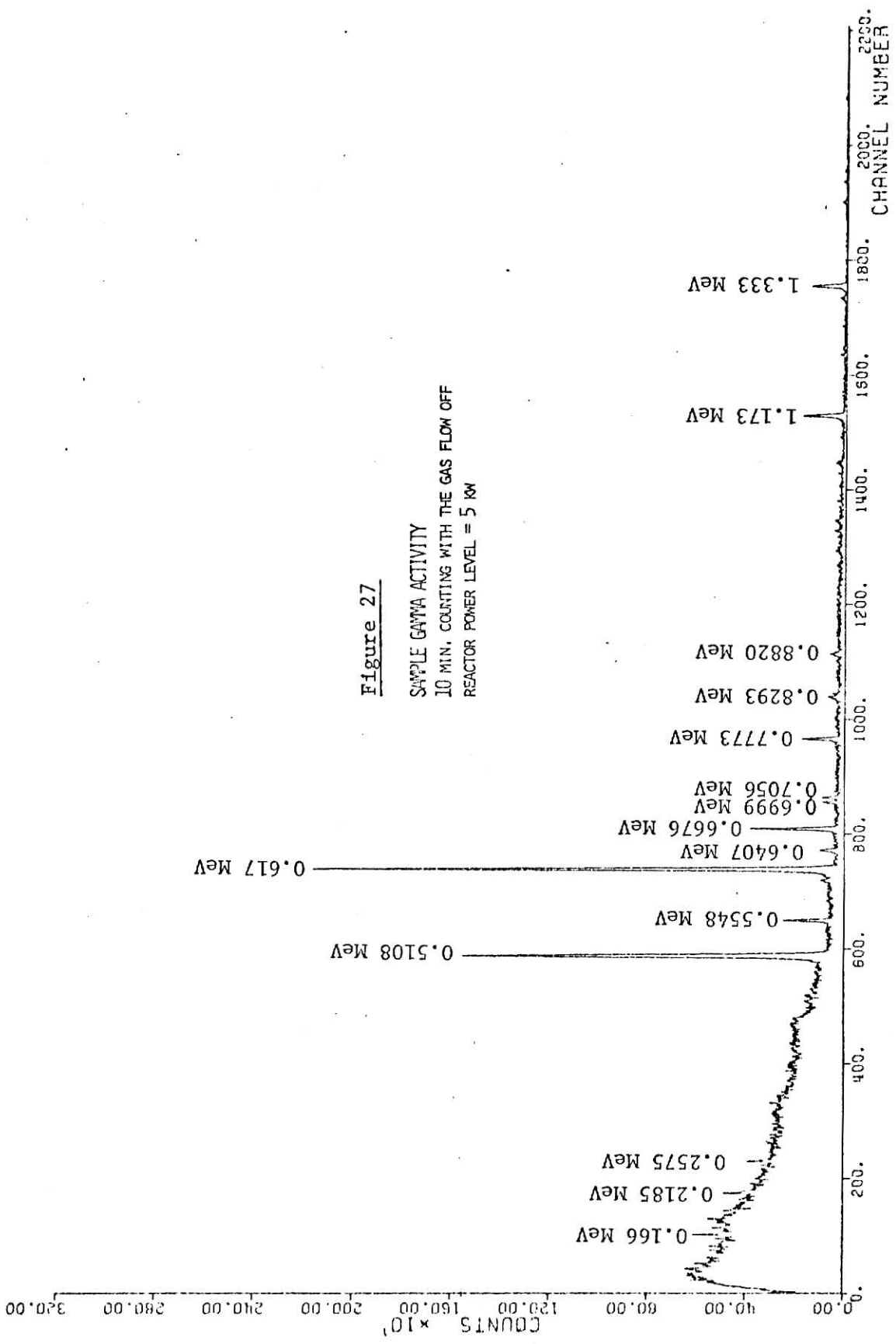

Figure 27

SAMPLE GAMMA ACTIVITY
10 MIN. COUNTING WITH THE GAS FLOW OFF
REACTOR POWER LEVEL = 5 KW

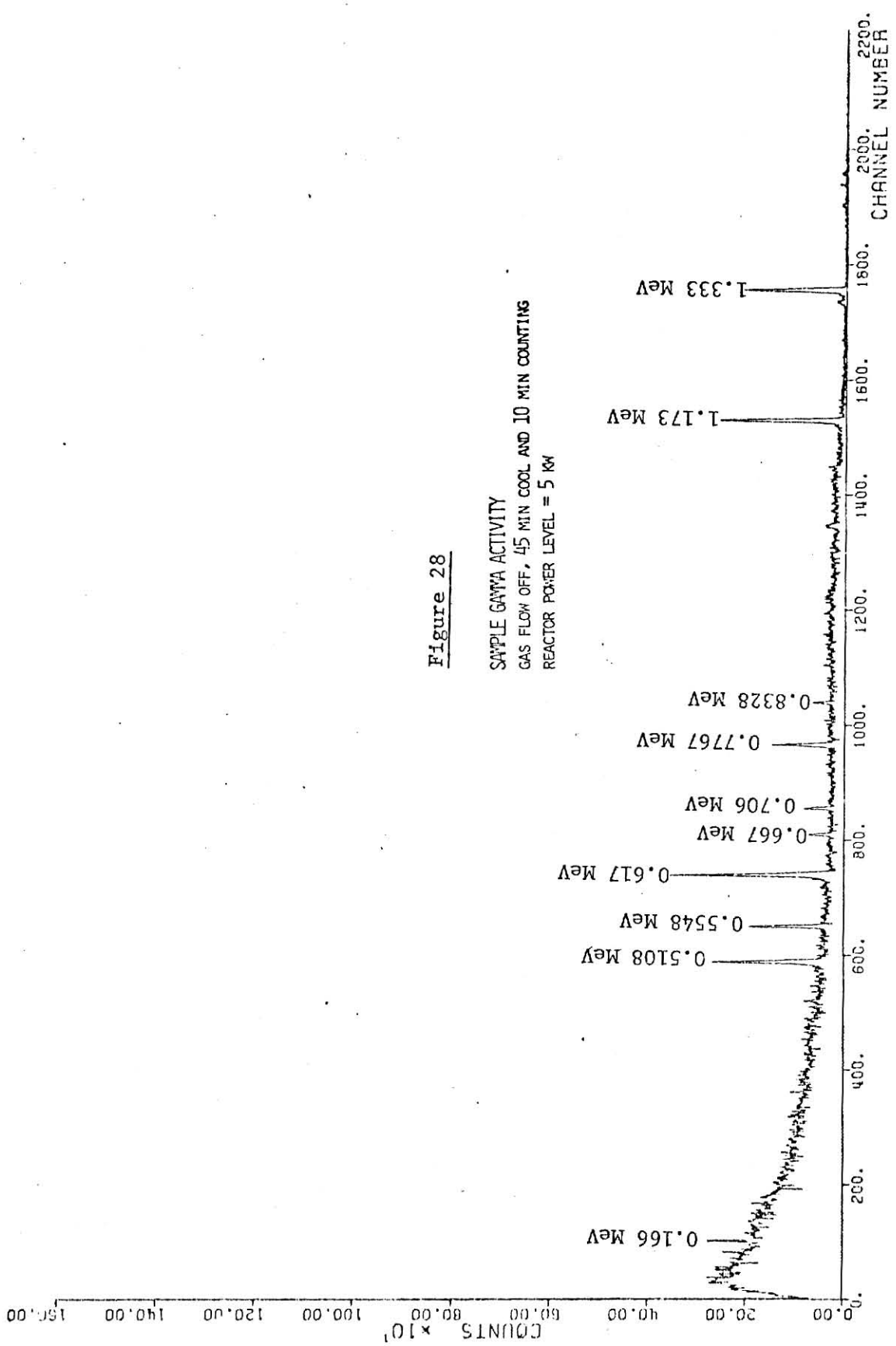

Figure 28

SAMPLE GAMMA ACTIVITY
GAS FLOW OFF, 45 MIN COOL AND 10 MIN COUNTING
REACTOR POWER LEVEL = 5 KW

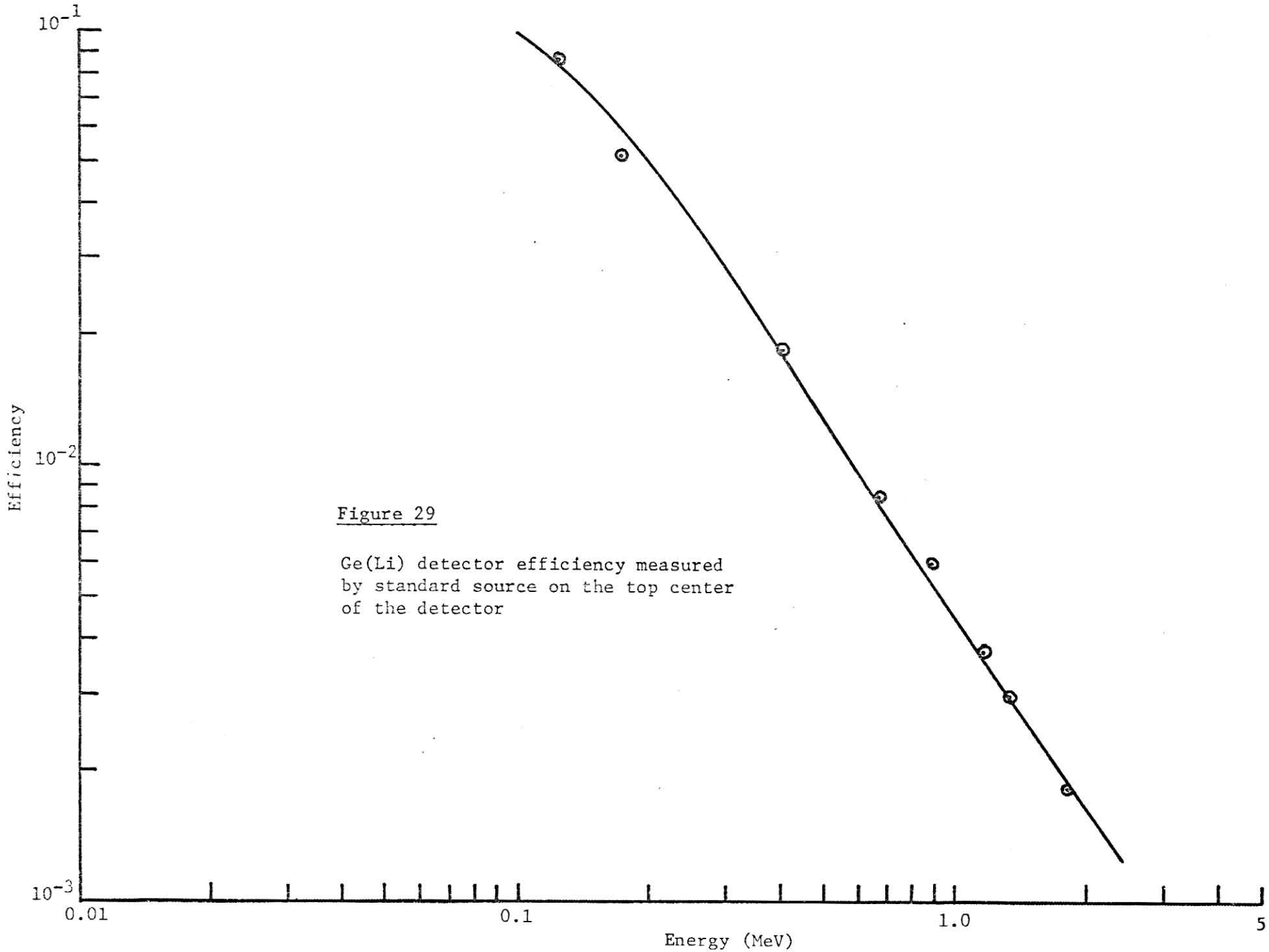

Figure 29

Ge(Li) detector efficiency measured by standard source on the top center of the detector

Table 8. Predominant peak energies and their possible contributors

Energy (keV)	Contributors to Peak	Half-life	Intensity (tabulated) %	Intensity (calculated) %
124.844	Xe-142	1.22 s	6.2	0.558
	Mo-108	1.50 s	11	0.99
	Nd-149	1.8 h	0.1	0.001
155.356	Nd-149	1.8 h	5.2	0.345
	Xe-142	1.22 s	12.7	0.864
	Ba-142	10.8 m	0.58	0.04
218.509	I -134	53.2 m	0.24	0.011
	Xe-139	39.1 s	77.0	3.39
	Rh-107	21.7 m	0.1	0.005
	Rb-93	58.9 s	0.001	0.0005
	Ce-146	14 m	21	0.924
257.536	Te-133M	55.4 m	1.0	0.038
	Sb-130	41 m	3.9	0.148
	Nd-149	1.8 m	0.33	0.013
	Xe-138	17.1 m	32.5	1.24
	Tc-108	8.3 s	-	-
	Mo-108	1.5 s	-	-
295.854	Sb-131	23 m	1.95	0.051
	Xe-139	39.7 s	24	0.624
393.776	Rb-92	45.3 s	0.16	0.003
	Nb-99	2.6 m	3	0.06
	Rh-107	21.7 m	8.8	0.17
	Te-133	12.9 m	0.8	0.015
	Xe-139	39.7 s	.8	0.15
420.741	Ag-121	3 s	0.001	0.00002
	Kr-90	32.2 s	0.35	0.006
	I -133	21 h	0.26	0.004
434.223	I -134	53.2 s	4.15	0.063
	Kr-90	32.2 s	3.2	0.05
	Ru-108	4.5 m	43	0.65
	Sb-131	23 m	2.64	0.039
510.858	Sn-127	2.12 h	1.1	0.014
	Kr-87	76.3 m	0.053	0.001
	Xe-140	13.6 s	-	-
	I -133	21 h	1.5	0.023
	Rh-108	4.5 m	10	0.15
	Ba-142	10.8 m	0.3	0.005

Table 8 (Continued)

Energy (keV)	Contributors to peak	Half-life	Intensity (tabulated) %	Intensity (calculated) %
531.436	Xe-138	17 m	1.2	0.0024
	I -135	6.7 m	0.5	0.006
539.951	Kr-90	32.1 s	38.8	0.427
	I -134	53.2 m	7.6	0.084
	La-141	42.4 s	40.1	0.44
	Xe-142	1.22 s	-	-
554.143	Kr-87	76.3 m	0.03	0.003
	Kr-90	32.2 s	6.6	0.066
	Rh-107	21.7 m	0.008	0.00008
	Nb-90	2.6 m	0.001	0.00001
	Sr-91	9.75 h	61.5	0.615
	Xe-138	17 m	0.08	0.0008
586.783	Kr-89	3.16 m	18.6	0.19
	Kr-92	1.84 s	0.11	0.0011
	La-144	42.4 s	-	-
603.104	Rb-91	66.6 s	4	0.039
	Br-87	55.7 s	50 *	0.49 *
	Ba-142	10.1 m	0.36	0.0036
	Br-84	31.8 m	1.75	0.017
	Xe-142	1.22 s	21.8 *	0.236
617.296	Br-80	17.6 s	7	0.068
	Pd-117	20.1 h	43.7	0.42
	Xe-142	1.22 s	76.3 *	0.73 *
	I -133	21 h	0.37	0.004
	Kr-90	32.2 s	1.4	0.015
604.712	Xe-140	13.6 s	6.6 *	0.057
	In-188	4.4 m	10.3	0.096
	La-142	95.4 m	47.5	0.46
667.623	Br-80	17.6 m	1.0	0.008
	Sb-129	8.9 h	2.5	0.02
	I -132	2.28 h	98	0.78
	Sb-131	23 m	1.67	0.014
699.253	Ba-141	18 m	1.2 *	0.009 *
	Rb-89	15.6 m	0.3	0.002
706.282	Sb-134	10.3 s	57	0.43
	I -133	21 h	1.6	0.012
	I -135	6.7 h	0.7	0.005
724.557	Xe-139	39.7 s	0.9	0.0066
	Cs-139	9.76 m	2.4	0.018

Table 8 (Continued)

Energy (keV)	Contributors to peak	Half-life	Intensity (tabulated) %	Intensity (calculated) %
735.100	Cs-140	67.9 s	10	0.07
	Br-84	31.8 m	1.24	0.009
	Pr-146	24 m	8.9	0.062
	Xe-142	1.22 s	15.7 *	0.11 *
	Kr-92	1.84 s	0.26	0.002
762.57	Br-88	15.9 s	-	-
	Ag-122	1.5 s	-	-
	Sr-91	9.7 h	0.53	0.0036
	Kr-89	3.16 m	1.45	0.01
776.57	Rb-89	15.6 m	0.073	0.0004
	Kr-89	3.16 m	1.3	0.008
	Ag-115	21 m	3.1 *	0.002
808.577	Xe-142	1.22 s	6.9 *	0.041
	I -135	6.7 h	0.06	0.0004
	Ag-118	2.8 s	-	-
832.802	Rb-90	2.57 m	49.4	0.29
	Ba-141	18 m	3.8 *	0.022
	Br-85	2.87 m	5.3	0.03
	Nb-98	51 m	10	0.059
882.707	I -134	53.2 m	64.9	0.357
1032.422	Rb-89	15.6 m	64.1	0.269
	Ba-142	10.8 m	0.54	0.0022
	Ru-107	4.2 m	4	0.0168
1118.878	Kr-90	32.3 s	53	0.223
	Br-84	31.1 m	0.14	0.001
	Xe-137	3.8 m	0.2	0.0012
	Kr-89	31.6 m	1.9	0.008
1250.168	Kr-88	2.85 h	1.0	0.0032
	Sb-128	8.9 h	1.0	0.0032
1363.442	La-142	95.4 m	2.19	0.006
	Br-86	59 s	11.7	0.031
1421.495	Rb-89	15.5 m	0.098	0.0003
	Sr-94	1.29 m	1.0	0.0026
	Kr-90	32.3 s	3.7	0.0096
1437.779	Rb-91	66.6 s	0.8	0.002
	Br-84	31.8 m	0.06	0.0002
	Ba-141	18.0 m	1.8 *	0.005 *

Table 8 (Continued)

Energy (keV)	Contributors to peak	Half-life	Intensity (tabulated) %	Intensity (calculated) %
1462.557	Kr-87	76.3 m	0.053	0.0001
	Kr-90	32.3 s	0.4	0.001
	Br-86	59.0 s	5.6	0.014
	Br-87	55.7 s	37.2 *	0.09
	Rb-92	4.53 s	0.05	0.0001
1476.716	Rb-89	15.6 m	0.38	0.0009
	Sr-91	9.75 h	0.15	0.0004
	Nb-132	2.6 m	11.0 *	0.026 *
	Br-87	55.7 s	32.8 *	0.08
	I -132	2.28 h	0.124	0.0003
1565.920	Br-86	59 s	65.1	0.16
	Ge-80	22.7 s	4.5	0.011
	I -135	6.7 h	1.2	0.003
1798.841	Rh-108	17 s	-	-
	Ba-141	18 m	1.3 *	0.002 *
1772.646	Y -95	10.9 m	4.8 *	0.009 *
	Kr-89	22.1 m	0.86	0.002

s second
m minute
h hour

* relative intensity

Data contained in columns 2,3,4 were obtained from Ref. 41.

Table 9. Assignments of isotopes to the observed gamma-ray spectrum

Calculated Energy(MeV)	Isotope	$T_{1/2}$		I %	Listed Energy(MeV)
0.1248	Kr-90	32.2	s	58	0.122
0.1554	Xe-138	17.1	m	5.7	0.1539
0.1660	Kr-88	2.8	h	7.0	0.1660
0.1858	Br-82	35.5	h	70.0	0.1820
0.1968	Kr-88	2.8	h	35.0	0.1961
0.2185	Xe-139	39.7	s	77.0	0.219
	Br-82	35.5	h	23.6	0.2215
0.2401	Kr-90	32.2	s	17.0	0.242
0.2575	Xe-138	17.1	m	32.5	0.258
0.2900	Xe-139	39.7	s	10.0	0.2899
0.2959	Xe-139	39.7	s	24.0	0.296
0.3938	Xe-139	39.7	s	8.0	0.394
0.4030	Kr-87	76.3	m	48.0	0.4027
0.4207	Kr-90	32.2	a	0.35	0.419
0.4342	Xe-138	17.1	m	20	0.4345
0.4555	Xe-137	13.1	m	30	0.4556
0.5109	Br-80m	4.42	h	-	0.511
	Br-80	17.6	m	0.3	0.511
0.5314	Xe-138	17.1	m	0.2	0.5301
0.5399	Kr-90	32.2	s	38.8	0.5396
0.5541	Br-82	35.5	h	70.1	0.5543
0.5868	Kr-92	1.84	s	0.11	0.585
0.6031	Br-84	31.8	m	1.75	0.6048
	Br-87	55.7	a	50 *	0.604
0.6173	Br-82	35.5	h	43.3	0.619
	Br-80	17.6	m	7.0	0.616
	Br-80m	4.42	h	7.0	0.616

Table 9 (Continued)

Calculated Energy (MeV)	Isotope	$T_{1/2}$		I %	Listed Energy (MeV)
0.6407	Br-80	17.6	m	0.3	0.639
	Br-80m	4.42	h	0.3	0.639
0.6676	Kr-89	3.16	m	2.0	0.669
0.7063	Br-80	17.6	m	0.2	0.704
	Br-80m	4.42	h	0.2	0.704
0.7246	Kr-91	7.9	s	1.0	0.721
0.7351	Br-84	31.8	m	1.29	0.736
0.7625	Br-88	15.9	s	-	0.761
0.7766	Br-82	35.5	h	83.3	0.7765
0.8026	Br-86	59.1	s	2.9	0.803
0.8328	Br-85	2.87	m	5.3	0.832
0.8827	Br-84	31.8	m	41	0.881
	Br-84m	6.0	m	98	0.881
1.0324	Br-84	6.0	m	1.0	1.029
1.118	Kr-90	32.3	s	53	1.1187
1.2502	Kr-88	2.8	h	1.0	1.2500
1.318	Br-82	35.5	h	27.5	1.3117
1.3634	Br-86	59.1	s	11.7	1.3616
1.4215	Br-87	55.9	s	1.0 *	1.419
1.476	Br-82	35.5	h	16.66	1.4748
	Br-87	55.9	s	32.8	1.470
1.565	Br-86	59.1	s	65	1.5646

lives, number of counts under the peaks, and the gamma energies associated with these contributors as listed in reference 41 by observing the decay scheme of each isotope. The results of these assignments are presented in Table 9 in which the calculated peak energy as observed from Figure 26 are listed in column 1, while column 2 shows the energy of the assigned isotope as reported in the "Atomic Data and Nuclear Data Tables" [41]. The computed energies were found to be in agreement with those listed in reference 41 within an error of ± 2 keV.

After studying the fission-product transfer with the Ge(Li) detector and identifying probable bromine delayed-neutron precursors, the NaI(Tl)-BF_3 coincidence counter was operated with the methanol sample container located between the neutron and gamma-ray detectors and with the reactor operating at 5 kW and the bromine gas-flow system operating at about 500 ml/min.

The detectors were first operated in singles mode, i.e., noncoincident mode, to study their behavior. For the neutron detectors this simply consisted of measuring the count rates from the BF_3 counters with the bromine gas-flow system on or off. The count rates were measured with the scaler driven by the output of the single-channel analyzer whose window was on the peak of the BF_3 pulse height distribution. Three minutes were allowed before the start of each measurement to account for any buildup or decay of the precursors. The average of four trials gave a neutron detector count rate of 0.49 ± 0.04 counts/sec with the gas flow off and 1.11 ± 0.05 counts/sec with the gas flow on.

The NaI(Tl) detector was operated in the singles mode by switching the linear gate in the gamma-ray channel from "gated" to "normal". An ungated bromine spectrum obtained using the reactor power level and flow rates as described above is shown in Figure 25. The 0.617 MeV and 0.511 MeV gamma-ray peaks resulting from ^{80}Br and ^{82}Br, respectively, dominate the NaI(Tl)

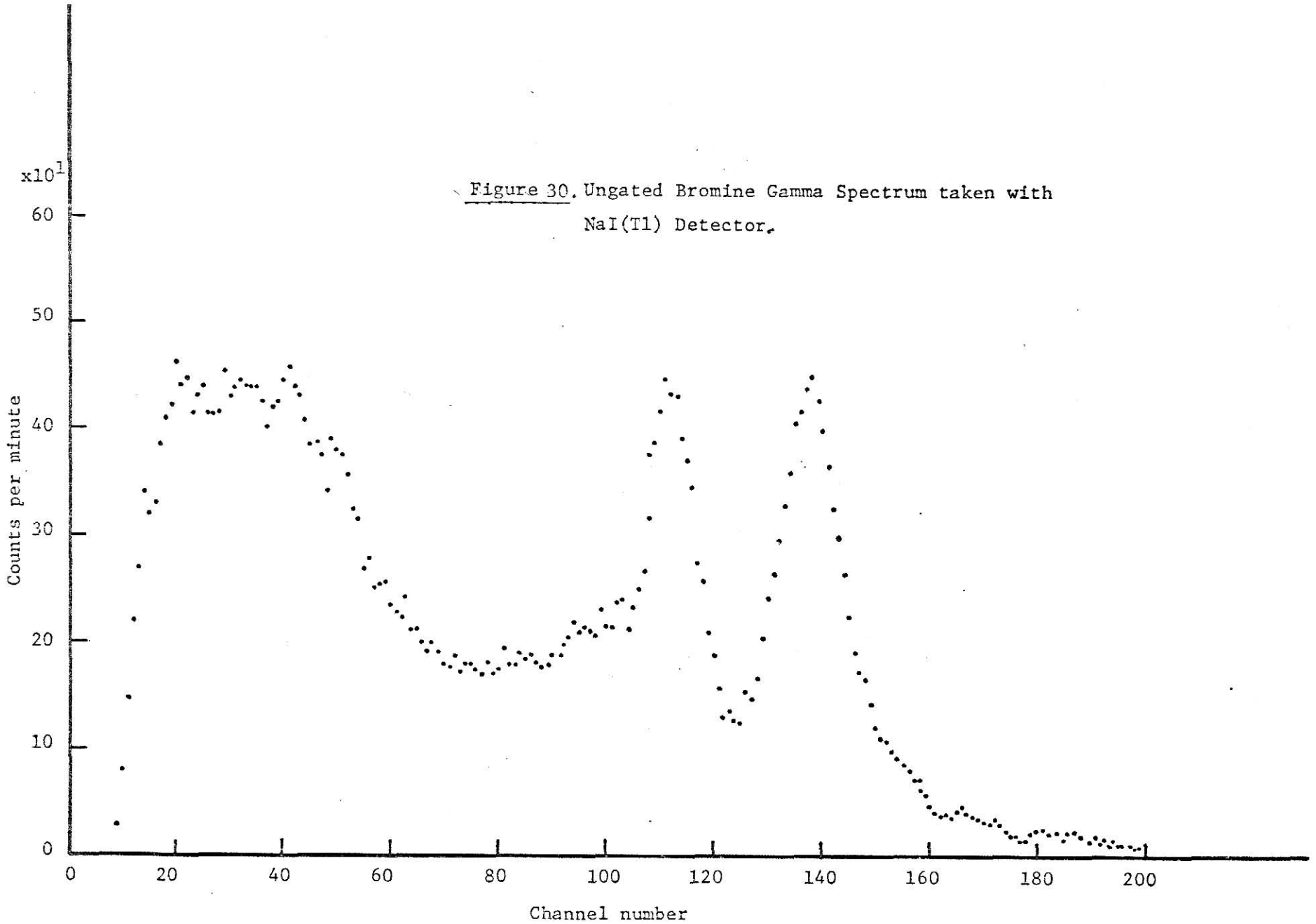

Figure 30. Ungated Bromine Gamma Spectrum taken with NaI(Tl) Detector.

gamma-ray spectrum. The count rate in the NaI(Tl) detector was 726 counts/sec as determined from Figure 38.

Since the gamma-ray count rate is

$$N_\gamma = 726 \text{ counts/sec},$$

the neutron count rate is

$$N_n = 0.62 \text{ counts/sec},$$

and since the absolute efficiencies for the neutron and gamma-ray detectors are

$$\varepsilon_\gamma = 0.01$$

and

$$\varepsilon_n = 0.04 \quad ,$$

the neutron and gamma-ray production rates are

$$A_n = \frac{N_n}{\varepsilon_n} = 15.5 \text{ sec}^{-1}$$

and

$$A_\gamma = \frac{N_\gamma}{\varepsilon_\gamma} = 72600 \text{ sec}^{-1} \ .$$

If the fraction of precursors which decay via an excited state in the final nucleus is assumed to be

$$\frac{A_{n\gamma}}{A_n} = 0.1,$$

then

$$A_{n\gamma} = (0.1)(15.5) = 1.55 \text{ sec}^{-1}$$

and the true coincidence count rate would be

$$C_T = \varepsilon_\gamma \varepsilon_n A_{n\gamma} = 6.2 \times 10^{-4} \text{ sec}^{-1} \qquad \text{(IV.1)}$$

and the random coincidence count rate would be

$$C_R = \tau \varepsilon_n \varepsilon_\gamma A_n A_\gamma = 1.12 \times 10^{-2} \text{ sec}^{-1} \ , \qquad \text{(IV.2)}$$

for a true-to-random coincidence ratio of

$$R = \frac{C_T}{C_R} = 0.055. \qquad \text{(IV.3)}$$

Although this ratio and the true count rate C_T are not adequate for a practical measurement, a one-hour coincidence measurement was performed to demonstrate the operation of the complete coincidence counting system. The resulting true-plus-random coincidence spectrum and the random spectrum are shown in Figures 31 and 32, respectively. The internal discrimination levels in the two linear gates were not identical and account for the lower number of counts observed in the random spectrum below channel 230 compared to the number of counts below channel 30 in the true-plus-random coincidence spectrum. Above channel 30 in the true-plus-random spectrum 46 counts were observed and above channel 230 in the random spectrum 38 counts were recorded; thus the true-to-random coincidence ratio

$$R = \frac{C_T}{C_R} = 0.211 \quad {}^{+\,0.265}_{-\,0.211}$$

is consistent with the value obtained in equation IV.3.

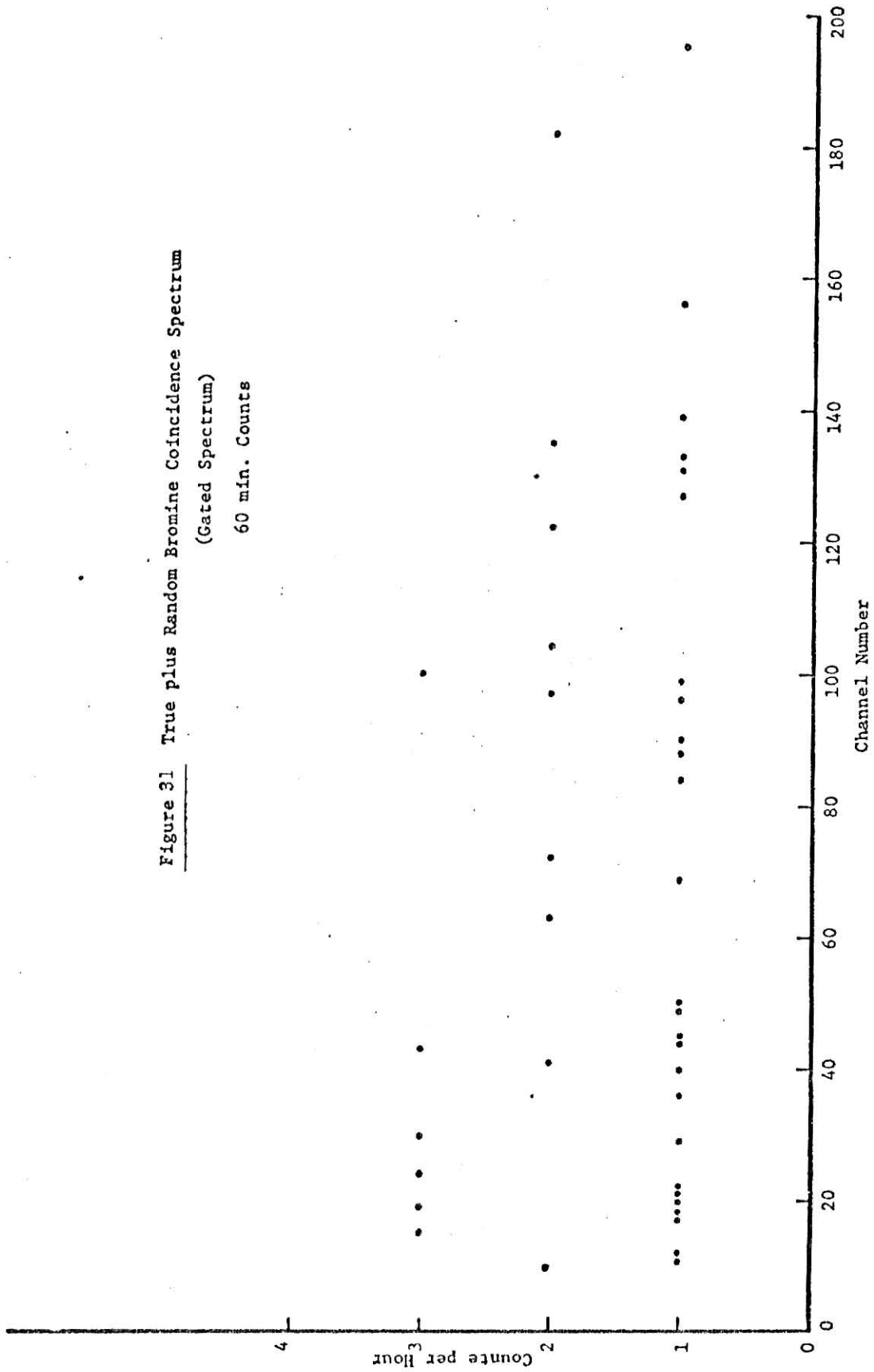

Figure 31 True plus Random Bromine Coincidence Spectrum
(Gated Spectrum)
60 min. Counts

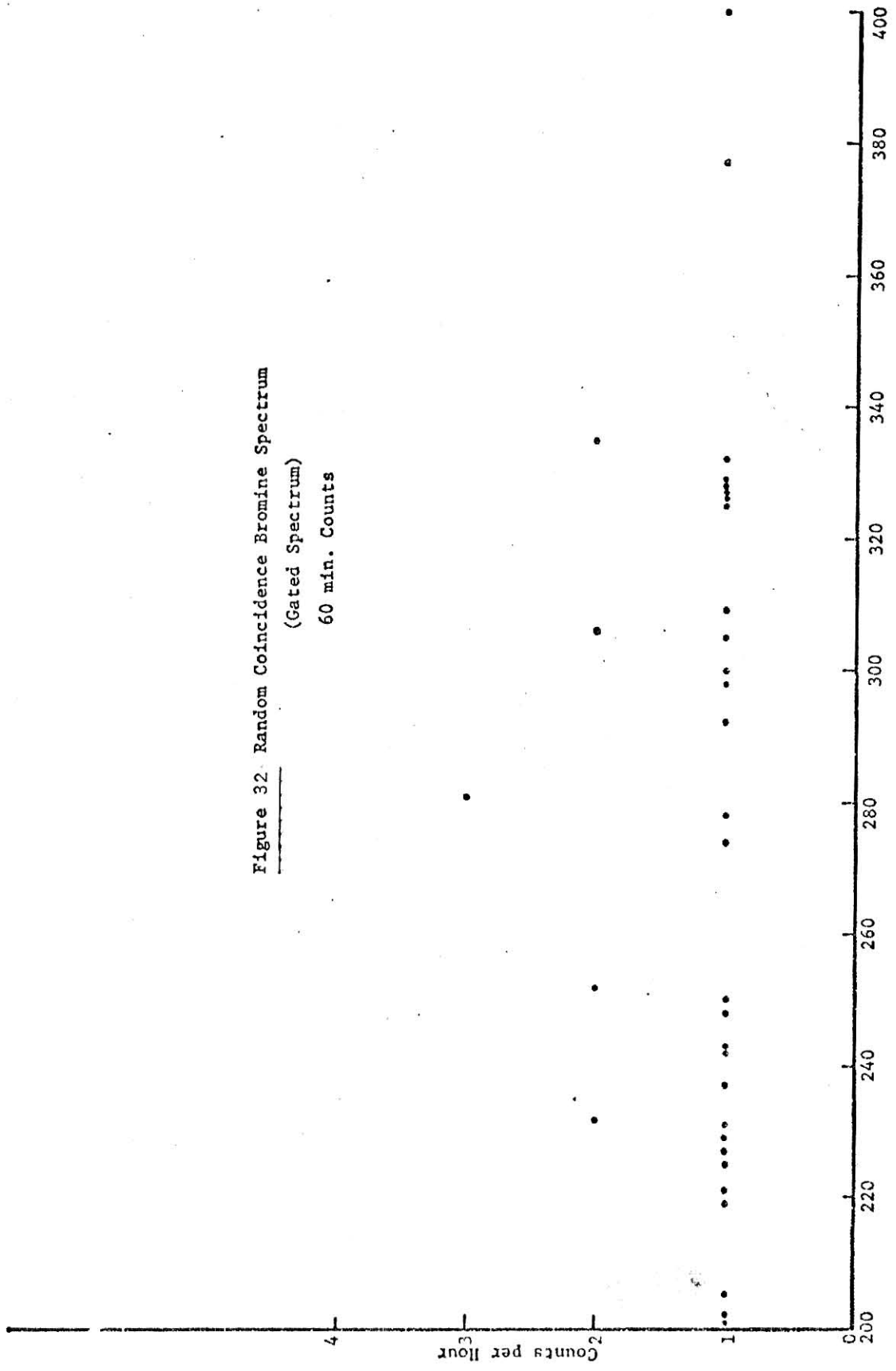

Figure 32 Random Coincidence Bromine Spectrum
(Gated Spectrum)
60 min. Counts

Chapter V.

V.1 Summary, Recommendations and Conclusions

To determine the feasibility of delayed-neutron gamma-ray coincidence measurements for investigating delayed-neutron decay modes, radiochemical separation was performed on a uranyl nitrate solution irradiated by thermal neutrons in the thermal column of the KSU TRIGA Mk II nuclear reactor. By sweeping the gaseous and bromine fission products using a nitrogen-bromine mixture as a carrier gas, spectroscopy could be performed on the fission products of interest.

The uranium sample solution preparation and installation in the reactor presented no serious physical problems. Limits stipulated by 10CFR20 [50] for radiological health considerations did not present serious problems at the fission rates needed. The bromine liquid and vapor can be handled, with a carefully designed transport system, without hazard in the reactor and reactor bay.

Evidence was found in the Ge(Li) gamma-ray spectra for the presence of lines from bromine delayed-neutron precursors with mass numbers 87 and 88. The bromine fission products with mass numbers 89, 90, 91, and 92 with very short half-lives (< 5 seconds) are not observed, probably because their half-lives are shorter than the transit time of the gases from the irradiation cell to the counting position, as the latter was estimated to be of the order of 5 seconds for the flow rates used. The Ge(Li) gamma-ray spectra also show the presence of numerous other lines which are not delayed-neutron precursors, such as ^{80}Br, ^{82}Br, ^{84}Br, and ^{85}Br. The isotopes ^{80}Br and ^{82}Br were produced by activation of the carrier gas which bubbled through the irradiation cell. The presence of ^{84}Br, ^{85}Br, ^{87}Br, and ^{88}Br shows that bromine fission products

are effectively transported from the irradiation cell to the coincidence counter, although contaminations from the noble gases krypton and xenon were also observed.

Methanol was found to trap bromine effectively at the counting position and therefore CCl_4 (which was used by Perlow and Stehney [33] but which is less desirable from the standpoint of safety) was not needed.

The neturon detectors operated stably after some discharge problems in the distribution box were eliminated. An acceptable background ($\sim$ 1/2 count/sec) was obtained from the neutron detectors after stability was reached.

Even with a natural uranium irradiation sample, the background obtained by the neutron and gamma detectors was found to be adequately low at the required reactor power level.

The electronic system was successfully assembled from commercial modules except for the time-delay unit, which could be replaced with commercial pulse generators. The count rates observed in the neutron and gamma detectors were similar to those anticipated. The coincidence-counting system operated successfully within the limitations imposed by the resolution and efficiency of the detectors used, although the true-to-random coincidence ratio was found to be too low for practical coincidence measurements.

Three modifications to the present experiment are recommended to permit practical neutron-gamma coincidence measurements.

1. Ge(Li) detector

   If the NaI(Tl) crystal is replaced with a very large Ge(Li) detector ($\sim$100 cm^3), the excellent energy resolution obtained will compensate for the loss in intrinsic detection efficiency for the Ge(Li) compared to a 3 x 3" or a 6 x 4" NaI(Tl) detector. The reasons for this are that (1) a much smaller true-to-random ratio can be tolerated because of the much improved energy resolution, and (2) since true

coincidences due to inelastic scattering can be readily identified (because of the much improved resolution), the Ge(Li) detector housing can be placed in contact with the precursor sample.

2. ^{3}He counters

   If the 10 BF_3 counters are replaced with 25 4-atm ^{3}He counters, the neutron detector efficiency will be greatly improved.

3. Gas-flow system

   If the bromine-to-nitrogen ratio in the gas-flow system is adjusted to maximize the ratio of fission-product bromine to activated bromine, the neutron-gamma ratio at the counting location will be substantially improved. Also, if the alcohol trap for the bromine is designed to be slowly but continuously drained and replenished, the buildup of long-lived fission products will be reduced and the alcohol will never become saturated with bromine.

If these three improvements are made, it is reasonable to assume that

$$\varepsilon_\gamma = 0.01,$$

$$\varepsilon_n = 0.2,$$

$$R = 0.1, \text{ and}$$

$$\frac{A_\gamma}{A_n} = 1000,$$

where the symbols have the same meaning as in Chapter III.

If it is also conservatively assumed, as before, that

$$A_n = 10\, A_{n\gamma} \quad ,$$

then

$$R = 0.1 = \frac{C_T}{C_R} = \frac{\varepsilon_\gamma \varepsilon_n A_{n\gamma}}{\tau\, \varepsilon_\gamma \varepsilon_n A_n A_\gamma}$$

$$= \frac{A_{n\gamma}}{\tau\, (10A_{n\gamma})A_\gamma}$$

$$= \frac{1}{10\, \tau\, A_\gamma}$$

or

$$A_\gamma = \frac{1}{\tau} = \frac{1}{25 \times 10^{-6}\ \text{sec}} = 4 \times 10^4\ \text{sec}^{-1} \quad .$$

Thus the true count rate is

$$C_T = \varepsilon_\gamma \varepsilon_n A_{n\gamma}$$

$$= \varepsilon_\gamma \varepsilon_n\ (0.1\ A_n)$$

$$= \varepsilon_\gamma \varepsilon_n\ (0.1)(\frac{A_\gamma}{1000})$$

$$= (0.01)(0.2)\ (0.1)(\frac{4 \times 10^4}{1000})\text{sec}^{-1}$$

$$= 8 \times 10^{-3}\ \text{sec}^{-1}$$

$$\cong 5000\ \text{week}^{-1}.$$

About 5000 true-coincidence counts per week and about 50000 random-coincidence counts per week are reasonable count rates for a difficult coincidence experiment. It is concluded, therefore, that with the modifications to the

system recommended above, successful coincidence data can be obtained for the investigation of the decay modes of the bromine delayed-neutron precursors.

ACKNOWLEDGMENTS

The author wishes to express his gratitude to Dr. M. S. Krick, who suggested this work, for his guidance and help throughout the course of this study. Sincere appreciation is given to the Department of Nuclear Engineering for their financial support which made this study possible. Special thanks are given to the staff of the electronics shop and of the Kansas State TRIGA Mk II nuclear reactor in the Department of Nuclear Engineering for their cooperation in scheduling and performing the experiment. I am also grateful to Dr. J. F. Merklin for his help in the sample preparation and to Mr. J. Razvi for his assistance and valuable suggestions during the performance of this study. I also wish to thank Mrs. M. Brisbin for her efforts and dedication in typing this work.

Last but not least, the author is ever grateful to his wife, Cida, for her patience and forbearance throughout the course of this thesis.

REFERENCES

1. Jahnsen, T., Pappas, A. C., and Tunnal, T., "Delayed Neutron Emission, Theory and Precursor Systematics", Delayed Fission Neutrons: Proceedings of a panel held in Vienna 24-27 April 1967, IAEA, Vienna, 1968 p. 35.

2. Roberts, R., Meyer, R. C., and Wang, P., Phys Rev. 55 (1939) 510.

3. Amiel, S., "Delayed Neutrons in Fission", Proceeding of the second IAEA Symposium on the Physics and Chemistry of Fission held by International Atomic Energy Agency in Vienna 28 July - 1 August, 1969, IAEA, Vienna, 1969.

4. Keepin, G. R., Augustson, R. H., and Walton, R. B., "Los Alamos Scientific Laboratory Safeguards Research and Development Program", in Proceedings of AEC Symposium on Safeguards Research and Development, Los Alamos Scientific Laboratory, October 27-29, 1969, WASH-1147.

5. Keepin, G. R., "Physics of Nuclear Kinetics", Chapters 6-10, Addison Wesley Publishing Company, Inc., Reading, Massachusetts.

6. Keepin, G. R., "Delayed Fission Neutrons Date in Reactor Physics and Design", Delayed Fission Neutrons: Proceeding of a panel held in Vienna 24-27 April 1967, IAEA, Vienna 1968.

7. Yiftah, S. and Shaphier D., "The Importance of Exact Delayed Neutron Data in Fast Reactor Dynamic Behavior", Delayed Fission Neutrons; Proceeding of a panel held in Vienna 24-27 April 1967, IAEA, Vienna, 1968.

8. Keepin, G. R., "Physics of Nuclear Kinetics", Chapter 4, Addison Wesley Publishing Company, Inc., Reading, Massachusetts.

9. Tomlinson, K. L. and Hermann, G., "Delayed Neutrons From Fission", AERE-R6993 Atomic Energy Establishment, Harwell (1972).

10. Kratz, K. L. and Hermann, G., "Delayed-neutron Emission From Short-lived Bromine and Iodine Isotopes", Nuclear Physics, A 229 (1974) p. 179-188.

11. Keepin, G. R., Wimmett, T. F., and Zeigler, R. K., "Delayed Neutrons From Fissionable Isotopes of Uranium, Plutonium and Thorium", Phys. Rev. 107 (1957) 1044.

12. Evans, A. E., Thorpe, M. M., and Krick, M. S., "Revised Delayed-Neutron Yield Data", Nucl. Sci. and Engg. 50 (1972) 80.

13. Hyder, H. R. McK. and Bachelor, R. J., "The Energy of Delayed Neutrons From Fission", Nucl. Energy 3 (1956) 7.

14. Shalev, S. and Cuttler, J., "Fissile Nuclear Data", Trans. Am. Nucl. Soc. 14 (1971) P. 373.

15. Pappas, A. C. and Rudstam, G., "An Approach to the Systematics of Delayed Neutron Precursors", Nucl. Phys. 21 (1960) 353.

16. Takahashi, K., "Application of the Gross Theory of β-decay Delayed-Neutron Emissions", Progr. Theor. Phys. 47 (1972) 1500.

17. Saphier, D. and Yiftah, S., "The Effect of Errors in the Delayed-Neutron Data on Fast Reactor Static and Dynamic Calculations", Nucl. Sci. and Engg. 42 (1972) 272.

18. Masters, C. F., Thorpe, M. M., and Smith, D. B., "The Measurement of Absolute Delayed-Neutron Yields from 3.1 and 14.9 MeV Fission", Nucl. Sci. and Engg. 36 (1969) 202.

19. Shpakov et. al., "Delayed Neutron Yields in the Fission of ^{239}Pu and ^{232}Th by 14.5 MeV Energy Neutrons", Soviet Journal of Atomic Energy, 11 (1962) 1190.

20. McGarry, W. I., Omohundro, R. J., and Holloway, G. E., Bull. Am. Phys. Soc., Series II, 5, No. 1 (1960) 33.

21. Keepin, G. R., "Physics of Nuclear Kinetics", Chapter 4, Addison Wesley Publishing Co., Inc., (1965), Reading, Massachusetts.

22. Krick, M. S. and Evans, A. E., "The Measurements of Total Delayed-Neutron Yields as a Function of the Energy of the Neutrons Inducing Fission", Nucl. Sci. and Engg. 47 (1972) 311.

23. Garvey, G. T. et al., "Set of Nuclear Mass Relations and a Resultant Mass Table", Rev. Mod. Phys. 41 (1969) S1.

24. Crawford, G. I., et. al., "Population of Excited States in Delayed Neutron Emission", J. Phys. A, Vol. 7, No. 12, 1974, L 141-L143.

25. Gunther, H., Siegert, G., Wünsch, K., and Wollnik, H., "Gamma Ray Energies of Short-Lived Rb, Sr, and Y Isotopes Indicating Delayed Neutron Emission To Excited States", Nucl. Phys. A242 (1975) 56-61.

26. Pappas, A. C., Rep. LNS-MIT-63, AECU-2806 (1953) Part IV.

27. Pappas, A. C., Int. Conf. Peaceful Uses Atomic Energy (Proc. Conf. Geneva, 1958) 15, IAEA (1958) 373.

28. Keepin, G. R., "Interpretation of Delayed Neutron Phenomena", J. Nucl. Energy 7 (1958) 13.

29. Bohr, N. and Wheeler, J. A., Phys. Rev. 56 (1956) 426.

30. Bonner, T. W., Bame, S. J., and Evans, J. E., "Energy of Delayed Neutrons from Fission of ^{235}U", Phys. Rev. 101 (1956) 1514.

31. Evans, R. D., Chapter 17, § 3, "The Atomic Nucleus", McGraw-Hill, New York, (1955).

32. Blatt, J. M., Weisskopf, V. F., "Theoretical Nuclear Physics", Chapter 8, 6A, John Wiley, New York, (1952).

33. Perlow, G. J. and Stehney, A. F., "Delayed Neutrons from 15.5 sec ^{88}Br", Phys. Rev. 107 No. 3 (1957) 116.

34. "Neutron Proportional Counters", Catalog 12, Reuter Stokes, Cleveland, Ohio.

35. Birks, J. B., "The Theory and Practice of Scintillation Counting", Chap. 12, Macmillan Co., New York, 1964.

36. Nuclear Safeguards Research and Development", LA-4315-MS, Los Alamos Scientific Laboratory, (1968).

37. Nicholson, P. W., "Nuclear Electronics", London, John Wiley and Sons, 1974.

38. "The Integrated Circuit Catalog for Design Engineers", 1st Edition, Texas Instruments Incorporated, Dallas, Texas.

39. Radiological Health Handbook, U. S. Dept. of Health, Education and Welfare, January, 1970.

40. Price, W. J., "Nuclear Radiation Detection", 2nd Ed. McGraw-Hill Book Company, Chap. 7.

41. "Atomic Data and Nuclear Data Tables", Vo 13, Nos 2-3, February 1974, Academic Press Inc., New York and London.

42. Saudor Denne, "Semiconductor Detectors for Nuclear Radiation Measurements", Wiley-Interscience, John Wiley and Sons (1971).

43. Data General Technical Manual, NOVA 1220 Computer, Data General Corp., (1972).

44. Lederer, C. M., Hollander, J. M. and Perlman, I., "Table of Isotopes", 6th Ed., John Wiley and Sons, Inc., New York (1967).

45. Tuttle, R. J., "Delayed-Neutron Data for Reactor Physics Analysis", Nucl. Sci. Engg. 56, 37-71 (1975).

46. Tomlinson, L., "Theory of Delayed Neutron Physics", Nuclear Technology, Vol. 13 (1972) 42.

47. Shalev, S. and Rudstam, G., "The ^{137}I Delayed-Neutron Energy Spectrum", Trans. Am. Nucl. Soc. 14 (1971) 373.

48. Sloan, W. R. and Woodruff, G. L., "Spectrum of Delayed Neutrons from Thermal-Neutron Fission of Uranium-235", Nucl. Sci. Engg. 55, 28-40 (1974).

49. Gauvin, H. and de Tourreil, J., in Symposium on Physics and Chemistry of Fission, 2nd Ed. P. 621, International Atomic Energy Agency (1969).

50. United States Atomic Energy Commission, "Standards For Protection Against Radiation", Rules And Regulations, Title-10 Part 20.

51. Price, W. J., "Nuclear Radiation Detection", 2nd Ed. McGraw-Hill Book Company, Chap. 4.

52. Hughes, D. J., "Pile Neutron Research", Addison-Wesley, (1953).

APPENDIX A

Proposed

Reactor Experiment No. 37

Investigation of Bromine and Iodine Fission Products

Submitted by

M. M. Farghaly

Nuclear Engineering Department

Kansas State University

Investigation of Bromine and Iodine Fission Products

Object: To perform a continuous activation of a sample solution containing natural uranium inside the open tangential beam port of the TRIGA Mark II reactor.

I. Sample Preparation and Experimental Procedure:

(Ref. Fig. 1)

The sample is a solution containing 2 g of natural uranium disolved in 1M HNO_3 and 0.5M $KBrO_3$. The total volume of 15 ml will be contained in the cell "C" which will be located at an irradiation distance of about 6 inches from the mouth of the tangential beam port (TBP) of the TRIGA Mark II reactor. The sample will be irradiated by a collimated beam of neutrons through a cylindrical collimator located inside the TBP of the reactor. The cell "C" containing the sample solution will be held within the collimator by a soft protective material. The neutron flux inside the collimator and at the irradiation position was determined and was found to be in the order of 10^6 neutrons/cm^2-sec with the reactor operating at a power level of approximately 2 kW. A small empty plastic vessel will be located downstream from the irradiation cell to catch any active solution that might be carried out of it by foaming. A stream of air will be flowing to the glass vessel D where it gets mixed with the halogen of interest. The mixture will be bubbled through the irradiation cell at a flow rate of about 1 liter/min. The gas flow will carry the halogen activity from the irradiation cell "C" to trap "B" where any excess fission products can be trapped and then to the reservoir "A" (which is the counting

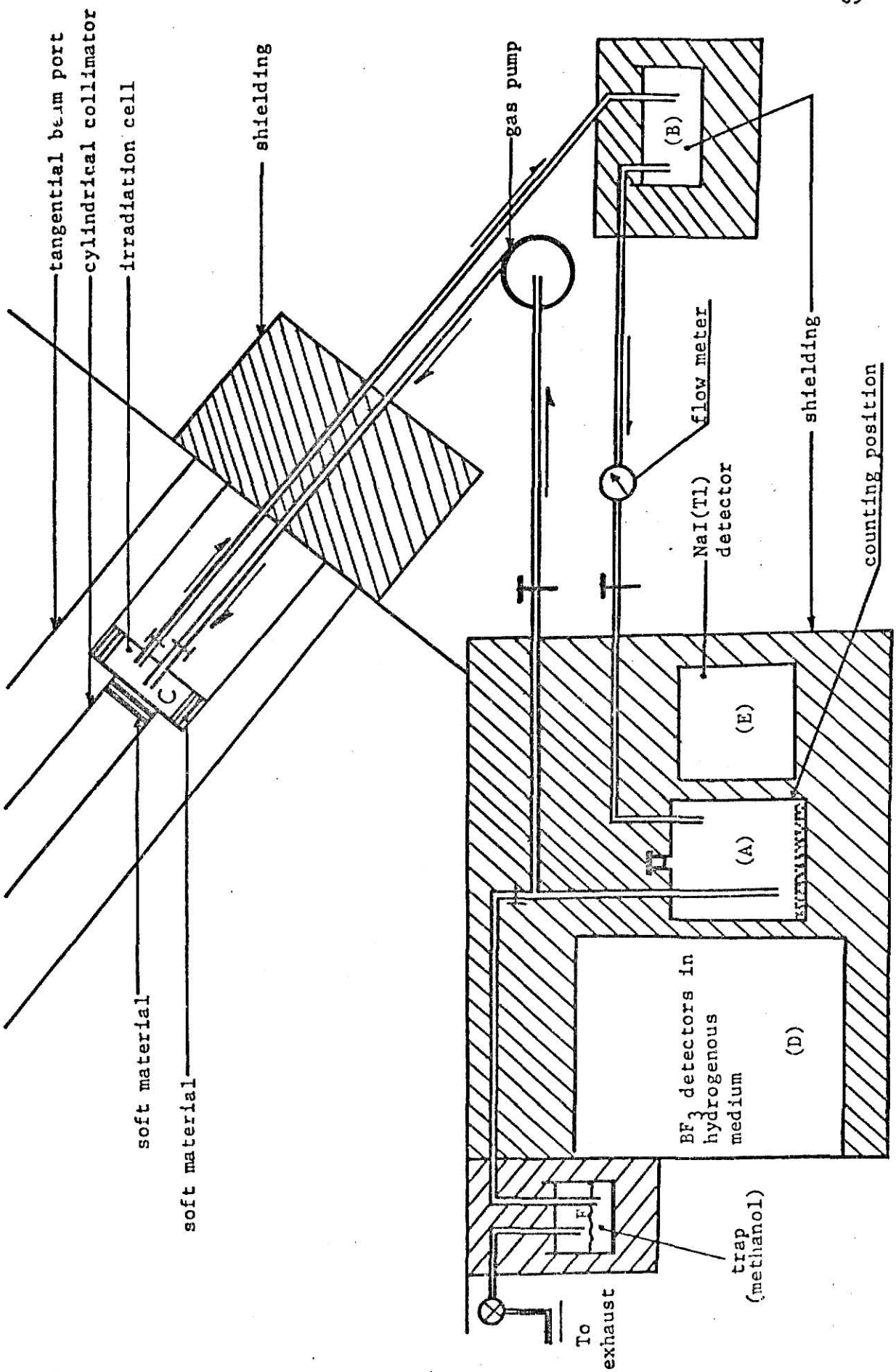

Figure 1 Closed Loop Experimental setup

position) containing CCl_4 or an activated charcoal serving as a trap where bromine (or iodine if it is the case) will remain and from there through some traps to a vacuum pump and then to the exhaust vent of the reactor bay. The gaseous fission products will be collected in the reservoir "A" and will be counted by an n-gamma coincidence setup consisting of a 3 x 3 inch NaI(Tℓ) detector for gamma counting on one side of the reservoir and an array of BF_3 counters connected in parallel and contained in a hydrogenous box for neutron counting on the other side.

II. Radiation Safety Concerns:

1. Irradiation Cell and Sample Preparation:

The sample will be prepared in the chemistry laboratory as follows: Two gm of natural uranium will be dissolved in 1M HNO_3 and 0.5M $KBrO_3$. 15ml (approximately) of the solution will be contained in a glass cell enclosed in a plastic bag which will prevent any leakage of the radioactive solution from the cell "C" to the surrounding space in the collimator avoiding any corrosion damage of the collimator inner walls. Further, the capsule cell will be supported by soft materials to the walls of the collimator. Also, a barrier of Al sheets, which is transparent to the beam of neutrons coming from the reactor core, will be placed behind the irradiation cell to avoid any transfer of the sample to the smaller diameter of the collimator in case of any irradiation cell leakage. Since the activity we are dealing with is relatively low, the damages that might occur due to any accidental breakage of the cell will not be of great significance.

2. Shielding Considerations:

The beam port will be opened during the experiment in accordance with Reactor Experiment No. 16: "Profile of Gamma, Fast Neutron, and Slow Neutron Radiation in Beams from Open Port". The shielding materials will be positioned in front of the open port on a platform. The reservoir "A" will be located between the NaI(Tℓ) detector and the BF_3 detectors as explained before in part II of this report. These three components (reservoir A, NaI(Tℓ) and BF_3 detectors) will be enclosed in a cavity of approximately 60 x 60 x 60 inches as shown in Figure 2. The concrete shielding of this unit will be extended to the flasks E and D.

3. Tubing Material and Trapping Unit Shielding:

The tubing coming from flask "D" to the irradiation cell "C", from the irradiation cell "C" to the trap "B" and from the trap "B" to the reservoir "A" will be glass enclosed in another hard material tubing like Al or hard plastic. The other tubing connecting the remaining of the system will be Tygon which is quite radiation-resistant and easily machined. The total length of the tubing used for the gas flow system (with an inner diameter of 1/4 inch and 3/16 inch wall thickness) will not exeeed 25 feet. Attempts will be made to have the least possible tubing length exposed in the room. The trapping unit will be an empty glass flask with glass tubing coming into and from it. This flask will be located inside a 12 x 12 x 12 inch shielding unit of concrete blocks.

After the reactor has been brought to an ititial low operating power level, the area around the experimental shielding will be surveyed by neutron and gamma survey meters to ensure that any local radiation is well below the levels required by 10CFR20.

III, The Expected Activity Estimations:

Assume that the saturation activity is produced at a reactor power level of 2 kW (which is the reactor power level required for the purpose of this experiment). The saturated activity, in the worst case, of the radioactive gases can be estimated as follows: The gaseous fission products that might be of great importance during the course of this experiment are those of bromine (Br), iodine (I), and xenon (Xe). The saturated activity of a fission product can be expressed by the following equation

$$A_{sat} = \sum_i y_i^j * \text{Fission Rate},$$

where y_i^j is the fractional fission yield of the isotope i of the element j and the fission rate required for this experiment is on the order of 3500 fissions/sec.

For bromine as a good approximation consider the sum of the fission yields of the isotopes of mass numbers 82 through 89 which gives a value of 0.1587. Applying the above formula for the saturated activity one gets

$$A_{sat}^{Br} = 0.0152 \text{ microcuries.}$$

Proceeding the same way as above, the saturated activity due to iodine and xenon was found to be, approximately, as follows:

$A_{sat.}^{(I-131)} = 0.0026$ microcuries
$A_{sat.}^{(I-132)} = 0.0039$ microcuries
$A_{sat.}^{(I-133)} = 0.0064$ microcuries
$A_{sat.}^{(I-134)} = 0.0068$ microcuries
$A_{sat.}^{(I-135)} = 0.0058$ microcuries
$A_{sat.}^{(Xe-131)} = 0.0026$ mocrocuries
$A_{sat.}^{(Xe-133)} = 0.0024$ microcuries
$A_{sat.}^{(Xe-135)} = 0.0024$ microcuries

According to Appendix A of the TRIGA R-88 license, the volume of the reactor bay is 144000 ft^3 (40.78 x 10^8 cm^3), so the maximum concentration per unit volume in the reactor bay that might be reached in case of an extreme accident such as the complete loss of the radioactive materials from the experimental system can be obtained from the table below.

Element (Atomic #)	Isotope	Concentration in Air (microcuries/ml)
Bromine (35)	Br-82 to 89	3.7×10^{-12}
Iodine (53)	I-131	6.3×10^{-13}
	I-133	1.6×10^{-12}
	I-135	1.57×10^{-12}
Xenon (54)	Xe-131	6.5×10^{-13}
	Xe-133	5.8×10^{-12}
	Xe-135	5.8×10^{-12}

Comparing the values of the above table with the corresponding values of MPC indicated in 10CFR20 one can see that the worst case concentrations produced during the performance of this experiment will be much lower than those indicated in the "Standards for Protection Against Radiation", 10CFR20. Also, the activity produced due to I-131 through I-135 is far below the 5 mCi limit specified in the technical specifications of the R-88 license. As for the activity of the sample itself, the main radioactive elements produced are: uranium, bromine, and potassium. The saturated activity of each

of these radioactive elements can be expressed as:

$$A_{sat} = \text{capture rate} + 8 \text{ fission rate.}$$

The capture rate is equal to $N \sigma_c \phi_{th}$ and fission rate is $N\sigma_f \phi_{th}$ where N is the # of atoms of the nuclide under consideration, σ_c is the capture cross section and σ_f is the fission cross section. The values of these cross sections are shown in the table below.

Element	σ_c(b)	σ_f(b)	Mass in the Sample (gm)
U-235	101	580	0.0144
U-238	2.7		1.9858
K-41	1.1		1.35
Br-79	11.4		20.2
Br-81	3.2		19.8

From the above table, the saturated activity can be calculated as:

$$A_{sat} = (0.6023 \times 10^{24})(10^{6})(10^{-24}) \left(\frac{0.0144*101}{235} + \frac{1.9858*2.7}{238} + \frac{1.35*1.1}{41} + \frac{20.2*11.4}{79} + \frac{19.8*3.2}{81} + 8* \frac{0.0144*580}{235}\right) =$$

$$4.052 \times 0.6023 \times 10^{6} = 2.44 \times 10^{6} \text{ dis/sec} =$$

$$\frac{2.44 \times 10^{6}}{3.7 \times 10^{10}} = 66 \ \mu\text{Ci}$$

Then the maximum total saturated activity that could be produced in the sample will be less than 66 μCi. As for the activity of the noble gases that might be produced during the course of this experiment, the most important noble gases from the safety point of view are Xenon and Krypton. The former has been already considered and the values

of its saturated activity is given in the table of part III of this report. For Krypton, the saturated activity is:

$$A_{sat} = \sum_i Y_i * \text{Fission rate} = 0.0173 \text{ microcuries}$$

considering the volume of reactor bay (40.78×10^8 cm^3), the saturated activity permit volume would be 4.24×10^{-12} microcuries/cm^3. The total saturated activity per unit volume due to the released noble gases will be 17×10^{-12} microcuries per mℓ which is far below the estimated limits of the MPC in restricted areas, so on pumping those gases to the exhaust, there would be negligible hazard.

BIBLIOGRAPHY

1. M. S. Krick, Reactor Supervisor, Kansas State University, personal communications.

2. Kansas State University 250-kW TRIGA Mark II Pulsing Reactor Mechanical Maintenance and Operating Manual, General Dynamics/ General Atomic Division.

3. Radiological Health Handbook, U. S. Department of Health, Education, and Welfare - January 1970.

4. United States Atomic Energy Commission, "Standards For Protection Against Radiation," Rules And Regulations, Title-10, Part 20.

5. Barrow, M. G., Physical Chemistry, second edition, 1966.

6. Glasstone, S. and Sesonske, A., Nuclear Reactor Engineering (1967).

M E M O

TO: Reactor Safeguards Committee

FROM: M. S. Krick

SUBJECT: Amendment to Experiment #37

DATE: 18 June 1975

It is proposed that experiment #37 (Investigation of Bromine and Iodine Fission Products), which specifies use of the tangential beam port, be amended to allow the experiment to be performed in other beam ports or in the thermal column subject to the same fission-product activity limitations as initially described. Please indicate your approval or disapproval of the following amendement.

Experiment #37, Amendment 1

Any of the four beam ports or the thermal column may be used for the experiment. Other provisions of the experiment are unchanged.

	Approve	Disapprove
N. D. Eckhoff	N. Dean Eckhoff (for REF)	
L. D. Ellsworth		
R. E. Hightower	R E Hightower	
M. S. Krick	M S Krick	
J. P. Lambert	J. P. Lambert	
H. C. Moser		
J. K. Shultis	J K Shultis	

APPENDIX B

Appendix B.

Neutron Flux Calculation

Foil Activation Method

The activation method of neutron flux measurement makes use of the production of radioactive nuclei by the absorption of neutrons in a detecting material. The radioactive nuclei so produced decay with the emission of nuclear radiation and can be detected. Some of the most widely used detecting materials are indium, gold, and cobalt in the form of foils and wires. If the flux is constant over the volume of the foil then the rate of production R of the radioactive nuclei depends on the absorption cross section of the detecting material and on the neutron flux in the following manner [42].

$$R = N_D \int_0^\infty dE\ \sigma_a(E)\phi(E) \qquad \text{(B-1)}$$

where N_D = Number of nuclei in the detector

σ_a = microscopic activation cross section

ϕ = neutron flux

E = neutron energy.

For the purpose of this discussion, the thermal flux and the fast flux can be defined as [43]:

$$\phi_{th} = \int_0^{E_c} dE\ \phi(E) \qquad \text{(B-2)}$$

$$\phi_f = \int_{E_{Tc}}^{E_{max}} dE\ \phi(E) \qquad \text{(B-3)}$$

where E_{Tc} is the thermal cutoff energy.

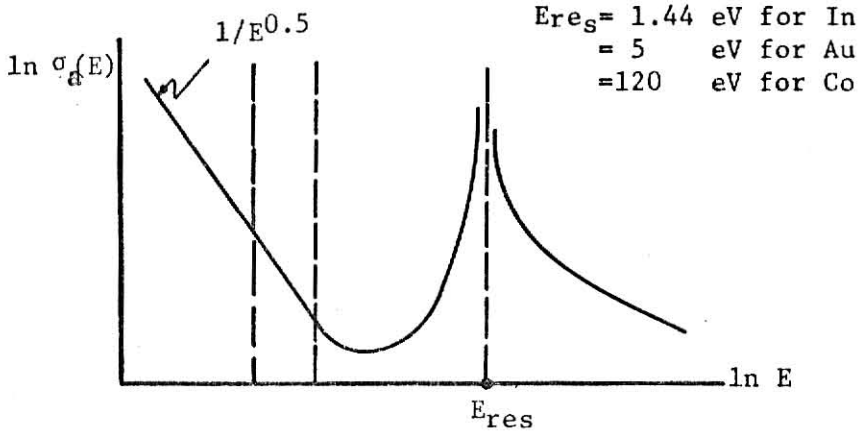

Figure B-1

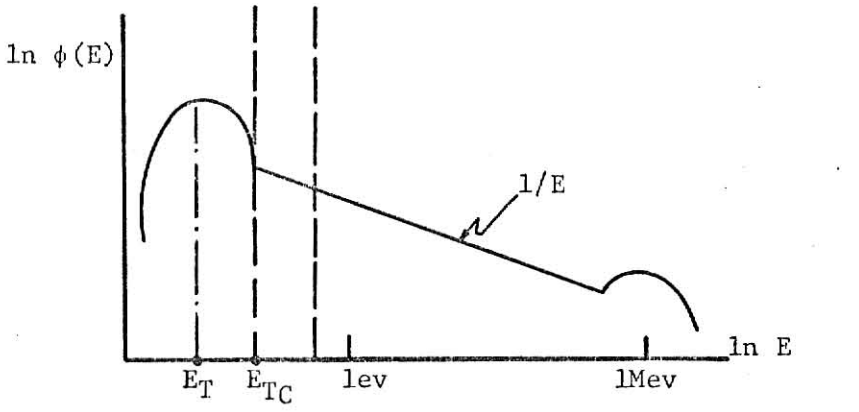

Figure B-2

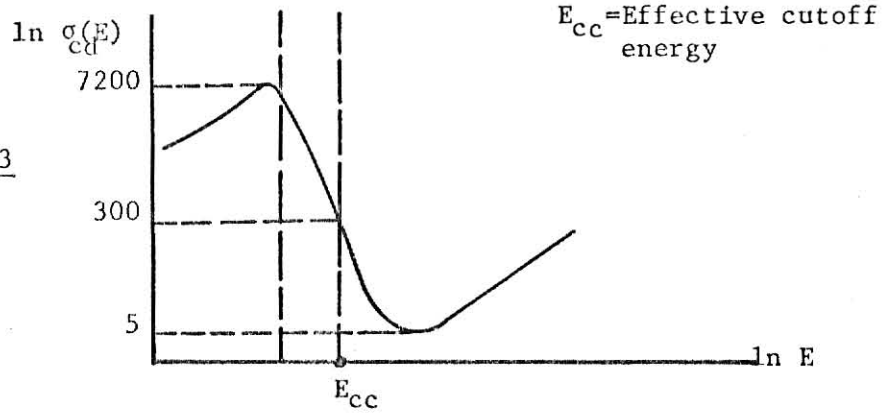

Figure B-3

Energy dependent absorption cross sections for resonance absorbers and for cadmium are shown in Figures B-1 and B-3, respectively. In these plots

E_{cc} = effective cutoff energy for cadmium

and

E_{res} = resonance energy.

Figure B-2 shows the neutron flux $\phi(E)$ vs. E with the thermal cutoff energy E_{Tc} indicated.

To measure the thermal flux, ϕ_{th}, one must differentiate between the activation produced by thermal neutrons and by fast neutrons. The common way of doing this is to make two measurements, one with a bare foil and one with a cadmium covered foil. If one assumes that no neutrons with $E<E_{CC}$ get through the cover and that all neutrons with $E>E_{CC}$ do pass through it, then the activity per unit mass of the foil $\hat{R}$ is given by the relation [42]

$$\hat{R} = \frac{F_{CD}\, C\lambda}{n\, m\, \gamma} \left[(e^{\lambda t_1}-1)(e^{-\lambda t_2} - e^{-\lambda t_3}) \right]^{-1} \qquad \text{(B-4)}$$

where F_{CD} = cadmium cover flux depression factor

γ = percentage of nuclei that decay by the observed decay mode

λ = decay constant of the foil material

m = mass of the activated foil

C = net number of counts observed by the counting system

n = efficiency of the detector used in the counting system

t_1 = time of foil activation

t_2 = cooling time

t_3 = time during which the foil is counted.

The parameters of equation (B-4) above are indexed with the letter b for bare foil and with the letter c for covered foil.

The fast flux, ϕ_o and the thermal flux ϕ_{th} are then given by [42]

$$\phi_o = \frac{\hat{R}_c}{N_D(RI)} \tag{B-5}$$

$$\phi_{th} = \frac{\hat{R}_b - \hat{R}_c}{N_D \bar{\sigma}} - \phi_o \sqrt{\frac{16E_T}{\pi}} \left(\frac{1}{\sqrt{E_{Tc}}} - \frac{1}{\sqrt{E_{cc}}} \right) \tag{B-6}$$

where $\bar{\sigma}$ = microscopic absorption cross section

(RI) = resonance integral of the foil material, and

where E_T, E_{Tc}, and E_{cc} are the same quantities defined previously.

Using this method of foil activation, the thermal flux in the tangential beam port and in the thermal column of the TRIGA Mk II nuclear reactor were measured by using pairs of bare and cadmium covered gold foils attached to a rod at different distances inside each irradiation facility. The foils were irradiated at a reactor power level of 10 kW for two hours and were counted using a Ge(Li) gamma-ray spectrometer controlled by a NOVA 1220 computer.

Using

E_{Tc} = 0.2 eV

E_{cc} = 0.4 eV

E_T = 0.03 eV

$\bar{\sigma}$ = 98.8×10^{-24} cm^2

RI = 1530×10^{-24} cm^2

γ = 0.955

n = 0.01

F_{cD} = 1.09 for covered foils

1.00 for bare foils

λ = 2.9757×10^{-6} sec^{-1}

N_D = 3.06×10^{21},

the values of the thermal fluxes computed are shown in Tables B-1 and B-2.

Table B-1. Neutron flux distribution inside the tangential beam port (TBP).

Foil Pair #	Distance from the mouth of TBP (inches)	Thermal flux, ϕ_{th} (neutron/cm^2-sec)
0	0.00	4.03×10^6
1	15.00	4.95×10^6
2	36.6	10.6×10^6
3	55.9	3.5×10^7
4	74.7	1.24×10^8
5	94.2	1.92×10^9

Table B-2. Thermal neutron flux inside the thermal column.

Foil Pair #	Distance from the mouth of the thermal column	Thermal flux, ϕ_{th} (neutrons/cm^2-sec)
1	4.5 ft.	2.8×10^7
2	7 ft.	4.9×10^8

APPENDIX C

APPENDIX C.

Specifications and General Features of the Components and Equipment shown in Figure 19.

1. ORTEC 442 Linear Gate and Stretcher

Linear Input
- Polarity: Positive unipolar, or bipolar with positive portion leading
- Amplitude: +0.1 to +10 volts, linear range; ±12 volts maximum
- Rise Time: 100 nsec to 10μsec
- Input impedance: 1000 ohms

Gate Input
- Function: Optional external control for switch selectable coincidence or anticoincidence mode triggering
- Input Pulses: 3 volts, 100 nsec min. width

Linear Output
- Polarity: Positive
- Amplitude: +0.1 to 10 volts, equal to peak of the accepted linear input
- Rise Time: 300 nsec

Gate Period
- Function: Adjusts duration of gating control from leading edge of Gate Input pulse; has been adjusted to 25 μsec.

2. ORTEC 420 A Timing Single Channel Analyzer

Signal Input
- Amplitude Range: 50mV to 10V
- Pulse Width Range: 200 nsec to 20 μsec
- Polarity: Postive Unipolar, or positive portion leading bipolar

SCA Outputs
- Pulse Shape for positive outputs, i.e., gate outputs
  - Amplitude: +5v
  - Rise Time: 20 nsec
  - Pulse Width: 500 nsec

3. TMC 402 Pulse Height Analyzer

Signal Input
- Polarity: Negative
- Amplitude: 0 to 50 mV
- Rise Time: 0.5 μsec is ideal
- Fall Time: 1 to 3 μsec. The total width of the pulse presented should not be less than about 1.0 μsec. at 50% amplitude.

4. Amplifiers

4.1 TC220 Linear Amplifier

First differentiator	=	1 msec
Second differentiator	=	1.6 μsec
Coarse gain	=	8.0
Fine gain	=	0.54
Integrator	=	0.4 μ sec
Polarity:		negative
Output impedence:		50 Ω

4.2 ORTEC-410 Linear Amplifier

Polarity: Positive unipolar output signal or Bipolar. RC pulse shaping with variable time constant ranging from 0.1 to 10 microseconds.
Delay line shaped pulse is 0.8 μsec wide.
Input impedence: 125 ohms
Output impedence: 93 ohms
Total gain: RC shaping mode - 0.35 to 480
Delay line shaping mode - 0.75 to 1300
Input attenuation factors: 1,2,5,10,20,50
Fine gain: 1.0 to 3.0
Coarse gain: X1, X3, X9
Rise time: Unipolar output - 80 nsec
Bipolar output - 100 nsec
Maximum bandpass: within 3db from 700 Hz to 4.3 MHz.

5. Continuously Variable Time Delay Passive Network AD-YU Model 2011

Time delay: 0 to 11 μsec
Bandwith: 10 megacycles for the cutoff frequency
Rise time: less than 0.1 μsec
Input impedence: 20 μμf shunted by 1 Mohm with input cathode follower, and 600 ohms without input cathode follower
Output impedence: 100 ohms (nominal)
Maximum input voltage: 24 volts peak to peak without clipping
Output signal amplitude: 3 db below input amplitude with maximum delay at low frequencies and 1 db below input with zero delay.

Accuracy of time delay: ± 2% of the time delay at any point.

A NEUTRON-GAMMA COINCIDENCE COUNTING SYSTEM FOR THE INVESTIGATION OF BROMINE DELAYED-NEUTRON PRECURSORS

by

Mahmoud M. Farghaly

B.S., University of Alexandria, 1967
M.S., University of Sao Paulo, 1971

AN ABSTRACT OF A MASTER'S THESIS

submitted in partial fulfillment of the

requirements for the degree

Master of Science

Department of Nuclear Engineering

KANSAS STATE UNIVERSITY

Manhattan, Kansas

1975

ABSTRACT

A neutron/gamma-ray coincidence counting system was developed for the investigation of the decay modes of bromine delayed-neutron precursors. The precursors were obtained as fission products by the irradiation of a sample solution containing natural uranium in the thermal column of the Kansas State University TRIGA Mark II nuclear reactor. A nitrogen-bromine gas-flow system was constructed for the transfer of the bromine fission products from the irradiation position to the coincidence counter. A lithium-drifted germanium [Ge(Li)] gamma-ray spectrometer was used to study the the radioisotopes transferred by the gas-flow system. Isotopes of bromine, krypton, and xenon were observed; the bromine isotopes included ^{80}Br and ^{82}Br, which were activation products of the transfer gas. Evidence was found for the presence of the delayed-neutron precursors ^{87}Br and ^{88}Br.

The coincidence counting system was designed to determine the energy distribution of the gamma rays detected in coincidence with delayed neutrons. The neutron detector consisted of 10 BF_3 counters in a paraffin moderating assembly. The gamma-ray spectrometer consisted of a 3 x 3 in. NaI(Tℓ) detector and a multichannel pulse height analyzer. The detectors were operated in singles and coincidence modes using fission products from the uranium sample. The coincidence system operated satisfactorily within the limitations set by the resolution and efficiencies of the detectors used, although the true-to-random coincidence ratio was found to be too low for practical coincidence measurements. It is estimated that the use of ^{3}He neutron detectors and a very large Ge(Li) detector will permit a useful coincidence spectrum to be measured in approximately a week's operating time.